Abstract

Since the first observation of nuclear magnetic resonance (n.m.r.) in ferromagnetic cobalt (1), n.m.r. has been used extensively to study the electron-nucleus hyperfine interaction in magnetically ordered materials (2). This thesis describes an unsuccessful attempt to extend such studies to the magnetically ordered phases of terbium and holmium metals. Detailed calculations of the intensity of the predicted n.m.r. signal in terms of linewidth and electronic susceptibility at the n.m.r. frequency are given for the heavy rare earth metals gadolinium to thulium, and a comparison is made with europium and with iron, cobalt and nickel.

With the exception of gadolinium, which has a closed 4f electrons shell configuration, the hyperfine interactions at $0^{o}K$ in the heavy rare earth metals vary from $\pm$ 800 Mc/sec. in dysprosium to 6,500 Mc/sec. in holmium. These are an order of magnitude higher than in most magnetically ordered materials and we show that this, combined with relatively weak exchange interactions, is likely to lead to a very strong nuclear spin-spin coupling. The corresponding short spin-spin relaxation times and line broadening may make n.m.r. difficult to observe. A qualitative discussion of spin-lattice relaxation mechanisms shows that the spin-lattice relaxation times will probably be shorter than in the 3^{d} transition metal

ferromagnets.

In a magnetically ordered material n.m.r. is excited indirectly through the electronic magnetisation and electron-nucleus hyperfine coupling, leading to enhancement of the oscillatory field exciting the n.m.r. We have measured as a function of temperature the combination $|\mu| + \mu'' = \mu_R$ of the components of the complex permeability $\mu' - j\mu''$ in crystal specimens of terbium and holmium metals and in a terbium polycrystal, in the region of the respective predicted n.m.r. frequencies. The results are used to elucidate the enhancement of n.m.r. in these metals, and it is shown that in the ferromagnetic phases domain wall motion at the n.m.r. frequency is largely absent. Measurement of μ_R at $\doteq$ 3,000 Mc/sec. on a crystal of dysprosium metal in the temperature range 20°K to 280°K is also reported. In all cases peaks are found in μ_R at the magnetic ordering transitions and in the ordered phases μ_R varies from $\doteq$ 1.2 to $\doteq$ 8.

Incidental to the permeability measurements, measurement of the d.c. resistivities of terbium, holmium and dysprosium crystals have been made throughout the temperature range 10°K to 280°K. The current flow in each case is at a specified angle between the c-axis and the basal plane. Resistivity measurements on a terbium polycrystal have also been made from 77°K to 280°K. The

results are consistent with the most reliable data of other workers.

Qualitative measurement of microwave absorption at 3,000 Mc/sec. in a powder sample of terbium shows no peak at the ferromagnetic to antiferromagnetic ordering transition ($\pm 220^{\circ}K$), and also that the microwave magnetic permeability at $77^{\circ}K$ is considerably larger than in bulk terbium. Low frequency and d.c. susceptibility measurements confirm the absence of an ordering transition at $220^{\circ}K$, and show that ferromagnetism sets in at the normal Neel temperature ($\pm$ $230^{\circ}K$) and persists continually to low temperatures. Observation of microwave power absorption in the strained surface of a terbium single crystal also shows one magnetic ordering transition only, at $230^{\circ}K$.

A continuous wave variable frequency spectrometer depending on a double modulation principle and partial saturation of the n.m.r., operating in either in the region of 3,000 Mc/sec. or 6,500 Mc/sec. (the terbium and holmium predicted n.m.r. frequencies) has been developed. This is capable of detecting a fractional change $\delta Q/Q$ of 5×10^{-5} in the quality factor Q of a coaxial cavity containing the specimen. In application to a search for n.m.r. in terbium and holmium crystals, the specimens formed the centre conductor of the cavity. The extent of the search made is 2954 to 3078 Mc/sec. at $77^{\circ}K$, and 2957 to 3010 Mc/sec. at

72°K in terbium, and from 6320 to 6570 Mc/sec. at ≐ 20°K in holmium. The measured permeability at the n.m.r. frequency is combined with the calculations of the n.m.r. absorption intensity and the measured spectrometer sensitivity to show that, subject to the necessary partial saturation conditions being fulfilled, no n.m.r. signal less than of order 10 Mc/sec. broad is present in the holmium, or less than of order 0.4 Mc/sec. in the terbium. These results are consistent with the estimated magnitude of the contribution to n.m.r. linewidth due to nuclear spin-spin coupling.

<u>References</u>

1. A.C. Gossard and A.M. Portis: Phys. Rev. Letters 3, 164 1959.

2. Chapters 5 and 6 in "Magnetism" IIA. G.T. Rado and H. Suhl, editors, Academic Press. 1965.

SOME MAGNETIC RESONANCE EXPERIMENTS ON SOLIDS

Thesis submitted for the degree
of Doctor of Philosophy at the
University of Oxford

by

T.G. Emeleus
of
Wadham College

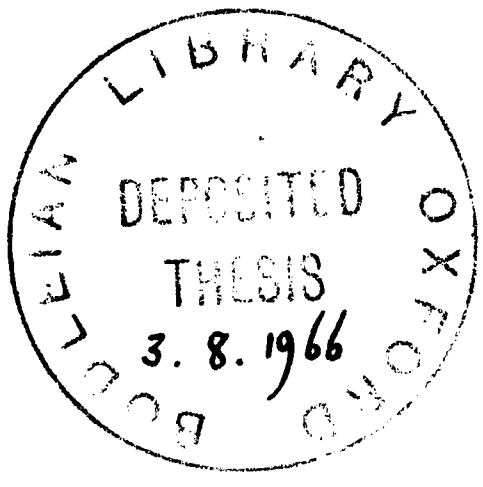

The Clarendon Laboratory
Hilary Term 1966.

Acknowledgements

The author wishes to make grateful acknowledgement to:

Professor B. Bleaney, for providing the facilities of the Clarendon Laboratory and for many invaluable suggestions and discussions;

Dr. J. M. Baker, who supervised the work for the first and fourth years, for continual encouragement and advice;

Dr. M.A.H. McCausland, who supervised the work for the second and third years, for continual encouragement and advice, and for constructing much of the electronic equipment;

Drs. L. Drain and B. Forsyth of A.E.R.E. Harwell, for grinding and X-ray analysis of the terbium powder specimen;

Members of Dr. Garton's group, for annealing the specimens;

Dr. J. Owen, for use of the Faraday susceptibility balance;

Drs. J. Leisegang, D.T.R. Edmonds, G. Murray and many other members of the Laboratory, for helpful discussions;

Mr. E.J. Jenkinson and Mr. H. Lock, in whose workshops much of the apparatus was constructed;

Mrs. C.E. Hacker, for typing the thesis;

The Ministry of Education for Northern Ireland, for the provision of a Research Studentship (1962 to 1965).

Contents

Chapter 1. Magnetic ordering and hyperfine interactions in heavy rare earth metals.

(i) Magnetic ordering 1.1

(ii) The hyperfine interaction 1.7

Chapter 2. N.m.r. enhancement, relaxation and linewidths in magnetically ordered heavy rare earth metals.

(i) Introduction 2.1

(ii) General discussion of n.m.r. enhancement in magnetically ordered materials 2.2

(iii) N.m.r. enhancement in the heavy rare earth metals 2.4

(iv) Relaxation, saturation and linewidths 2.11

(v) Summing up 2.22

Chapter 3. Specimens and cryogenic apparatus.

(i) Preparation of the rare earth metal specimens 3.1

(ii) Low temperature microwave apparatus 3.4

(iii) Electrical resistivity apparatus 3.13

(iv) Low frequency magnetic susceptibility apparatus 3.15

Chapter 4. Microwave magnetic permeability of terbium, holmium and dysprosium metals.

(i) Introduction 4.1

(ii) Experimental methods 4.6

(ii) Experimental methods 4.6

(iii) Experimental results
(a) Electrical resistivity measurements 4.13

(b) Calibration of the cavities 4.19

(c) Experimental values of μ_R for terbium, holmium and dysprosium 4.26

(iv) Discussion of results: application to n.m.r. 4.41

Chapter . Field dependence of microwave absorption in bulk terbium, and some magnetic properties of terbium powder.

(i) Introduction 5.1

(ii) Field dependence of microwave absorption in bulk terbium 5.1

(iii) Some magnetic properties of terbium powder 5.5

(iv) Discussion of results 5.8

Chapter 6. The search for n.m.r. in terbium and holmium metals.

(i) Introduction 6.1

(ii) Microwave generation, handling and detection 6.5

(iii) Modulation stabilizing and signal processing 6.7

(iv) Sensitivity of the spectrometers 6.15

(v) The search for n.m.r. 6.19

(vi) Conclusion 6.21

Appendices

Chapter 1.

Magnetic Ordering and Hyperfine Interaction in Heavy Rare Earth Metals.

1. (1) Magnetic Ordering

The rare earth metals exhibit a wide variety of forms of co-operative magnetism in the temperature range $0^{o}K$ to $300^{o}K$. A comprehensive survey and theoretical discussion of rare earth metal magnetism has been given by Elliott (1). The metals of particular interest in the present work are terbium, dysprosium and holmium. Their magnetic properties are conveniently reviewed in the context of the second half of the 4f transition group where, along with gadolinium, erbium and thulium, they form an interesting series illustrating systematic development of several magnetic properties as the 4f shell is filled. The crystal structure of all six metals is basically hexagonal close packed, with c/a ratios 1.57 to 1.59, a little smaller than the ideal value of 1.63. However, in the ferromagnetic phases, magnetostrictive effects tend to distort the lattice (2). This is illustrated by the orthorhombic distortion observed in dysprosium below $86^{o}K$ (3). These rare earth metals may be regarded as an assembly of tripositive ions in a sea of conduction electrons. The two 6s and one 5p electrons

of the atom form into conduction bands, leaving the partially filled 4f shell well screened from the crystal field by the complete 5s shell.

With the exception of gadolinium, each of these metals shows at least two magnetic ordering transitions, the transition temperatures, details of the magnetic ordering, the ground state configurations of the ions and parameters of interest in the exchange interaction are given in Table 1. (1). Figure 1.1 illustrates the magnetic ordering referred to in this table.

Although the magnetic ordering transitions show up in many of the bulk magnetic and electrical properties of the rare earth metals, determination of the detailed magnetic structure has been done almost entirely by neutron diffraction. (5). Elliott has shown (1) in a relatively simple way how the many kinds of magnetic ordering thus found may be accounted for by a combination of crystal field effects and a long range oscillatory exchange via the conduction electrons. Using the method of Rudermann and Kittel (6) he derives the expression

$$E_{ij} = (9/2)\pi^2(\lambda-1)^2(\underline{J}_i\cdot\underline{J}_j)F(2k_oR_{ij})/E_o$$

for the energy of the ith moment due to the jth. R_{ij} is the distance between the ions, k_o the conduction electron wave-vector and $F(x) = (x.\cos(x) - \sin(x))/x^4$.

Table 1.1.

	$4f^n$	L	S	J	λ	$(\lambda-1)^2 J(J+1)$	T_1 °K	order	T_2 °K	order
Gd	7	0	7/2	7/2	2	15.75	289	ferro	-	-
Tb	8	3	3	6	3/2	10.5	229	helix	220	ferro
Dy	9	5	5/2	15/2	4/3	7.08	179	helix	86	ferro
Ho	10	6	2	8	5/4	4.5	132	helix	35	distorted helix
									19.4	cone
Er	11	6	3/2	15/2	6/5	2.55	85	LW	50	complex
									20	cone
Tm	12	5	1	6	7/6	1.17	56	LW	22	anti-phase.

Notes: This is based on Table II of reference 1. Slight modifications to the transition temperatures and the ordering columns are based on recent results reviewed in reference 4, and also the present work.

Figure 1.1

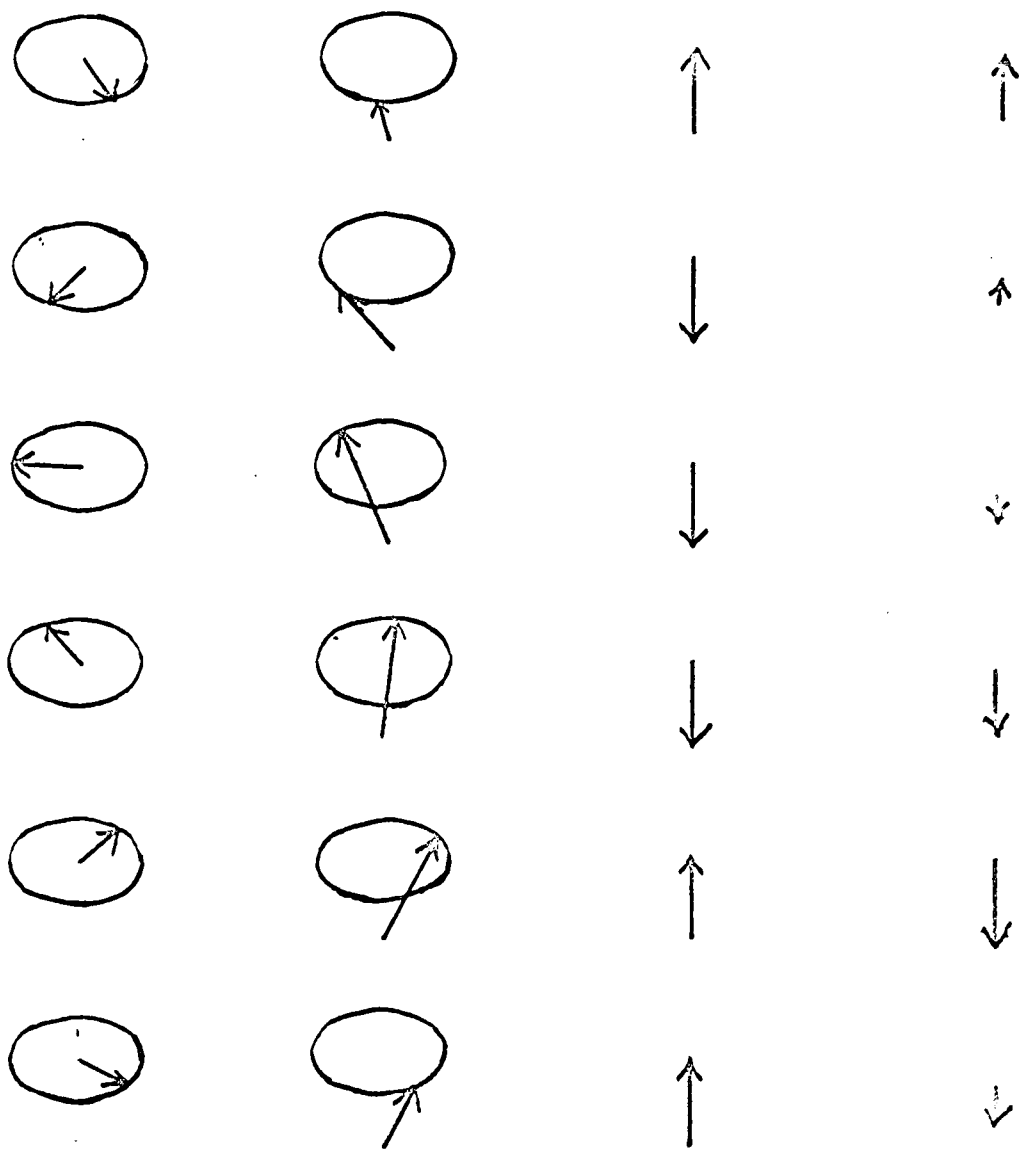

a. b. c. d.

types of ordering :--

a. plane helix

b. conical

c. antiphase

d. LW (longitudinal wave)

K is a measure of the overlap between the conduction and 4f electrons, and λ the spectroscopic splitting factor. Assuming that k, F(x) and E_o do not vary appreciably through the series, the exchange interaction will vary approximately as $(\lambda-1)^2(\underline{J}_i.\underline{J}_j)$, or $(\lambda-1)^2J(J+1)$. The magnetic ordering temperature T_1 is also a measure of the exchange, and so the smooth approximately linear variation of T_1 with $(\lambda-1)^2J(J+1)$ through the series indicates the essential correctness of this model.

The potential energy of a rare earth ion in a hexagonal crystal field such as that experienced in the metals has the form

$$V = V_2^0\langle r^2\rangle\alpha Y_2^0(\underline{J}) + V_4^0\langle r^4\rangle\beta Y_4^0(\underline{J}) + V_6^0\langle r^6\rangle\gamma Y_6^0(\underline{J}) + V_6^6\langle r^6\rangle\gamma(Y_6^6(J) + Y_6^{-6}(\underline{J})).$$

where the $Y_n^m(J)$ are the operator equivalents of spherical harmonics. The first term dominates this expression and is present because of the departure of the c/a ratio to values lower than the ideal value of 1.63 (7). Physically it describes the interaction of the crystal field with the electric quadrupole moment of the 4f shell, and its effect is to concentrate the electrons in the hexagonal plane. Assuming a free ion model, the principal axis of the quadrupole moment is parallel to the magnetic dipole moment of the shell. As a direct result, this crystal

field term provides the major contribution to the large axial magnetic anisotropy found in the non S-state heavy rare earth metals.

In terbium, dysprosium and holmium α is negative and the effect of the V_2^0 crystal field term is to favour alignment of the magnetic moments perpendicular to the c-axis. This orientation is found experimentally in terbium and dysprosium throughout their co-operative phases, and in holmium between 132°K and 19.4°K. Below 19.4°K higher order crystal field terms stabilize conical ordering. In erbium and thulium α is positive, favouring alignment of the magnetic moments parallel to the c-axis. This alignment is found experimentally in thulium throughout its co-operative phases, and in erbium from 50°K to 85°K. However, below 50°K the situation is again complicated by higher order crystal field terms.

In gadolinium, which is an S-state ion, the electronic quadrupole interaction is no longer present in first order and the anisotropy energy is very much smaller than in the other heavy rare earth metals. It is found experimentally that gadolinium is a classical ferromagnet with its relatively small anisotropy energy varying in a complicated way with temperature.

1. (ii) The Hyperfine Interaction

In the rare earth metals terbium to thulium the hyperfine interaction is dominated by the coupling between the nuclear magnetic moment and the spin and orbital motion of the 4f electrons. Freeman and Watson (8) show that the energy due to this is of order

$$\mathcal{E}_{orbital} = g_n\beta_n \left\{ g\beta \cdot \frac{\underline{I}\cdot\underline{J}}{J(J+1)} \frac{1}{\langle r^3 \rangle} \right\},$$

where $\langle r^3 \rangle$ refers to the 4f electrons and β and β_n are respectively the Bohr and nuclear magnetons. J is the angular momentum quantum number for the 4f shell. In the paramagnetic phase thermal effects average $\underline{J}$ nearly to zero, and in the magnetically ordered phases, $\underline{J}$ may be replaced by its temperature dependent expectation value $\langle J_z \rangle$, where z is the direction of the local magnetization vector. $\langle J_z \rangle$ is nearly zero at the highest magnetic ordering temperature, and rises close to the maximum free ion value at $T=0^{\circ}K$. In the magnetically ordered phases, $\mathcal{E}_{orbital}$ may then be written as

$$\mathcal{E}_{orbital} = g_n\beta_n A I_z \langle J_z \rangle$$

$$= g_n\beta_n I_z H_e.$$

At $T = 0^{\circ}K$, this corresponds to a hyperfine field H_e of order 10^6 to 10^7 oersteds, and a hyperfine interaction

of 10^3 to 10^4KMc/sec. Bleaney (9,10) estimates that core polarisation and conduction electrons will contribute at most a few percent to the magnetic hyperfine interaction, and that other magnetic effects will be much smaller than this.

The 4f electrons also produce an electric field gradient at the nuclear sites. This is parallel to the magnetic moment of th e ion and, with the exception of thulium, which has I = 1/2, it interacts with the large nuclear quadrupole moments found in the heavy rare earth metals causing a significant term in the hyperfine interaction. The total nuclear Hamiltonian in the co-operative state will then take the form

$$H = a'I_z + P(I_z^2 - \tfrac{1}{3}I(I+1)), \text{ where } a' = a\langle J_z\rangle.$$

This gives a spectrum of 2I lines, with the transition $I_z = m$ to $I_z = m-1$ occuring at the frequency $a' + P(2m-1)$.

In the case of europium and gadolinium, which are S-state ions, and the 3d transition metal ferromagnets, where the orbital contribution no longer dominates the hyperfine interaction. several smaller effects sum together to give an interaction one or two orders of magnitude less than that found when the orbital contribution is fully effective. This makes interpretation of the observed hyperfine interactions in these metals much more difficult than in the series terbium to thulium.

Using electron spin resonance data, Bleaney has estimated the parameter a' at $0^{o}K$ for the whole series of rare earth metals (9,10). His estimates are based on the assumptions that the rare earth ion in the metal has the same core polarization and value of $\langle r^{3} \rangle$ as in the salts, and that conduction electrons make a negligable contribution. Some of these estimates, together with experimental results obtained by several methods are shown in Table 1.2. For the non S-state ions agreement between Bleaney and experiment is within experimental error. For europium and gadolinium the estimates have proved to be too large (13,14). However, the values of a' obtained experimentally in magnetically ordered GdN (14) and EuS (15) are in good agreement with Bleaney, and so it is probable that the discrepancy in the metals is due to a conduction electron contribution to the hyperfine field.

The primary aim of the present work was to use the technique of nuclear magnetic resonance (n.m.r.) to observe directly the hyperfine interaction in magnetically ordered terbium and holmium. The frequency ranges explored were those estimated by Bleaney, corrected to the experimental temperature using published values of the saturation magnetization σ (16,17) and the relation

Table 1.2.

Isotope	Isotopic abundance (percent)	I	aJ(calc) Mc/sec	a'_o(exp) Mc/sec	P(calc) Mc/sec	P(exp) Mc/sec
Eu 151	48	5/2	-360		-.059	
153	52	5/2	-160	123(a)	-0.15	
Gd 155	15	3/2	+41	30.7(b)	<1	
157	16	3/2	+56	48.6(b)	<1	
Tb 159	100	3/2	+3180	(+)3130(c)	3100	+440(c)
Dy 161*	19	5/2	-820±20	-825±30(d)	150±30	160±12(d)
163	25	5/2	+1140±20		+180±30	200±40(d)
Ho 165	100	7/2	+6500	6680(c) 6450(c) 6100(c)	+63	150±50(c)
Er 167*	23	7/2	-940	-950±30(d)	-.8	
Tm 169*	100	1/2	-2360	2230±100(d) 2330±120(d)	0	

References: (a) refers to (13)
(b) refers to (12)
(c) results quoted in (10)
(d) results quoted in (11)

* = Mossbauer nucleus.

$\frac{\nu_T}{\nu_{T=0^oK}} = \frac{\sigma_T}{\sigma_{T=0^oK}}$, where ν is the n.m.r. frequency. This relation applies only to the $I_z = 1/2$ to $I_z = -1/2$ transition, which occurs at frequency $a' = a\langle J_z \rangle$, and it follows from the proportionality of σ to $\langle J_z \rangle$ in the free ion model. However, Mossauer measurements of ν_T in dysprosium show that agreement with this model becomes poor at temperatures approaching T_n (18). No n.m.r. was observed in the present work, and this negative result is discussed in more detail particularly in chapters two and six.

Of the three published observations of n.m.r. in magnetically ordered rare earth metals, in europium (13), gadolinium (12) and terbium (19), the last mentioned has proved to be spurious (20). The resonances in europium and gadolinium occur at frequencies much lower than those expected in the non S-state heavy rare earth metals, and so the physical mechanisms of n.m.r. excitation and the technical problems involved will differ considerably from those encountered in the present work. Other unsuccessful attempts to observe n.m.r. in holmium (21) and terbium (22) are also known to the present writer.

Chapter 1: References

1. R.J. Elliott: Chapter 7 in "Magnetism" IIA, G.T. Rado and H. Suhl editors, (Academic Press 1965)

2. J.J. Rhyne and S. Legvold: Phys.Rev. 138, A507 1965.

3. A.E. Clark, B.F. de Savage and R. Bozorth: Phys. Rev. 138 A216 1965.

4. K.P. Belov, R.Z. Levitin and S.A. Nikitin: Sov. Phys. Uspekhi 7, 179 1964.

5. W.C. Koehler, H.R. Child, E.O. Wollan and J.W. Cable: J.Appl. Phys. 34, 1335 1963.

6. M. Rudermann and C.Kittel: Phys. Rev. 96, 99 1954 .

7. F.W. de Wette: Phys. Rev. 123, 103 1961.

8. A.J.Freeman and R.E. Watson: Chapter 4 in "Magnetism" IIA, G.T. Rado and H. Suhl editors.

9. B. Bleaney: J. Phys. Soc. Japan 17 Supp. BI, 435 1962.

10. B.Bleaney: J. Appl. Phys. 34 1024 1963.

11. S. Ofer, M.Rakavy, E. Segal and B.Khurgin: Phys. Rev. 138 A241 1965.

12. R.E. Gegenwarth and J.I. Budnik: Bull. Am. Phys. Soc., (11) 10 591 1965.

13. G.A. Uriano and R.L. Streever: Phys. Letters 17 205 1965

14. E.L. Boyd and R.J. Gambino: Phys. Rev. Letters 12, 20 1964.

15. E.L. Boyd: Bull. Am. Phys. Soc. (2) 8, 439 1963.

16. D.E. Hegland, S. Legvold and F.H. Spedding: Phys. Rev. 131, 159 1963.

17. D.L. Strandberg, S. Legvold and F.H. Spedding: Phys. Rev. 127, 1046 1962.

18. Manchester University Mossbauer Group: G. Bowden: private communication 1966.

19. J. Herve and P. Veillet: Compt. Rend. 252, 99 1961.

20. J. Herve: private communication 1964.

21. J. Itoh: private communication 1964.

22. A.C. Gossard: Ph.D. thesis, University of California (unpublished) 1960.

Chapter 2

N.M.R. Enhancement, Relaxation and Linewidths in Magnetically Ordered Heavy Rare Earth Metals.

2. (1) Introduction

In a magnetically ordered material n.m.r. is excited indirectly through the electronic magnetization and the electron-nucleus hyperfine coupling, rather than by direct interaction between the nuclei and the applied alternating field H_1. H_1 induces a transverse component M_t in the local electronic magnetization M and, since the hyperfine field H_e is everywhere parallel to M, this leads to a transverse component H_1' in H_e. H_1' is usually very much greater than H_1, and a correspondingly enhanced n.m.r. signal is observed. Details of this enhancement mechanism have been given in many papers and are reviewed by Portis and Lindquist in reference (1).

In general, the enhancement may be due either to the motion of the domain walls in a ferromagnet at the n.m.r. frequency or, in absence of domain wall motion, to the response of the bulk electron magnetism to the applied alternating field. Portis and Lindquist (1) show that the former mechanism produces considerably more enhancement than the latter. In the following two sections we show that the weaker non-domain wall enhancement mechanism is most likely to apply to n.m.r.

in the heavy rare earth metals, excluding gadolinium, and we discuss this mechanism in detail, making estimates of its effectiveness in the various metals.

In section (iv) we discuss relaxation, saturation and broadening of n.m.r. in the heavy rare earth metals, and show that in the case of holmium, thulium and terbium the presence of a probable very strong nuclear spin-spin coupling may make n.m.r. difficult to observe.

2. (ii) General discussion of n.m.r. enhancement in magnetically ordered metals.

In most observations of n.m.r. made on magnetically ordered metals, the metals are ferromagnetic and the n.m.r. frequency is less than 300Mc/sec. (1). The dominant enhancement mechanism is due to motion of the domain walls at the applied frequency, and considerable reduction of the n.m.r. signal size occurs when the walls are removed by applying a static magnetic field or by using monodomain particles. The response of the electronic magnetism of a metallic ferromagnet to a high frequency field is very complicated. When no static field is applied, this response depends rather critically on factors such as the size of the ferromagnetic domains, the effective mass of the domain walls and eddy current damping of domain wall motion (2,3). Although these factors vary considerably from one metal to another, in all cases domain wall motion

is damped out as the frequency of the applied field is increased, and in general is significantly decreasing in importance at frequencies above a few hundred Mc/sec. With the exception of gadolinium, the hyperfine interactions at $0^{\circ}K$ in the heavy rare earth metals lie in this frequency range. We may then expect less domain wall enhancement of n.m.r. than is commonly observed at lower frequencies, and a corresponding increase of excitation of n.m.r. in the bulk domains, as these will now be less effectively shielded by demagnetizing fields.

The measurements of magnetic permeability of terbium and dysprosium metals at ≈5,000kc/sec. reported in chapter four confirm the absence of significant domain wall motion in these particular cases. Furthermore, in many of their magnetically ordered phases, the heavy rare earth metals are antiferromagnetic, and in these circumstances domain wall enhancement may be excluded completely. In the following section we calculate the n.m.r. response in the heavy rare earth metals, making the assumption that domain wall motion is effectively absent. The enhancement mechanism is then essentially that discussed by Bortis and Lindquist (1) for single domain particles.

2. (iii) N.M.R. enhancement in the heavy rare earth metals.

It is usual to observe magnetic resonance at microwave frequencies by detecting the change it produces in the quality factor Q of a resonant cavity containing the specimen. In this section we start by calculating the change in magnetic susceptibility of an ordered magnetic material due to n.m.r., and then relate this to the fractional change $\delta Q/Q$ it produces in the cavity quality factor for the particular case of a metallic specimen. We then evaluate the relative magnitudes of $\delta Q/Q$ for the heavy rare earth metals, and also make comparison with the effect of domain wall enhanced n.m.r. in ferromagnetic iron, cobalt and nickel, and europium and gadolinium.

Suppose that at some point in the specimen the applied alternating field has a component H_t perpendicular to the local magnetization vector $\underline{M}$. H_t will produce a transverse component in $\underline{M}$ of $M_t = M_s \delta\theta$, where M_s is the specimen saturation magnetization and $\delta\theta$ the angle through which H_t tips $\underline{M}$. The effective field at the nuclei, $\underline{H}_e$, is parallel to $\underline{M}$, hence H_t causes a transverse field H_t' at the nuclei given by:-

$$H_t' = M_s \delta\theta,$$

hence

$$H_t' = M_t (H_e/M_s).$$

Writing $H_e/M_s = \beta$, we have:-

$$H_t' = \beta M_t.$$

The nuclear magnetization will then have a transverse component $\underline{m}_t$ where:-

$$\underline{m}_t = \chi_n \cdot (\underline{H}_t + \underline{M}_t\beta) \qquad \text{equation 1a.}$$

This in turn will produce a transverse field acting on the electron spin system, and hence:-

$$\underline{M}_t = \chi_e \cdot (\underline{H}_t + \underline{m}_t\beta) \qquad \text{equation 1b.}$$

In these equations χ_e and χ_n are respectively the electronic and nuclear magnetic susceptibilities and they will, in general, be complex and anisotropic. The high magnetic anisotropy in the heavy rare earth metals means that anisotropy effects in χ_e will, in fact, be considerable. Furthermore, the spin orderings found in the heavy rare earth metals and the microwave cavity geometry used in the search for n.m.r. reported in chapter six, will lead to considerable variation of $\underline{H}_t$ over the specimen. For convenience, we ignore both the magnetic anisotropy and the variation in $\underline{H}_t$, and assume effective average values.

We define the total magnetic susceptibility $\chi' - j\chi''$ (i.e., electronic + nuclear) of the specimen by the equation:-

$$(\underline{M} + \underline{m})_t = (\chi' - j\chi'')\underline{H}_t \qquad \text{equation 2.}$$

Equations 1a and 1b may be solved for $(\underline{M} + \underline{m})_t$ in terms of $\underline{H}_t$, leading to the expression:-

$$(\underline{M} + \underline{m})_t(1-\chi_e\chi_n\beta^2) = \underline{H}_t(\chi_e+\chi_n + 2\chi_e\chi_n\beta).$$

Writing $\chi_e = \chi'_e - j\chi''_e$ and $\chi_n = \chi'_n - j\chi''$,

rejecting all but the leading terms and identifying X' and X'' in equation 2 gives:-

$$X' = \frac{1}{D}\left\{X'_e + \beta^2\left[X'_n(X'^2_e - X''^2_e) - 2X'_e X''_e X''_n\right]\right\}$$

$$X'' = \frac{1}{D}\left\{X''_e + \beta^2\left[X''_n(X'^2_e - X''^2_e + 2X'_e X''_e X'_n\right]\right\}$$

where D is given by:-

$$D = \left[1 + (X'_e X'_n - X''_e X''_n)\beta^2\right]^2 + (X'_e X''_n + X''_e X'_n)^2\beta^4.$$

Assuming that $D = 1$, and that terms in X'_n and X''_n are much smaller than those in X'_e and X''_e in absence of n.m.r., (this will be true at all but very low temperatures), the changes $\delta X'$ and $\delta X''$ in X' and X'' due to n.m.r. are given by:

$$\delta X' = \beta^2(X'_n(X'^2_e - X''^2_e) - 2X'_e X''_e X''_n) \qquad \text{equation 3a.}$$

$$\delta X'' = \beta^2(X''_n(X'^2_e - X''^2_e) + 2X'_e X''_e X'_n). \qquad \text{equation 3b.}$$

In Appendix A we show that the fractional change $\delta Q/Q$ in the quality factor Q of a microwave cavity due to changes $\delta X'$ and $\delta X''$ in the total magnetic susceptibility $X' - jX''$ of a metallic specimen is given by:-

$$\delta Q/Q = \frac{\alpha}{2|\mu|}\left\{\frac{\mu'}{|\mu| + \mu''}\delta X' + \delta X''\right\} \qquad \text{equation 4.}$$

where α is a factor depending on the design and construction of the cavity, and $\mu' - j\mu'' = 1 + X' - jX''$ is the magnetic permeability of the specimen. The fractional change $\delta Q/Q$ in Q due to n.m.r. is then obtained by substituting the expressions for $\delta X'$ and $\delta X''$ from equations 3 into equation 4.

The resulting expression gives the total change in Q, and assumes that the whole n.m.r. spectrum is observed simultaneously. However, in the heavy rare earth metals many of the isotopes of interest for n.m.r. purposes have a large nuclear quadrupole interaction, and it is probable that this will be resolved in the n.m.r. spectrum. The observed change in Q due to the single transition $I_z=m$ to $I_z=m-1$ will be smaller than the total change by + the normalized transition probability F, given by:-

$$F = \frac{|(m|I_+|m-1)|^2}{\sum_m |(m|I_+|m-1)|^2} \qquad \text{where } I_+$$

is the operator $I_x + jI_y$.

The present search for n.m.r. was made with a spectrometer depending on partial saturation of the resonance (4). Under these conditions, X_n'' may be neglected by comparison with X_n'. If the partially saturated resonance is then observed using a frequency modulation of depth $(\delta\nu)_{mod}$ much less than the n.m.r. linewidth , the fractional change in Q over a modulation cycle and due to a single line of the n.m.r. spectrum is:-

$$(\delta Q/Q)_{mod} = \frac{\alpha\beta^2 F}{2|\mu|}\left\{\frac{\mu'}{|\mu|+\mu''}(X_e'^2 - X_e''^2) + 2X_e'X_e''\right\}\frac{dX_n'}{d\nu}(\delta\nu)_{mod}$$

If an approximately Lorentzian dispersion signal is assumed the peak value of $\frac{dX_n'}{d\nu}$ is approximately

$\frac{1}{2}(X_{no})\ \frac{\nu_o}{2\pi(\delta\nu_o)^2}$, where $\delta\nu_o$ is the n.m.r. linewidth, X_{no} is the static nuclear susceptibility and ν_o the n.m.r. frequency. The complete expression for $(\delta Q/Q)_{mod}$ is then:-

$$(\delta Q/Q)_{mod} = \frac{\alpha\beta^2 F}{3\pi|\mu|}\left\{\frac{1}{|\mu|+\mu''}(X_e'^2 - X_e''^2) + 2X_e'X_e''\right\}(X_{no})\frac{\nu_o(\delta\nu)_{mod}}{(\delta\nu_o)^2}$$

The parameters F,β and X_{no} may be determined from well known properties of the heavy rare earth metals, and are given in Table 2.1. Due to probable broadening of n.m.r. through quadrupole effects (see section (iv)b of this chapter) we expect the I_z=1/2 to -1/2 n.m.r. transition to be most easily observed, and the values of F in the table refer to this transition. The n.m.r. linewidth $\delta\nu_o$ is difficult to estimate, and is discussed in 2. (iv). Experimental measurements of $|\mu|+\mu''$ are presented and discussed in chapter four, and are used there to estimate the order of magnitude of X_e' and X_e''. The cavity parameter α is of order unity, and specific values are calculated in Appendix A.

In Table 2.1 the factor $X_{no}\beta^2 F$ at 1^oK is calculated for the heavy rare earth metals. The quoted static nuclear susceptibility allows for the isotopic abundance of the relevant nucleus. Eu and Gd, and Fe, Co and Ni are also included for comparison. In the final column an attempt is made to estimate the magnitude of n.m.r. absorption

Table 2.1

Isotope	I	F	$\lvert g_n \rvert$	$X_{no}T$ x10^{10}	$\beta = \frac{H_e}{M_s}$	$X_{no}\beta^2\gamma$	Absorption rel. to Tm
Eu 151	5/2	9/35	1.38	1300	20	1.3×10^{-5}	(2.8)
153	5/2	9/35	.614	270	20	$.27\times10^{-5}$	(.60)
Gd 155	3/2	2/5	.161	3.5	13	2.4×10^{-8}	(.0052)
157	3/2	2/5	.215	5.5	13	4.4×10^{-8}	(.096)
Tb 159	3/2	2/5	1.27	1500	100	6.0×10^{-4}	2.6
Dy 161	5/2	9/35	.18	15	150	8.5×10^{-6}	.037
163	5/2	9/35	.25	28	160	18×10^{-7}	.078
Ho 165	7/2	4/21	1.15	5200	200	4.0×10^{-3}	17
Er 167	7/2	4/21	.16	23	220	2.3×10^{-5}	.10
Tm 169	1/2	1	.462	40	240	2.3×10^{-4}	1.0
Fe 57	1/2	1	.181	.35	15	$.79\times10^{-8}$	(.0017)
Co 59	7/2	(1)	1.31	19000	12	2.7×10^{-4}	(60)
Ni 61	3/2	(1)	.47	.4	12	9.2×10^{-8}	(.020)

Notes: g_n, the nuclear g factor, has been calculated on the basis of the table of nuclear moments in reference (20). The values of M_s used in calculation of β are calculated using a free ion model. Both H_e and M_s are temperature dependent; on the free ion model, however their ratio is constant. The ratio has been calculated from data appropriate to $0^{\circ}K$.

relative to thulium, which has a single 100°/o abundant nucleus and I = 1/2. The figures without brackets are simply $X_{no}\beta^2 F$ calculated relative to thulium. The figures in parenthesis are this quantity multiplied by an additional factor of 50, which is estimated by Portis and Lindquist (1) to be the overall increase in the fractional power absorbed due to n.m.r. when the observed X_e is due to domain wall motion rather then to non-domain wall processes. The final column then gives the relative magnitudes of n.m.r. absorption, assuming equal fractional linewidths, and equal values of $\frac{\delta\nu_{mod}}{\delta\nu_o}$ and X_e. It should be noted that X_e in the low frequency domain wall enhanced cases, could easily be one or two orders of magnitude greater than in the high frequency non-domain wall case. The relative size of n.m.r. signal will then be increased by an amount proportional to this, provided that total saturation is absent.

From the point of view of relative absorption, holmium and terbium appear as the most favourable heavy rare earth metals for attempts to observe n.m.r. For holmium, even in absence of domain wall enhancement, the calculated relative absorption is, assuming the same X_e, of the same order as the exceedingly intense absorption observed in cobalt (5). However, in spite of this encouraging feature, the discussion of the following

section suggests that both relaxation and inhomogeneous broadening may make n.m.r. difficult to observe in the heavy rare earth metals.

2. (iv) Relaxation, Saturation and Linewidths.

When the microwave field exciting n.m.r. in a solid is sufficiently large, the absorption signal saturates and decreases in size, while the dispersion signal maintains approximately constant size, and the line-width decreases (4). Under these conditions of partial saturation, and provided there is a short enough spin-spin relaxation time, an effective spin temperature may be defined in a frame of reference rotating with the nett magnetic moment of the spin system. Using this model, Redfield (4) has shown that the partially saturated dispersion signal depends on ω_m, the frequency of the field or frequency modulation used to observe the resonance. If the depth of modulation is much less than the n.m.r. linewidth, the derivative signals are given by:-

$$\frac{\partial X_1'}{\partial \nu} = \frac{1}{(1 + \omega_m^2 T_{1\rho}^2)} \frac{\partial X'}{\partial \nu}$$

and

$$\frac{\partial X_2'}{\partial \nu} = T_{1\rho} \frac{\partial X_1'}{\partial \nu} .$$

In these expressions, $\frac{\partial X_1'}{\partial \nu}$ is the signal observed

in phase with the applied frequency modulation, and $\frac{\partial X'_2}{\partial \nu}$ is that observed in quadrature with it. $\frac{\partial X'}{\partial \nu}$ is the signal observed in the limit of low modulation frequency. ν is the microwave frequency and $T_{1\rho}$ is the longitudinal relaxation time in the rotating reference frame, and is assumed to be the same as the longitudinal relaxation time measured in the laboratory frame. In the 3^d transition metal ferromagnets, the large enhancement of radio-frequency field due to motion of the domain walls makes such partial saturation conditions easily obtainable. Gossard et al (6) observed n.m.r. in Fe^{57} using a spectrometer exploiting this fact. Two modulation frequencies are applied, one much higher than $1/T_1$, and the other below $1/T_1$. The signals at the two frequencies are balanced against each other and the difference between them observed. In this way spurious instrumental resonances are eliminated and the n.m.r. is observed largely at the low frequency. A modification of this method has been used in the present search for n.m.r. in terbium and holmium (chapter 6), and so it is of considerable importance to examine possible nuclear relaxation mechanisms for these metals to estimate how effective this detection technique is likely to be.

The complete absence of n.m.r. data on the non S-state heavy rare earth metals necessitates extrapolation

of relaxation data from more or less different physical situations, and suggestion of new mechanisms which might apply particulary to this case. In either case, no detailed theoretical discussion is attempted.

a. Spin-spin relaxation.

In a magnetically ordered material with high isotopic concentration, the transverse relaxation is due to a spin-spin coupling mechanism first postulated by Suhl (7) and Nakamura (8). In this interaction, a nuclear spin excites a spin wave through the hyperfine coupling, and another nuclear spin causes it to be re-absorbed through its hyperfine coupling. The original form of this interaction does not involve real spin wave excitations, and leads to coupling between like nuclei only. It predicts spin-spin relaxation times T_2 which have no explicit temperature dependence, and which vary as $(\nu_e)/(\nu_n)^2$, where ν_e is the exchange frequency and ν_n the hyperfine interaction frequency in the fully ordered state. Beeman (9) has shown that a more complicated form of the Suhl-Nakamura interaction involving both real and virtual spin waves takes place between unlike spins also. The inclusion of real spin-waves introduces explicit temperature dependence, and the interaction tends to zero with temperature.

Experimental measurements of T_2 for

Ni^{61} (10), show that the spin-spin relaxation time is proportional to the concentration of the active isotope, and in Ni^{61} and Fe^{57} a small temperature dependence is found. In Table 2.2 we give representatitive values of T_2 in natural cobalt (100% Co^{59}) at various temperatures, taken from Weger's paper (10).

Table 2.2

temperature ^{o}K	1.35	4.2	77	295
T_2(milliecs)	.088	.088	.057	.025

In Table 2.3 we compare the values of $(\nu_e)/(\nu_n)^2$ for Fe^{57}, Co^{59} and Ni^{61} with those calculated for the heavy rare earth metals. The spin-spin relaxation times are taken from (10) and are room temperature values extrapolated to 100% active nuclei. T_o is the temperature at which magnetic ordering sets in. The values of ν_e are calculated on the crude assumption that $h\nu_e = kT_o$. The values of ν_n are taken from (1) and Table 1.2. The detailed Suhl-Nakamura expressions for T_2 contain a complicated factor multiplying $(\nu_e)/(\nu_n)^2$, and when evaluated for particular cases it is typically of order 1 to 100. It will be seen from Table 2.3 that the values of $(\nu_e)/(\nu_n)^2$ in the iron group differ from the measured values of T_2 by factors of this order.

Table 2.3

Isotope	$T_o(^oK)$	ν_n(kc/s)	T_2(msec)	$(\nu_e)/(\nu_n)^2$ (msec)
Fe 57	1043	47	1[illegible]	10
Co 59	1394	217	.025	.5
Ni 61	351	28	.27	20
Gd 155	269	30		6
157		47		3
Tb 159	229	3130		$5x10^{-4}$
Dy 161	179	820		$8x10^{-3}$
163		1140		$3x10^{-3}$
Ho 165	132	6500		$6x10^{-5}$
Er 167	80	940		$2x10^{-3}$
Tm 169	50	7360		$2x10^{-4}$

The complex spin structures and long range periodic exchange in the heavy rare earth metals would probably make it very difficult to calculate reliable values of the spin-spin interaction, and the estimates of $(\nu_e)/(\nu_n)^2$ given in the final column of Table 2.3 therefore should not be taken as too literal a guide to T_2. The general tendancy observed in other ferromagnets for T_2 to be shorter than $(\nu_e)/(\nu_n)^2$ suggests that T_2 in the heavy rare earth metals also could be shorter than indicated by these figures. However that may be, we may certainly expect the combination of weak exchange and large hyperfine interactions to favour a very strong coupling of the nuclear spins, and give correspondingly short values of T_2. This effect will be most apparent in holmium, terbium and thulium, and it is quite possible that lifetime broadening, which is of order $1/T_2$, will be embarrassingly large in these metals. We take up this point again in the final summing up of the chapter.

(b). <u>Quadrupole broadening.</u>

A significant contribution to the n.m.r. linewidth in the heavy rare earth metals is likely to arise through interaction of the nuclear quadrupole moment with the crystal field. Although the $I_z=1/2$ to $-1/2$ transition is not effected in first order by this, second order effects

become important if the spread in electric field gradients at the nuclear sites is large enough (11). In gadolinium, where the nuclei in the domain walls are at a wide variety of angles to the crystal field, this is particularly serious. The electric field gradients in the rare earth metals are enhanced by an antishielding factor of order 20 (12) and, taking this in to account, Edmonds estimates that the n.m.r. linewidth of order 9Mc/s observed in gadolinium (13) may be entirely accounted for by a second order quadrupole interaction.

In the non S-state heavy rare earth metals, the probable absence of domain wall motion means that n.m.r. will be expected in the domains. The electronic magnetic moments, and hence the nuclei, will then be aligned parallel to an easy direction of magnetization and a wide spread of angles relative to the crystal field will be avoided. In terbium, and dysprosium, and holmium above about 20°K, the high axial anisotropy causes the principal axis of the 4f electron shell quadrupole moment to lie in the hexagonal plane, and this in turn confines the nuclear magnetic moments to the plane. So long as the hexagonal symmetry persists, there will be no field gradients to interact with the nucleus, and one might even hope that first order quadrupole broadening of the n.m.r. transitions $I_z = m$ to $m-1$ for $m \neq 1/2$, would no longer be excessively

large. However, orthorhombic distortion of the lattice sets in with ferromagnetic ordering in both terbium and dysprosium, and will cause broadening of the transitions m≠1/2 in the ferromagnetic phases of these metals.

An additional source of electric field gradients at nuclear sites is provided by lattice strains and impurities in the specimens. Their effect is nearly impossible to estimate, and could well be significant. Microwaves penetrate only a few microns into the surface of a metal, and so any observation of n.m.r. will be confined to nuclei in a surface layer of this thickness. The method of specimen preparation described in chapter three is intended to minimize surface strains, but it is quite possible that sufficient remain to produce measurable broadening of the n.m.r.

(c). Spin-Lattice Relaxation Time, T_1 and the onset of saturation.

In iron, cobalt and nickel, T_1 has been measured and interpreted by Weger (14), and re-interpreted by Moriya (15). Experimentally, the relaxation of nuclei in the domain walls is faster than in the domains, and in the latter case T_1 is inversely proportional to temperature. Moriya's interpretation considers a relaxation mechanism due to fluctuations of the orbital current of the d-band electrons, and applies only to relaxation in the

ferromagnetic domains. It gives an adequate account of Weger's experimental values, which are given in Table 2.4

Table 2.4

Isotope	T_1
Ni^{61}	115/T millisecs.
Fe^{57}	2.5/T secs.
Co^{59}	80/T millisecs.

In the heavy rare earth metals the 4f orbital angular momentum is not quenched, and the spin and orbital angular momenta are strongly coupled. Moriya's division of relaxation by magnetic shell electrons into orbital and spin contributions will therefore no longer apply. However, in the rare earth metals, the high magnetic anisotropy shows that the total angular momentum $\underline{J}$ is strongly coupled to the lattice (16), and a modification of Moriya's orbital fluctuation theory will certainly apply. Lattice vibrations will produce transverse fluctuations in $\underline{J}$, and hence in the hyperfine field, which is largely orbital in origin. The strong coupling at each of the two stages of the process, spin to orbit, and orbit to lattice, could provide a strong relaxation of n.m.r.

With the exception of thulium, where $I = 1/2$, the nuclear quadrupole moments of the heavy rare earth

metals are also strongly coupled to the 4f electrons, and hence to the lattice. Although quadrupole relaxation is negligable in the 3d transition metals (15), the quadrupole interaction in the heavy rare earths is sometimes orders of magnitude larger, and in terbium is about 15°/o of the total hyperfine interaction. It is quite possible that this will significantly add to the coupling of the nuclei to the phonons.

Weger's interpretation of spin-lattice relaxation in the 3d transition metal ferromagnets is in terms of a spin-wave mechanism, augmented by the exchange interaction between the 4s conduction electrons and the 3d electrons. In the case of the rare earth metals, the coupling between magnetic ions is, in fact, due to conduction electrons and so spin waves will be coupled to the lattice even more directly than in the 3d ferromagnets. Furthermore, the magnetoelastic constants in the heavy rare earth metals are relatively large (17), and this will provide further direct coupling of spin-waves to the lattice, also making possible the mixed phonon-magnon excitations which dominate relaxation in some antiferromagnets (18). No attempt is made here to estimate the relative potency of orbital, spin-wave and quadrupolar relaxation in the heavy rare earth metals, but it seems safe to say that each mechanism will be at least as effective as its analogue in the 3d ferromagnet case, and possible considerably more so. We

may therefore expect spin-lattice relaxation to be at least as fast as in the domains in iron, cobalt and nickel, and it will probably be considerably faster.

As we stated at the beginning of section 2. (iv), the spectometer used to search for n.m.r. in terbium and holmium (chapter 6) depends for its operation on partial saturation of the resonance. Saturation sets in when $\gamma^2 H_1'^2 T_1 T_2 \gtrsim 1$, where γ is the gyromagnetic ratio for the nucleus under consideration, and H_1' is the microwave field at the nuclear sites. With the microwave power available, about 1 oersted of microwave field is obtainable at the surface of the specimen.

For the purpose of making a rough estimate of whether we can hope to obtain the necessary partial saturation conditions in terbium and holmium, we assume that X_e is real and is simply $\mu_R - 1$, where the values of μ_R (defined by $\mu_R = |\mu| + \mu''$) are those obtained experimentally and are given in chapter four. In holmium, the maximum X_e we can hope for is $\doteq 3$, occuring at 20°K, and, using the data of Table 2.1, this leads to a microwave field at the nuclei $H_1' = X_e \beta$ of $3 \times 200 = 600$ oersted. Using the data of Table 2.3 to estimate T_2 to be $\doteq 5 \times 10^{-8}$ sec., this leads to the requirement that $T_1 \gtrsim 2 \times 10^{-4}$ sec. In terbium, assuming that $X_e \doteq 0.2$, corresponding to the value of 1.[illegible] for μ_R at 77°K given

in chapter four, H_1' is of order 20 oersted. Taking T_2 to be $\doteq 5\times10^{-7}$ sec., this leads to the requirement that $T_1 \gtrsim 0.3$ sec.

It should be emphasised that there is much uncertainty in these estimates, and it is probable, particularly in the case of holmium, that the quoted estimates of both χ_e and T_2 are over optimistic. However, if these estimated conditions on T_1 are any guide to the conditions encountered in practice, it would probably be very difficult to meet them in the case of terbium, and relatively easy in the case of holmium.

2. (v) Summing up.

In the absence of more complete measurements of χ_e at the n.m.r. frequency throughout the heavy rare earth metals, it is difficult to make a critical assessment of which ones will provide the most favourable conditions for observation of n.m.r. The advantages of the large enhancement (Table 2.1) expected in holmium will probably be off-set by a very strong nuclear spin-spin coupling, and if T_2 is 10^{-3} seconds or less, as it may be, then the n.m.r. linewidth will be 100 kc/sec. or more. Indeed, unless the linewidth is less than about 10 kc/sec., there is little hope that the spectrometer we have used to search for the n.m.r. would be able to detect it.

In terbium, the tendancy shown by our measurements (chapter four) for χ_e to go to small values, of order

0.2 at low temperatures, shows that enhancement will be rather small. However, it is less likely that lifetime broadening will be prohibitively large, and we might expect broadening from this source of as little as 2 Mc/sec. However, even if it is possible to obtain the necessary saturation conditions, spectrometer sensitivity is probably not sufficient to detect a line of this width (see chapter 6). To obtain as long a T_1 as possible, it would be desirable to work at as low a temperature as possible.

Thulium has the weakest exchange of the heavy rare earth metals, and also a rather large hyperfine interaction (2360Mc/sec.), and the effects of a short T_2 are likely to be nearly as severe as in holmium. Furthermore, the 3-4 antiphase layer spin structure at low temperatures leads to 7 inequivalent lattice sites, and this would probably off-set the advantage of the absence of a nulcear quadrupole moment in concentrating the total spectrum in a single transition.

Dysprosium has a relatively unfavourable value of $X_{no}/\beta\ ^2F$ (Table 2.1), but the classical ferromagnetism observed below 86°K, combined with the small hyperfine interaction and correspondingly low n.m.r. frequency make it possible that a useful amount of domain wall enhancement may operate. However, as we have already observed, even if the spins are confined to the hexagonal

plane, quadrupolar broadening is likely to arise through the orthorhombic distortion of the lattice in the ferromagnetic phase. The exchange interaction in dysprosium is relatively large, and we might hope for a spin-spin relaxation time T_2 of a microsecond or so. This would greatly facilitate attempts to observe n.m.r. using either a spin-echo technique (19), or a double modulation technique depending on partial saturation, as in the present work.

Erbium, like dysprosium, has the advantage of a relatively small hyperfine interaction, and again we might expect domain wall enhancement of the n.m.r. However, the spin orderings in erbium are very complex, and the nuclear quadrupole moment of the nuclear isotope is about twice as large as in dysprosium (20). The conical ordering will cause nuclei in domain walls to have a wider spread of angles relative to the crystal field than in the case of dysprosium, and we may expect considerably greater quadrupole broadening. As in dysprosium, we might expect a spin-spin relaxation time of as long as a microsecond.

In conclusion, the combination of high n.m.r. frequencies, complex spin orderings, quadrupole effects and strong nuclear spin-spin coupling would probably make it difficult to detect n.m.r. in any of the heavy rare earth metals. It must be admitted that the present research was initiated assuming the validity of published n.m.r.

data for terbium (21) and it was not realized by us until sometime after that this was a spurious instrumental effect (22). However, n.m.r. has proved such a fruitful means of investigating ordered magnetic materials that it seems well worth attempting to extend such investigations to the heavy rare earth metals, even though the probability of success with available techniques may be rather small.

Chapter 2: References

1. A.M. Portis and R.H. Lindquist: Chapter 6 in "Magnetism" II A, G.T. Rado and H.Suhl editors.

2. M.H. Johnson and G.T. Rado: Phys.Rev. 75, 841 1949.

3. C. Kittell and J.K. Galt: Solid State Physics 3, 1956 F. Seitz and D.Turnbull editors.

4. A.G. Redfield: Phys. Rev. 98, 1787 1955.

5. A.C. Gossard and A.M. Portis: Phy.Rev. Letters, 3, 164 1959.

6. A.C. Gossard, A.M. Portis and W.J. Sandle: Phys. and Chem. of Solids, 17, 341 1960.

7. H. Suhl: Phys.Rev. 109, 606 1958.

8. T. Nakamura: Proy. Theoret. Phys. (Kyoto) 20, 542 1958.

9. D. Beeman, P. Pincus and F. Hartmann-Boutron: Phys. Rev. 139, A1880 1965.

10. M. Weger, E.L. Hahn and A.M. Portis: J. Appl. Phys. 32, 1245 1961.

11. A. Abragam: "Principles of Nuclear Magnetism" Page 234 (O.U.P. 1961).

12. D.T.R. Edmonds: verbal communication.

13. R.E. Gegenwarth and J.I. Budnick: Bull.Am. Phys. Soc., (11) 10, 591 1965.

14. M.Weger: Phys. Rev., 128, 1505 1962.

15. T. Moriya: Jour. Phys. Soc. Japan, 19, 681 1964.

16. R.J. Elliott: Chapter 7 in "Magnetism" II A, G.T. Rado and H.Suhl editors.

17. K.P. Belov, R.Z. Levitin and S.A. Nikitin: Sov.Phys. Uspekhi 7, 179 1964.

18. P. Pincus and J.M. Winter: Phys. Rev. Letters 7, 269 1961.

19. E.L. Hahn: Phys. Rev., 80, 580 1950.

20. I. Lindgren in "Perturbed Angular Correlations", E. Karlssohn, E. Matthias and K.Siegbahn editors. (North Holland 1964).

21. J. Herve and P.Veillet: Compt. Rend. Acad. Sci. (France) 252, 99 1961.

22. J. Herve: private communication.

Chapter 3.

Specimens and Cryogenic Apparatus

3. (i) Preparation of the rare earth metal specimens

In most of the experiments described in this thesis the specimens used are rare earth metal single crystal and polycrystal rods of about 6 cms. length and 5mm. diameter. The basic material was supplied by the Johnson-Matthey Company and was grown into single crystals and machined into uniform diameter rods by Metals Research Ltd. of Cambridge. The single crystals were grown using the "floating" molten zone technique and they were machined into uniform diameter rods on a spark lathe. Unfortunately the crystal growing process was not sufficiently advanced to produce large single crystal rods of any desired crystal orientation relative to the axis of the rod. The dimensions and crystal axis orientation of the specimens used are given in Table 3.1.

Table 3.1

Specimen	Length	Diameter	Angle between rod axis and crystal c-axis
terbium	6.0cm.	4.90±.03mm.	polycrystal
terbium	6.0cm.	4.20±.03mm.	76°
dysprosium	7.2cm.	4.89±.01mm.	84°
Holmium	4.7cm.	4.76±.03mm.	55°

As most of the experiments performed on these

specimens involve the absorption of microwaves at frequencies of 3,000Mc/sec. and above, it is important that the surface layer of the rods be as free as possible from strains and impurities. The microwave penetration depth at 3,000Mc/sec. (10cm. wavelength) is typically of order 10^{-3}cm. to 10^{-4}cm. The process used to obtain a suitable surface consists of annealing followed by etching. In the annealing process the specimen is wrapped in tantalum foil and annealed for three hours at 900°C in high vacuum. The subsequent cooling to room temperature takes place over a four hour period.

The efficiency of this process in reducing the number of crystal lattice defects is indicated by the change it produced in the residual resistivities of the dysprosium and holmium crystals (table 3.1).

Table 3.1

temperature	resistivity (ohm-mx10^8)		
	Ho	Dy	Tb(crystal)
14°K	11.00b	7.40b	———
	7.35a	6.17a	6.81a
11°K	5.70a	5.80a	6.65a

b = before annealing

a = after annealing

Electrical resistivity data for Ho, Dy and Tb published by the Ames group (1,2 and 3) indicates that the values of ρ at 11°K differ little from the true residual resistivity.

The tendancy of the present results to converge on a value for $\rho_{res.} \doteq 6 \times 10^{-8}$ ohm-m suggests that this value corresponds to impurity scattering, and is some 50 to 100% larger than in the Ames group crystals.

In spite of precautions taken during annealing, the surfaces of the rods are usually oxidized by the process. In all cases therefore, after annealing the specimens are polished with a diamond preparation until a shining metallic surface is obtained. They are then etched in a 40%/o concentrated nitric acid and 60%/o glacial acetic acid etch. In the case of the single crystals the etching process is continued until it is possible to see the single crystal character of the specimen. This is apparent by the intensity of light reflected off various parts of the surface. Two or three minutes in the etch is sufficient to obtain these conditions. In the case of the terbium polycrystal the etch vigorously attacks the boundaries between the crystallites, and the specimen was removed from the etch after 10 seconds.

A powder specimen of terbium was prepared by grinding under paraffin oil. The particles are irregular shapes and have dimensions of order one micron. Attempts were made to anneal this specimen under high vacuum. However, the high chemical activity of rare earth metals at high temperatures, combined with the finely divided nature

of the specimen caused it to oxidize during annealing. The experiments described for terbium powder were made on unannealed material.

3. (ii) Low temperature microwave apparatus

To study the interaction of microwaves with the rare earth metal rods, the rods are mounted as the centre conductor of a coaxial resonant cavity. The cavity systems used are mounted on the end of german silver tubes which carry the microwave power and thermal and electrical controls from the room temperature end of the apparatus to the cavity. A overall view of a typical low temperature microwave apparatus mounted in a metal dewar is shown schematically in figure 3.1.

All the cryogenic experiments are carried out inside a one piece metal dewar of design in common use in the Clarendon Laboratory (figure 3.2). A simple pumping system using an Edwards oil diffusion pump (11c.c model A102) working into an Edwards rotary pump (model ISC 150B) provides the necessary vacuum facilities. In all cases provision is made to evacuate the microwave cavity and fill it with helium gas. The coaxial cavitites and associated cryogenic mountings and controls divide into three distinct systems discussed separately below.

(a) 10cm. wavelength variable frequency cavity (figure 3.3)

The coaxial resonant cavity is one full wavelength

Figure 3.1

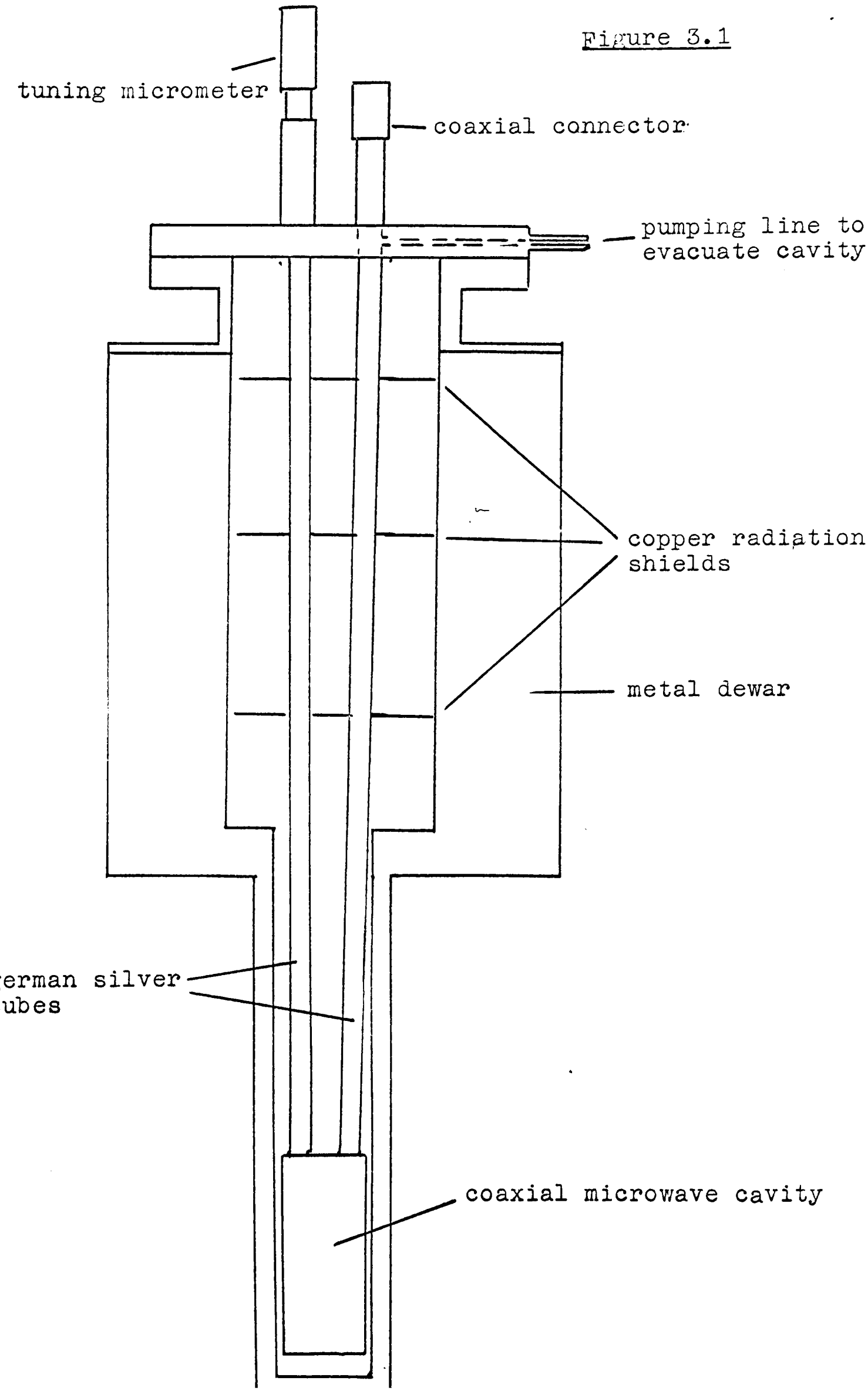
tuning micrometer
coaxial connector
pumping line to evacuate cavity
copper radiation shields
metal dewar
german silver tubes
coaxial microwave cavity

Figure 3.2

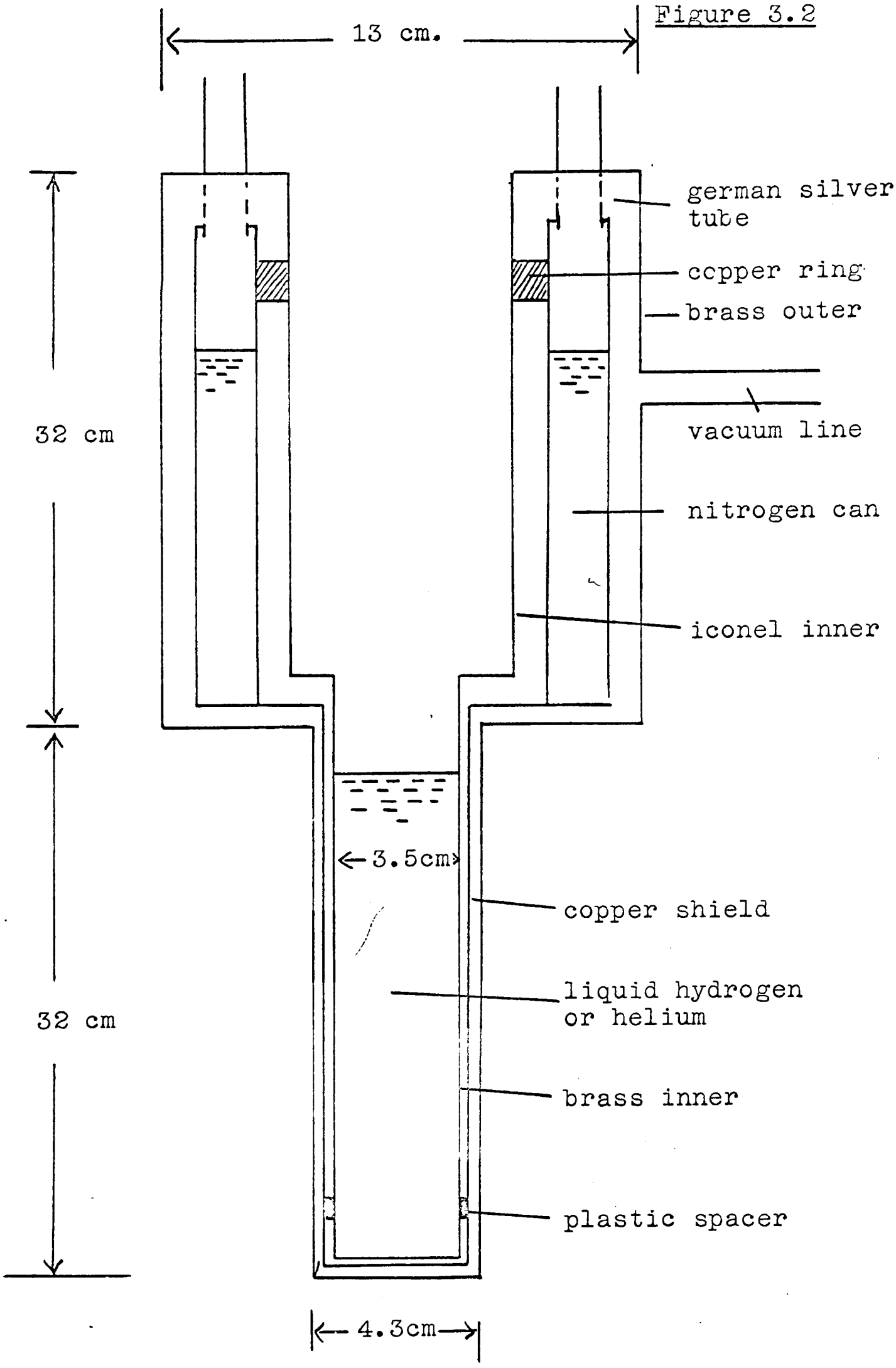

Metal dewar
(not to scale)

Figure 3.3

10 cm. wavelength variable frequency reflection cavity.

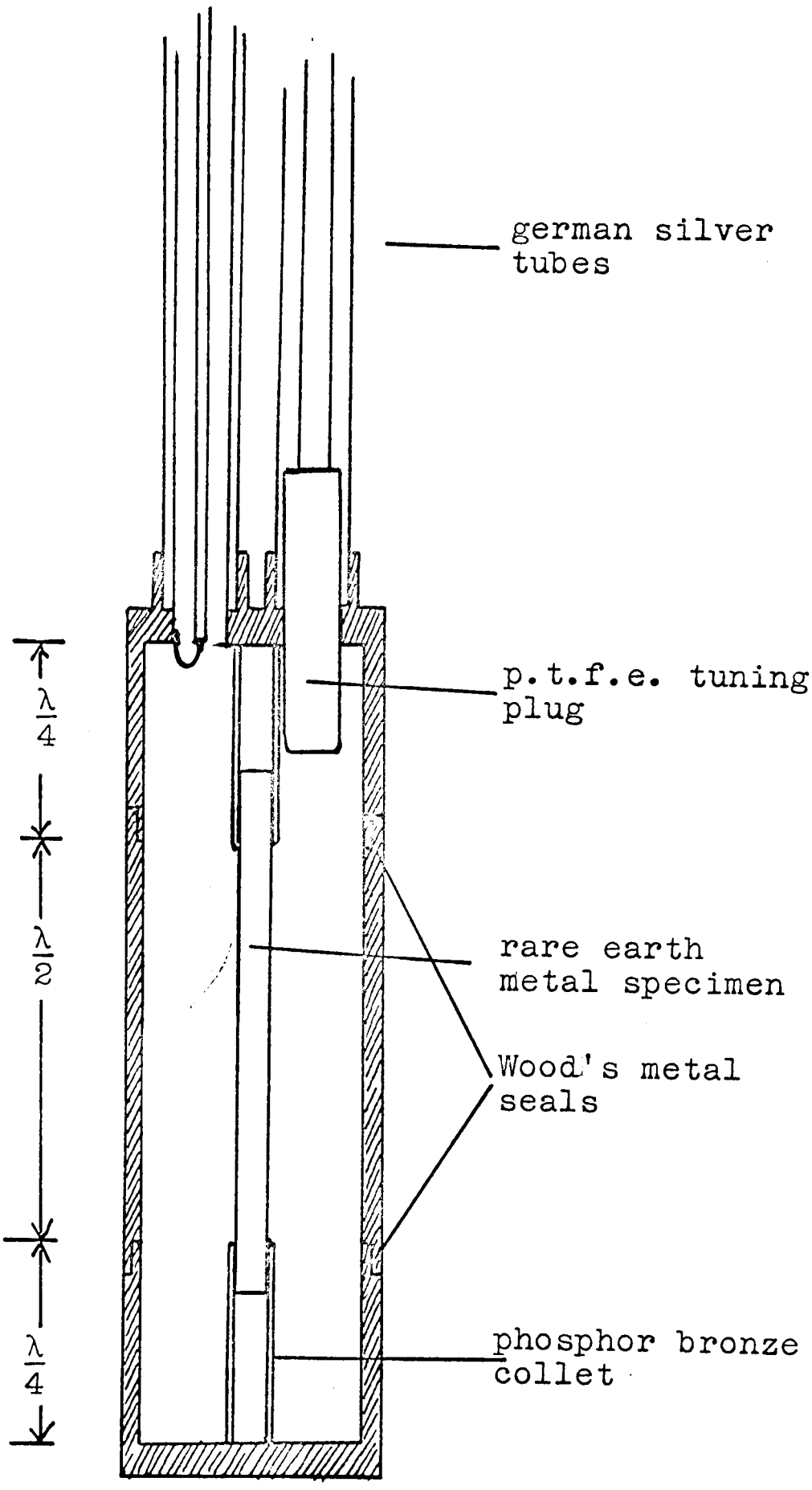

long, with the specimen forming the central half-wavelength section of the central conductor. The specimen is held in phosphor-bronze collets, the joins being approximately at points of zero current. The cavity is tuned using a plug of loaded polytetraflouroethylene (p.t.f.e.) controlled by a micrometer. This plug gives continuous tuning over 80 Mc/sec. The outside of the cavity is constructed in brass in three sections, and has joins at approximately at the points of zero current. These are made vacuum-tight using a low melting point solder (Wood's metal). The frequency range of the cavity may be extended by using a different length for the central section of the outer conductor. Microwave power is coupled into the cavity by a small copper loop on the end of the input coaxial line. By rotating this line any desired coupling may be obtained.

To minimize microwave losses in the metal walls of the cavity and in the collets, these are gold plated. This cavity has been used to investigate the absorption of microwaves in the dysprosium single crystal and the terbium polycrystal and, with slight modification to the collets, in the terbium single crystal.

(b) 4 to 5 cm. wavelength variable frequency cavity (figure 3.4)

This cavity is specially designed to have the holmium crystal as its centre conductor. It is a quarter wavelength resonant system tunable either by moving the centre conductor or by using a p.t.f.e. plug. Metal to metal contact between the centre conductor and the remainder of the cavity is avoided by bringing the specimen into the cavity through a thin p.t.f.e. collar and a microwave choke consisting of a re-entrant half wavelength section of coaxial line weakly coupled to the cavity. At its resonant frequency (6,520 Mc/sec.) this behaves as a nearly perfect reflector. The choke is, of course, less efficient away from its resonant frequency, but this is found not to be a serious effect.

The p.t.f.e. plug provides fine tuning over a range of 35Mc/sec., and by moving the centre conductor, the cavity may be tuned to any frequency in the range 6,000Mc/sec. to 8,000Mc/sec. As with the 10cm. cavity, the tuning mechanisms are controlled by micrometer heads, and power is coupled into the cavity by a copper loop on the end of the input line, which may be rotated. Again, to minimize losses in the brass parts of the cavity, these are gold plated.

Figure 3.4

4 to 5 cm. wavelength
reflection cavity.

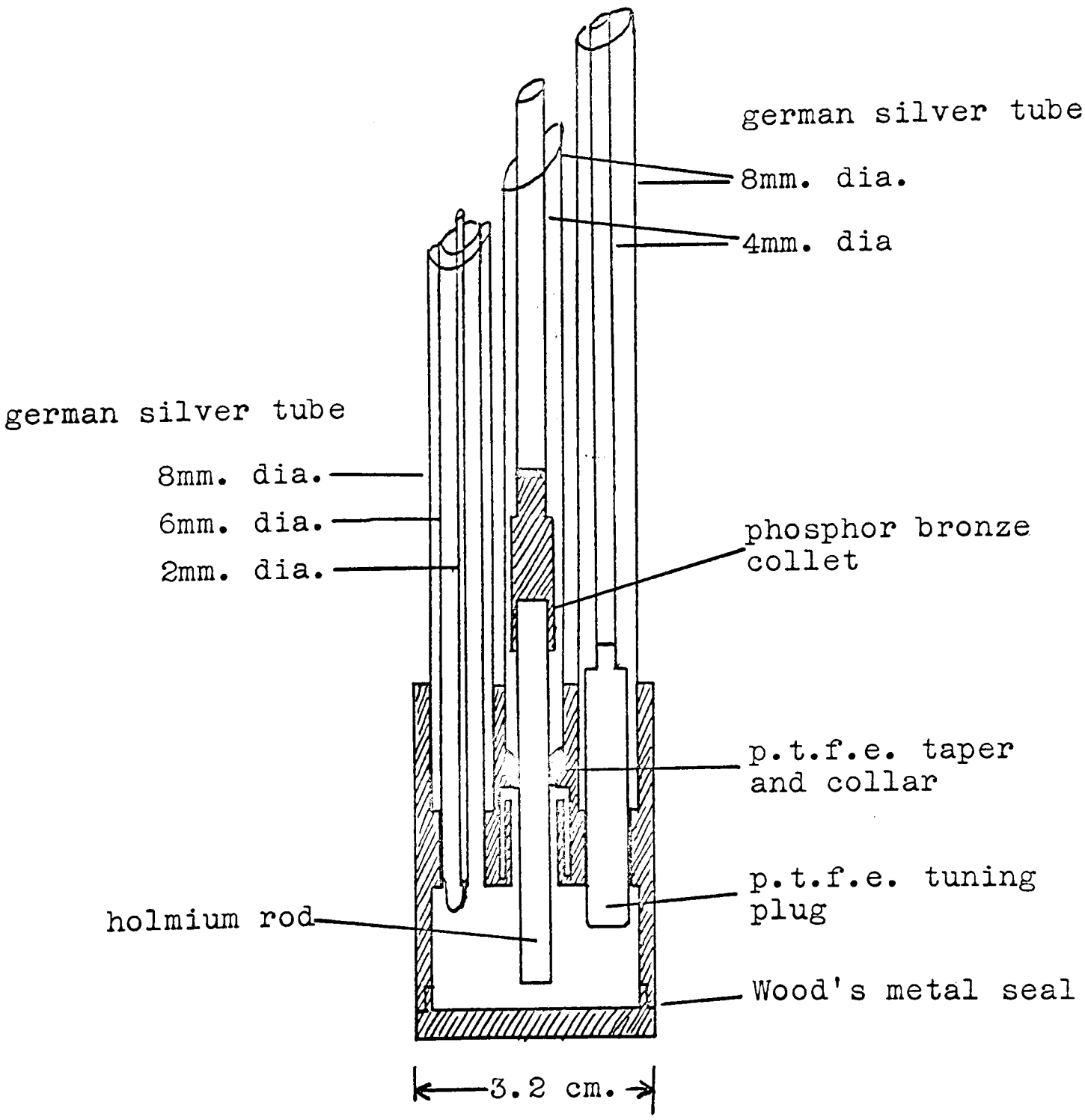

(c) Variable temperature microwave apparatus. (figure 3.5)

This apparatus provides a microwave resonant cavity which may be held at any desired temperature between that of the cryogenic liquid surrounding the vacuum jacket and above room temperature. Heat losses up the german silver coaxial line and to the vacuum jacket are balanced using the 350 ohm constantan heater coil. With the space surrounding the cavity evacuated, less than 1 watt dissipated in the heater coil is entirely adequate to compensate the heat losses and hold the cavity at any desired temperature. The temperature is measured using copper-constantan thermocouples calibrated at three fixed temperatures (in ice, solid CO_2 and liquid nitrogen), to determine a, b and c in an interpolation formula $V= a+bT+cT^2$, where V is the thermocouple voltage. The fixed temperature junction is kept in liquid nitrogen. These thermocouples are useful to 20°K. For temperatures below this, Allen-Bradley 1Kohm carbon resistors are used. Microwave power is capacitatively coupled into the cavity from the coaxial line. For work in the region of 3,000Mc/sec. (λ=10cm.) the quarter wavelength, choke-ended cavity illustrated in figure 3.5 is used. This apparatus has been used to obtain qualitative data on the absorption of microwaves as a function of static magnetic field and temperature in the terbium single crystal and polycrystal specimens. It may also be adapted to wavelengths of order

Figure 3.5

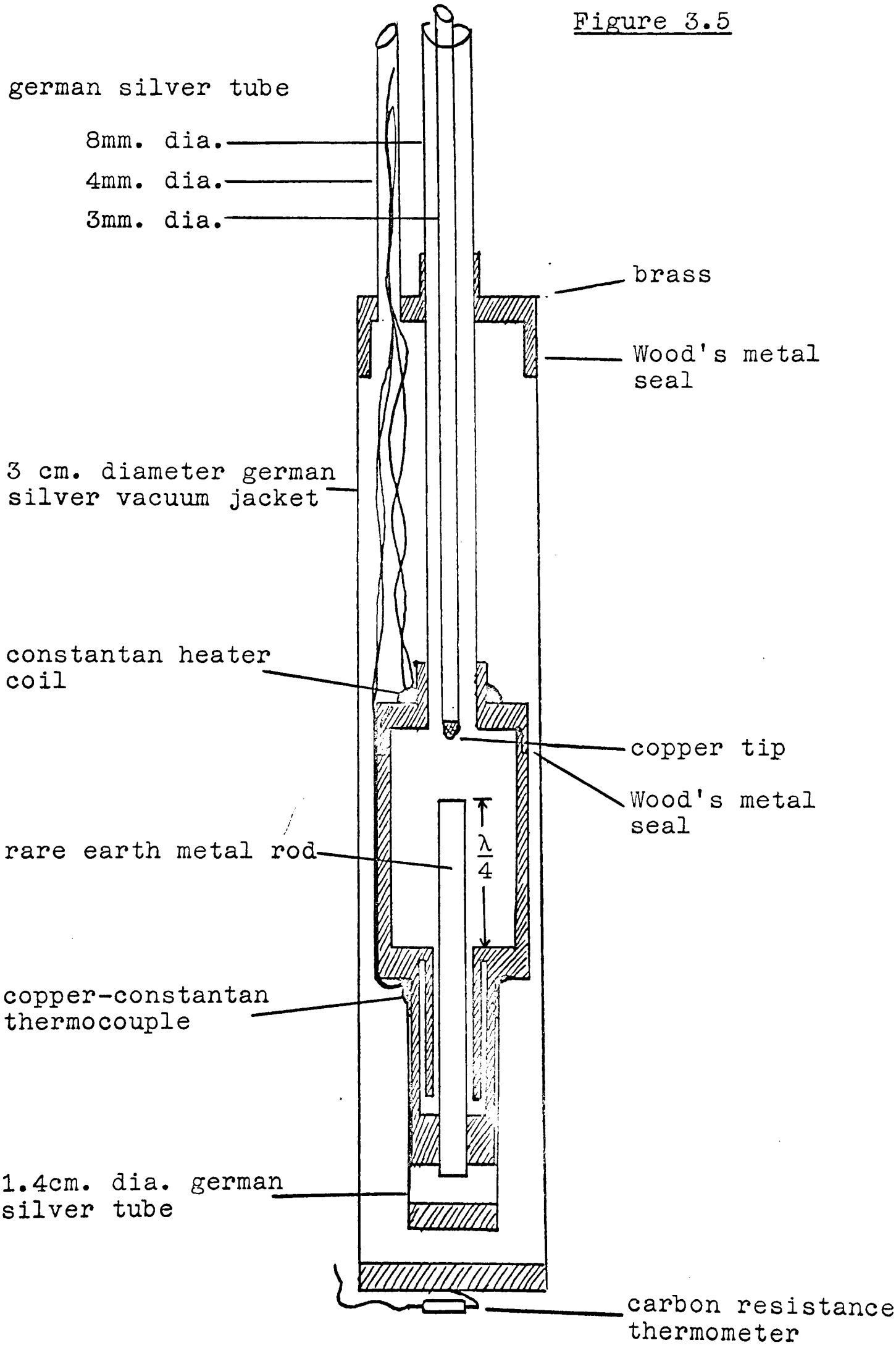
german silver tube
8mm. dia.
4mm. dia.
3mm. dia.
brass
Wood's metal seal
3 cm. diameter german silver vacuum jacket
constantan heater coil
copper tip
Wood's metal seal
rare earth metal rod
λ/4
copper-constantan thermocouple
1.4cm. dia. german silver tube
carbon resistance thermometer

4 to 5cm by using a 3/4 wavelength resonant cavity.

To study the variation of microwave absorption with temperature and static field in terbium powder, the powder is mounted in paraffin oil in a p.t.f.e. bath in the cavity. In this case a copper centre conductor is used. At $77^{\circ}K$, where the effect of a static magnetic field has been studied, the paraffin oil is frozen.

3. (iii) Electrical resistivity apparatus. (figure 3.6a)

The variable temperature microwave apparatus is readily adapted to provide a chamber in which various other experiments are performed. The microwave cavity is replaced by a brass cylinder and the centre conductor of the input coaxial line is removed. This apparatus has been used to measure as a function of temperature the electrical resistivities of the rare earth metal specimens. For these measurements the rare earth metal rod is mounted in the chamber as shown in figure 3.6a. A current is passed through it and the voltage between two knife edge contacts measured. The leads are brought up through the tube which normally forms the outer conductor of the input coaxial line. They then pass through a black wax vacuum seal at the room temperature end of the apparatus. The current is measured by determining the voltage developed across a 0.1 ohm manganin standard resistance. This voltage and the voltage across the specimen are both

Figure 3.6

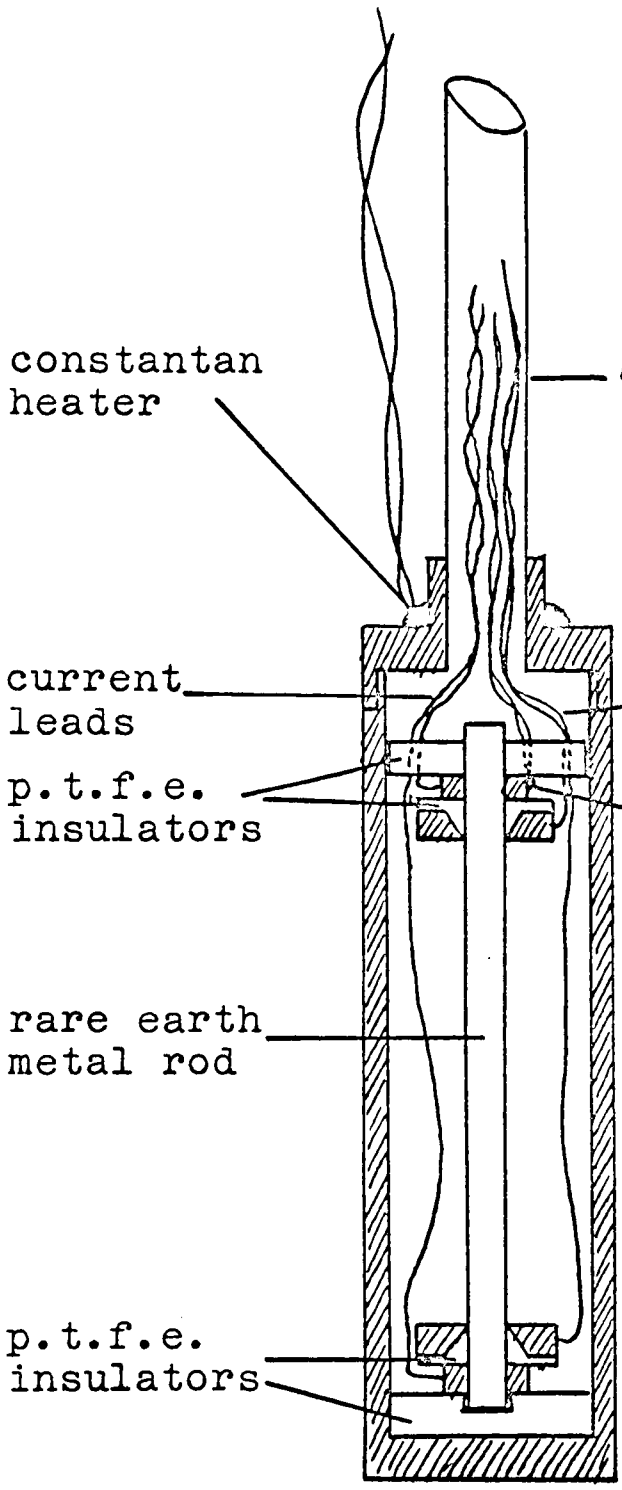

a.

Electrical resistivity apparatus

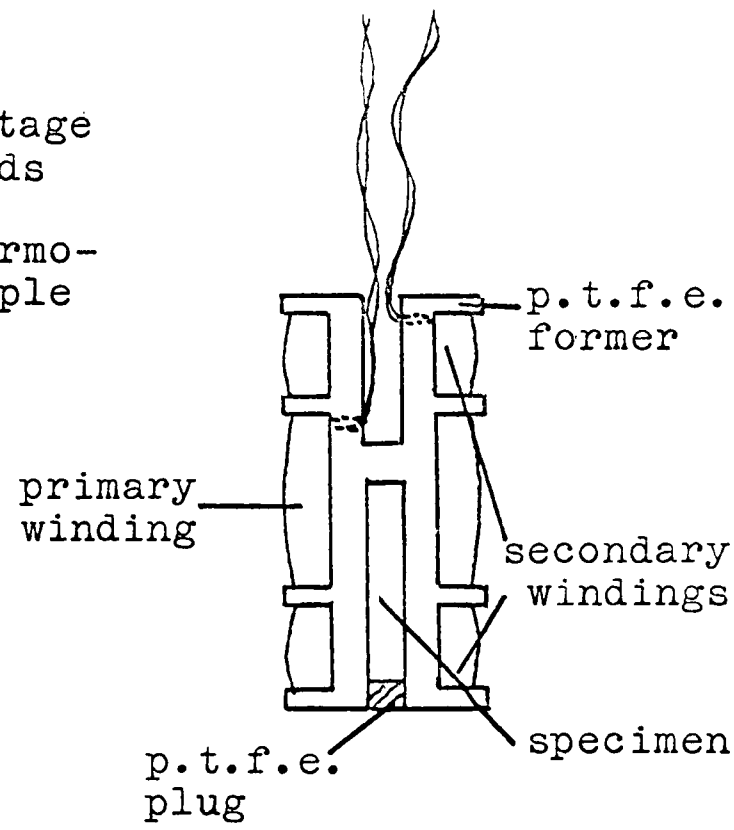

b.

Balanced mutual inductance

measured using a Tinsley potentiometer.

3. (iv) Low frequency magnetic susceptibility apparatus (figure 3.6b)

To measure the qualitative temperature variation of the low frequency magnetic susceptibility of the rare earth metals a small mutual inductance is used. The secondary of the mutual inductance consists of two sections wound in opposition to each other, so that when no specimen is present an alternating voltage across the primary gives no output across the secondary. When a specimen is in position, mounted as in figure 3.6b, a voltage dependent on the specimen magnetic susceptibility is developed across the secondary. The mutual inductance fits inside the experimental chamber used to contain the electrical resistivity apparatus. Application of the mutual inductance is discussed in chapter 5.

Chapter 3: References.

1. D.L. Strandberg, S. Legvold and F.H. Spedding: Phys. Rev. 127, 2046, 1962.

2. P.W. Hall, S.Legvold and F.H. Spedding: Phys. Rev. 117, 1960.

3. D.H. Hegland, S.Legvold and F.H. Spedding: Phys. Rev. 131, 185 1963.

Chapter 4

Microwave Magnetic Permeability of Terbium, Holmium and Dysprosium Metals.

4. (1) Introduction

In chapter two we showed that the magnitude and shape of the n.m.r. signal observed in a metallic ferromagnet depend on the components X'_e and X''_e of the electronic magnetic susceptibility at the n.m.r. frequency. It is therefore of considerable interest to obtain some estimate of these quantities. At microwave frequencies it is difficult, if not impossible, to make direct measurement of the magnetic susceptibility of a metallic ferromagnet. This is because of the small penetration depth, of order a few microns, of the microwaves into the specimen. However, it is possible to measure the surface impedance $Z_s = R_s + jX_s$ of a metal at microwave frequencies, and this has been made the basis of a large number of investigations of the high frequency magnetic permeability of several ferromagnets (1,2). The theory in this section relates the (complex) high frequency permeability of a magnetically ordered metal to the two components of the surface impedance, and shows how these may be determined by measurement of the properties of a microwave cavity containing the metal of interest. We consider particularly the application of the theory to a coaxial cavity in which

the specimen forms part of the centre conductor.

Maxwell's equations, applied to a conducting medium lead to the well known formula (5):-

$Z_s = (1+j)\sqrt{\pi\nu\mu\mu_o\rho}$, where ν is the frequency, μ_o the permeability of free space, and ρ and μ are respectively the electrical resistivity and magnetic permeability of the metal. Allowing for the fact that μ may be complex at high frequencies, we write $\mu = \mu' - j\mu''$ and, provided ρ is real, the real and imaginary parts of Z_s are then given by:-

$$R_s = \sqrt{\pi\nu\mu_o}\ \sqrt{|\mu|+\mu''} = \sqrt{\pi\rho\nu\mu_o\mu_R} \qquad \text{eqn. 1a.}$$

and $$X_s = \sqrt{\pi\rho\nu\mu_o}\ \sqrt{|\mu|-\mu''} = \sqrt{\pi\rho\nu\mu_o\mu_L} \qquad \text{eqn. 1b.}$$

where $|\mu| = \sqrt{\mu'^2+\mu''^2}$ and $\mu_R = |\mu|+\mu''$ and $\mu_L = |\mu|-\mu''$.

To determine μ completely, it is thus necessary to measure both R_s and X_s. The former may be obtained relatively easily by measuring the intrinsic quality factor Q_i of a cavity made partly or wholly of the material of interest. Q_i is defined by the relation:-

$$\frac{1}{Q_i} = \frac{P}{2\pi\nu E}, \qquad \text{eqn. 2.}$$

where P is the power dissipated, E the stored energy and ν is the resonant frequency. If the cavity is evacuated, we have:-

$$P = \frac{1}{2} R_a \int_a H^2 dS + \frac{1}{2} R_r \int_r H^2 dS$$

eqn. 3

where R_a and R_r are respectively the surface resistances of the specimen and of the rest of the cavity, and the integrals are taken over the corresponding areas. We define the intrinsic half power bandwidth $\delta\nu$ of the cavity by the relation $Q_i = \frac{\nu}{\delta\nu}$, and when we refer to the cavity (intrinsic) bandwidth $\delta\nu$, this is the quantity intended. From equations 2 and 3, we then have:-

$$\delta\nu = \frac{\frac{1}{2} R_a \int_a H^2 dS + \frac{1}{2} R_r \int_r H^2 dS}{2\pi \cdot \frac{1}{2}\mu_o \int_v H^2 dV}$$

$$= \frac{1}{2\pi\mu_o V} (A_a R_a + A_r R_r) \qquad \text{eqn. 4.}$$

where A_a, A_r and V are effective areas and volume, and are geometrical constants depending on the cavity and specimen configuration (Appendix B). Using equation 1a, equation 4 may then be written in the form:-

$$\delta\nu = A(T) + B\sqrt{\rho\mu_R} \qquad \text{eqn. 5}$$

where A(T) is temperature dependent, through its proportionality to R_r, and B is effectively independent of temperature. In principle knowledge of R_r and the cavity geometry is sufficient to determine A(T) and B theoretically. In the practical case of the coaxial cavities used in the present work (figures 3.3 and 3.4) approximate values of B may be calculated relatively easily (Appendix B). However, microwave losses occuring other than in the specimen include complicated effects arising where the input coaxial line and the dielectric tuner enter

the cavity, and these and other effects make reliable calculations of A(T) nearly impossible.

Alternatively, experimental measurement of the intrinsic bandwidths corresponding to a series of geometrically identical non-magnetic metallic specimens of known electrical resistivity enables $\delta\nu$ to be measured as a function of $\sqrt{\rho}$, and A(T) and B to be evaluated.

A complication arises if the surface of the specimen has roughness of dimensions comparable to the microwave penetration depth, δ. It is then found that the microwave surface resistance is greater than that which would be obtained from equation 1a. It is possible to apply a correction factor R(δ) for this effect, and the bandwidth formula, equation 5, then becomes:-

$$\delta\nu = A(T) + B\sqrt{R(\delta)\rho\mu_R} \qquad \text{eqn.5a.}$$

Provided the roughness is not too great, R(δ) may be approximated by

$$R(\delta) = 1 + C/\delta, \ (4), \qquad \text{eqn.6.}$$

where C is a constant. C may be determined experimentally by substituting the specimen into a cavity for which A(T) and B are already known. Provided ρ and μ_R are known at the experimental temperature, measurement of $\delta\nu$ enables R(δ) to be evaluated.

The reactive component X_s of the surface impedance,

and hence μ_L may in principle be determined by measuring the shift in the resonant frequency of a cavity containing the ordered magnetic specimen with respect to that of a geometrically identical cavity containing a specimen of known X_s. This shift is small and difficult to measure, and the substitution of one specimen for another must be made to a geometrical accuracy unobtainable with the available apparatus. Johnson and Rado (2) overcame this problem by pulsing a large current through the specimen, which was an iron rod forming the centre conductor of a coaxial cavity of resonant frequency 975Mc/sec. In this way they were able to saturate the magnetization of the iron and obtain a surface impedance due to electrical resistivity only.

In the present work, an attempt was made to overcome the substitution problem by using the 10cm. wavelength cavity (figure 3.8) and measuring the shift in cavity resonant frequency with a rare earth metal centre conductor between room temperature, where the surface impedance is almost entirely due to electrical losses, and lower temperatures, where magnetic ordering has set in. This shift is compared with the shift over the same temperature range when the centre conductor is a non-magnetic metal of known electrical resistivity. These attempts failed, partly because the expected shift in resonant frequency due

to the magnetism (a few hundred Ke/sec.), is an order of magnitude less than the shift in resonant frequency due to thermal contraction. As a result, we have confined measurement of high frequency permeability in the heavy rare earth metals to determination of μ_R, and the following sections describe the experimental methods used, and the results obtained.

4. (ii) Experimental Methods

(a) General introduction.

In all cases our measurements of μ_R for the heavy rare earth metals have been made using the two coaxial cavities described in 3. (ii)a and 3.(ii)b. The method used is essentially the same in both cases, and consists of calibration of the cavity to determine the parameters A(T) and B in equation 5, which relates the bandwidth $\delta\nu$ to the electrical resistivity and μ_R of the centre conductor. The specimen under investigation is then substituted as centre conductor, and the corresponding experimental values of $\delta\nu$ are obtained at various temperatures. These are combined with the results of electrical resistivity measurements, and μ_R is evaluated.

The cavity is calibrated by measuring at some fixed temperature the bandwidths corresponding to several non-magnetic centre conductors of known electrical resistivity. This gives the parameter B, which is temperature

independent, and also A(T) at that particular temperature. Measurements as a function of temperature of the bandwidth and electrical resistivity corresponding to any one of the non-magnetic centre conductors are then used to evaluate A(T) throughout the temperature range of interest.

The non-magnetic centre conductors used to calibrate the cavities are polished using a diamond preparation, and it is assumed that no roughness correction R(δ) need be applied. The reasonable agreement between the theoretical and experimental values of B (section 4 (iii)b) is taken as justifying this assumption. R(δ) is determined for the rare earth metal rods by measuring the corresponding cavity bandwidth at 273°K. Holmium, terbium and dysprosium all have their highest magnetic ordering transition temperatures considerably below this temperature, and so we assume that microwave losses are then all electrical in character, and μ_R is unity. In this way R(δ) is found to be unity to within experimental error in the case of all three single crystal specimens, and about 1.35 at this temperature for the terbium polycrystal.

The electrical resistivities of both the non-magnetic and rare earth metal centre conductors are measured as a function of temperature by the simple method outlined in 5. (iii).

(b) Cavity bandwidth measurement at constant temperature.

It is assumed that the absorption of microwaves in a cavity in the region of the resonant frequency follows a simple Lorentzian form. It may easily be shown that for such absorption, the difference in frequency $\delta\nu'$ between the points of inflection in the response curve is $\sqrt{3}$ times the frequency difference between the half power points. In general, for arbitrary coupling of the coaxial line to the cavity, the frequency difference $\delta\nu_L$ between the half power points measures the total power loss from the microwave fields in the cavity, including losses to the coaxial line. We say that these latter losses are "external" to distinguish them from losses intrinsic to the cavity, and they contribute an amount $\delta\nu_e$ to $\delta\nu_L$, which then may be written $\delta\nu_L = \delta\nu+\delta\nu_e$. The measured frequency difference between the half power points is known as the "loaded" bandwidth, and the corresponding quality factor $Q_L = \nu/\delta\nu_L$ where ν is the resonant frequency, is the "loaded" quality factor.

The quantity appearing in equation 5 is the intrinsic bandwidth $\delta\nu$, and to determine this, we measure $\delta\nu_L$ when the "external" losses are as small as possible. This measurement is made by setting the cavity up as part of a microwave reflection spectrometer (figure 4.1). The coupling of the coaxial line to the cavity is adjusted so that the power reflection coefficient is nearly unity.

Figure 4.1

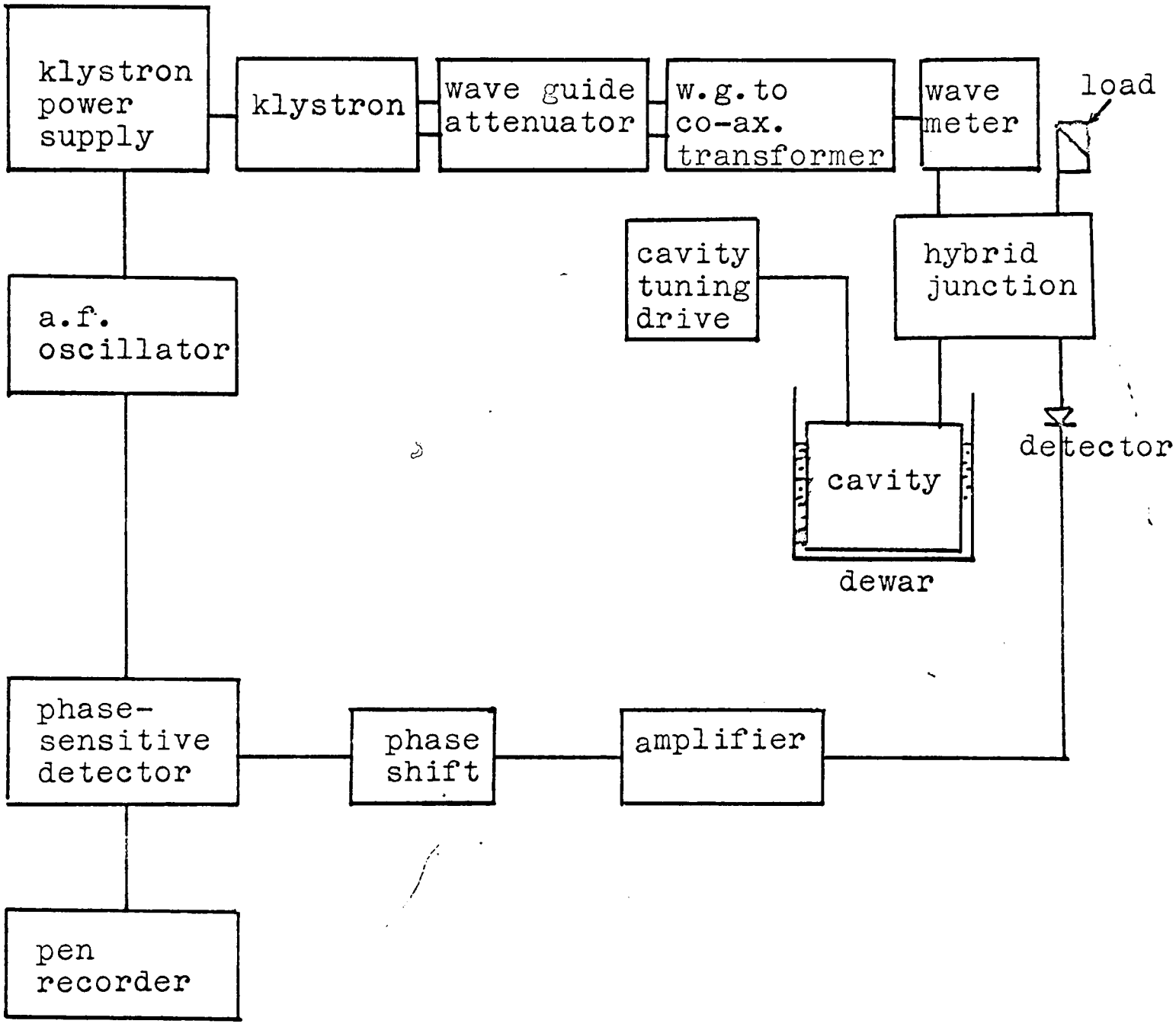
klystron power supply
klystron
wave guide attenuator
w.g.to co-ax. transformer
wave meter
load
cavity tuning drive
hybrid junction
a.f. oscillator
cavity
detector
dewar
phase-sensitive detector
phase shift
amplifier
pen recorder

The loaded cavity bandwidth then observed approximates closely to the intrinsic bandwidth (Appendix C). Experimentally, the coupling used corresponds to a power reflection coefficient greater than 0.990, leading to an observed bandwidth less than 0.5% larger than the intrinsic value. In the present work this small correction is ignored.

The microwaves are frequency modulated to a depth much less than the cavity bandwidth and the output of the phase sensitive detector is monitored with a pen recorder as the cavity is driven by a motor through the microwave frequency. The recorder chart then displays the derivative of the cavity resonance, enabling $\delta\nu'$ to be measured in terms of the cavity tuning rate. The tuning rate $\frac{d\nu}{dl}$, where l is the length of tuning plug in the cavity, is measured directly using a microwave frequency meter, and combining the two measurements gives $\delta\nu' = \sqrt{3}\delta\nu$ in Mc/sec.

(c) Cavity bandwidth as a function of temperature.

If the parameter $\delta\nu_e$, which is a measure of the coupling of the cavity to the input line, is known, the intrinsic bandwidth may be deduced from the power reflection coefficient (Appendix c). Alternatively, knowing $\delta\nu$ and the power reflection coefficient, $\delta\nu_e$ may be deduced. The value of $\delta\nu_e$ corresponding to any fixed geometrical

coupling is measured at various temperatures (usually 275°K, 195°K, 77°K and 20.3°K) by combining values of the intrinsic bandwidth determined by the method of 4.(ii)b with the corresponding power reflection coefficients. The variation of $\delta\nu_e$ throughout the temperature range of interest is then obtained by interpolation, and the inverse process is used to deduce $\delta\nu$ at any temperature in the range from the corresponding power reflection coefficient.

Two methods are used to determine the power reflection coefficient as a function of temperature. In the first of these the voltage produced by the microwave detector due to power reflected from the cavity is chopped at 400 c/sec., amplified and phase sensitive detected. The detector output is displayed on a recorder chart and continuously recorded as the cavity temperature changes. To calibrate the pen recorder reading in terms of the power reflection coefficient, the cavity is then tuned to well away from the microwave frequency. The microwave attenuation, measured by the waveguide attenuator, required to restore the recorder reading to any particular value, then gives the corresponding power reflection coefficient.

Due to changes in the cavity resonant frequency with temperature, special precautions are taken to maintain coincidence between the microwave frequency and the cavity resonance. The microwaves are frequency modulated at

100kc/sec. to a depth very much less than the bandwidth $\delta\nu$. The resulting signal is phase sensitive detected and the output fed back onto the klystron repeller in such a way as to stabilize the microwave frequency on the cavity resonant frequency. During a continuous temperature sweep over a wide range of temperatures it is found necessary periodically to make small adjustments to the cavity tuning to maintain approximately constant frequency. Otherwise the stabilizing system pulls the klystron across the mode and causes significant variation in the power output.

This continuous recording method was used to obtain the variation of $\delta\nu$ with temperature for the terbium single crystal and polycrystal specimens at $\sim$ 3,000Mc/sec. The variation in temperature is obtained either by pre-cooling the cavity and dewar with liquid nitrogen, removing the nitrogen and allowing the system gradually to warm up, or by filling the outer can only with liquid nitrogen and allowing the cavity to cool down slowly to 77°K.

The second method of determining the temperature variation of power reflection coefficient consists simply of direct measurements at a series of temperatures spanning the range of interest. As in the calibration of the recorder chart in the continuous recording method, these measurements are made by observing the microwave

detector voltage for the cavity on resonance, tuning the cavity well off resonance and measuring the attenuation in the microwaves required to restore the same detector voltage. This method is easy to operate when the temperature variation is slow, and was used to measure $\delta\nu$ as a function of temperature for the 10cm. cavity with the dysprosium rod as centre conductor, in the temperature range 280°K to 77°K. It was also used for holmium at 6377Mc/sec. A manostat was then operated to obtain constant pressure over liquid hydrogen, giving constant temperature anywhere in the range 11°K to 22°K.

Although the continuous recording method is more difficult to operate than the point by point one, it is potentially capable of providing more detailed information. In particular, it provides more precise values of the magnetic ordering transition temperatures.

4. (iii) Experimental Results.

(a) Electrical resistivity measurements.

The direction of microwave current flow in the centre conductor of coaxial cavity is parallel to the axis of the conductor. In some temperature ranges the rare earth metals show very high anisotropy in their electrical resistivity, and it is important that the d.c. resistivity be measured in the same direction as the

microwave current flow. The method of 3. (iii) conveniently meets this requirement.

Representitive results obtained for the non-magnetic centre conductors are given in Table 4.1

Table 4.1

$T^{o}K$	brass	copper	constantan
20	2.90	-	47.4
77	3.80	0.30	48.9
120	4.35	0.62	49.5
195	5.45	1.20	49.9
273	6.80	1.80	50.0

The resistivities are given in ohm-metresx10^{-8}

The measured resistivities of the rare earth metal specimens with the residual resistivity subtracted are shown in figures 4.2, 4.3 and 4.4. The temperature interval between measurements is typically 10 to 20 degrees Kelvin. However, this is reduced to two or three degrees in the region of magnetic ordering transitions. The results for the four specimens are discussed separately below.

1. <u>holmium.</u> (figure 4.2)

The measured resistivity is compared with a value calculated from oriented single crystal data of Strandberg et al. (5) using the formula

Figure 4.2

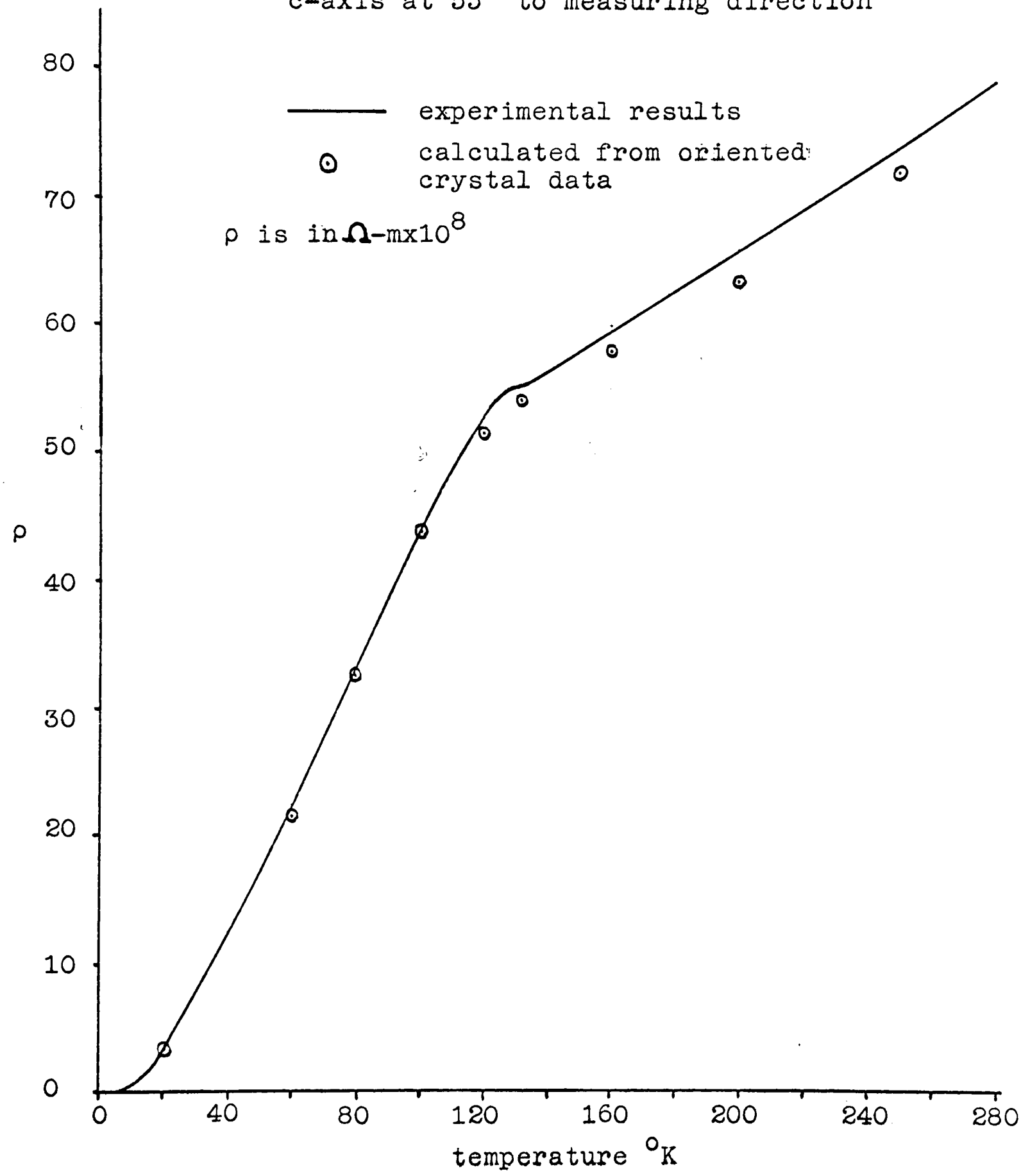
electrical resistivity of holmium crystal
c-axis at 55° to measuring direction
experimental results
calculated from oriented crystal data
ρ is in Ω-mx10^8
ρ
80
70
60
50
40
30
20
10
0
0
40
80
120
160
200
240
280
temperature °K

Figure 4.3

electrical resistivity of dysprosium crystal : c-axis at 84° to measuring direction.

ρ is in Ω-mx10^{8}

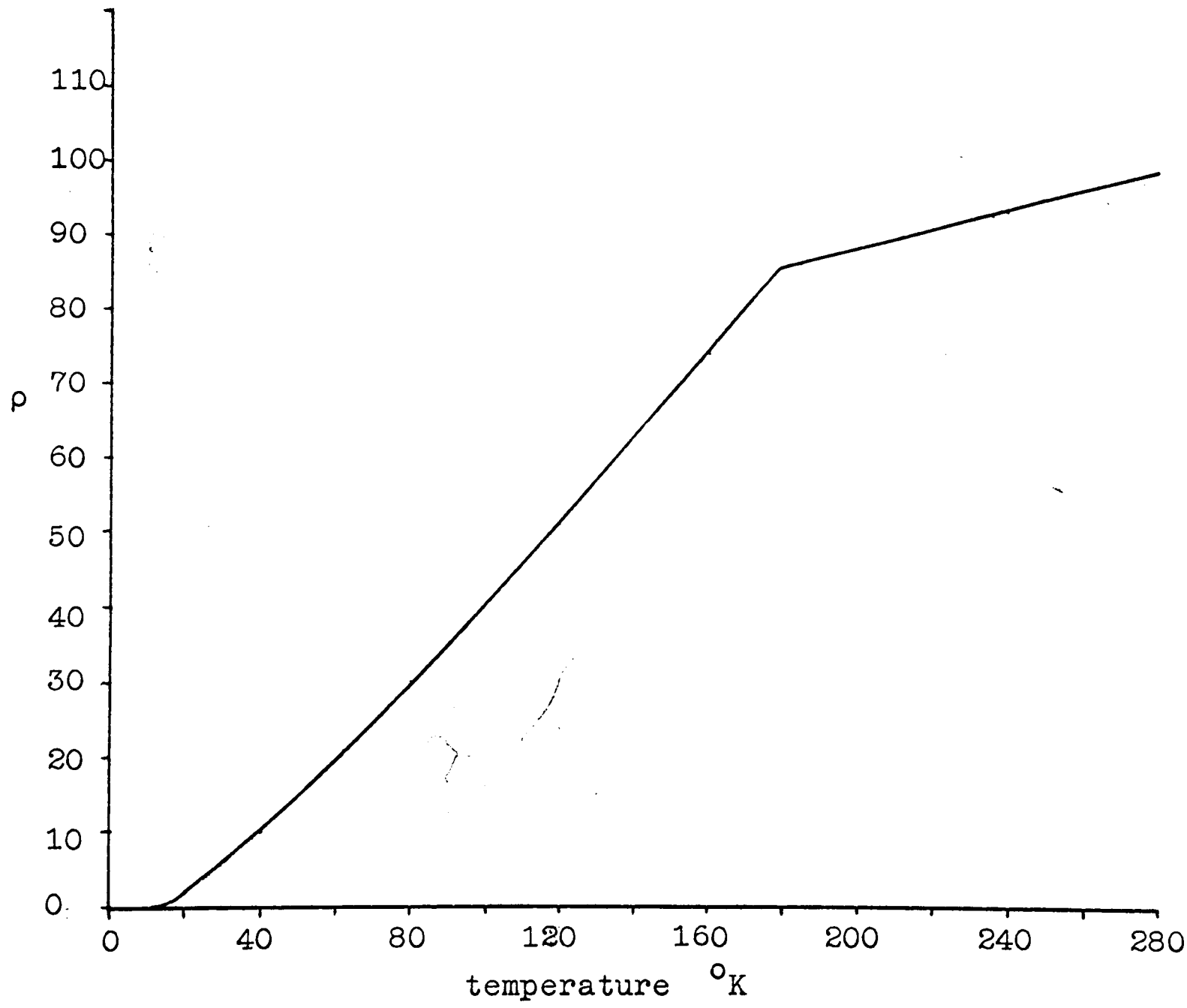

Figure 4.4

I. electrical resistivity of terbium crystal : c-axis at 76^{0} to measuring direction

II. measured polycrystal

⊙ calculated single crystal

ρ is in Ω-mx10^{8}

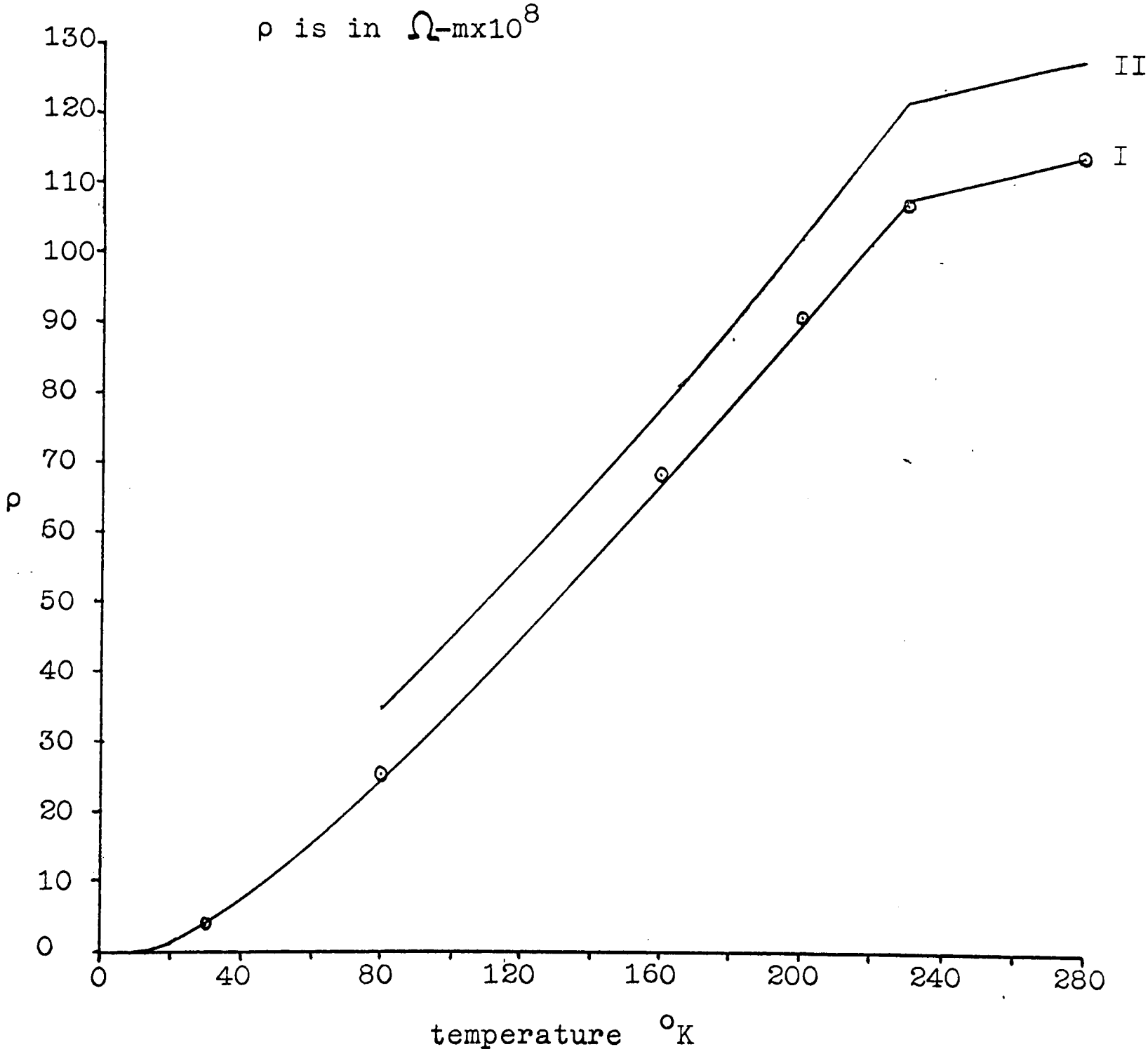

$$\rho_\theta = \rho_c \cos^2\theta + \rho_b \sin^2\theta.$$

ρ_c and ρ_b are respectively the c-axis and basal plane resistivities and θ is the angle between the c-axis and the measuring direction. Agreement between the measured and calculated values is reasonably good. A distinct kink in the resistivity curve occurs at 130±3°K. This is at the Neel temperature for holmium (6). No anomaly was found in the neighbourhood of 19.4°K, the Curie temperature.

2. <u>dysprosium</u> (figure 4.3)

In the dysprosium crystal the c-axis is nearly perpendicular to the measuring direction . The measured electrical resistivity will therefore be close to the basal plane value ρ_b. The results disagree with the predictions of Hall et al. (6) who analysed data obtained with crystals of intermediate orientation using the formula $\rho_\theta = \rho_c\cos^2\theta + \rho_b\sin^2\theta$. However there is good agreement between the present results and the basal plane resistivity for an oriented single crystal measured by Wilding (7). In particular, in his results the ferromagnetic to antiferromagnetic transition at 80°K is barely detectable in the basal plane resistivity. In the present work, there was no indication of this transition. The change in gradient in the resistivity versus temperature curve occurs at 178±1°K, the Neel temperature for dysprosium (6).

3. terbium. (figure 4.4)

The measured single crystal resistivity is compared with values calculated from oriented single crystal data of Hegland et al. (8) using the relation $\rho_{76^0} = \rho_c \cos^2 76^0 + \rho_b \sin^2 76^0$. The two values agree to within experimental error. The change in gradient occurs at 229.5±1°K, corresponding to the Neel temperature of terbium.

Measurements on the polycrystal were not extended to below 77°K. The change in gradient occurs at 229±2°K. The deeply pitted surface of the specimen makes the cross sectional area rather uncertain, and this, combined with the undetermined residual resistivity accounts for the measured resistivities being some 10% larger than those of Colvin et al. (9).

4. (iii)b Calibration of the cavities.

Our measurements of μ_R have been made at 3000Mc/sec. on the two terbium specimens, at 3050Mc/sec. on the dysprosium single crystal, and at 3077Mc/sec. on the holmium crystal. The three sets of cavity calibrations which were necessary are discussed separately below, and the values obtained of the parameter B in equation 5 are given in Table 4.2.

1. Calibration of the 10cm. cavity (figure 4.6) at 3000Mc/sec., with specimen centre conductors of 4.9mm. diameter.

4.9mm is the specimen diameter for which the collets

in this cavity are designed, and it is the diameter of the terbium polycrystal and dysprosium single crystal rods. Measurements at 273°K of the bandwidths $\delta\nu$ corresponding to copper, brass and constantan centre conductors, and to the two rare earth metal rods, are plotted against $\sqrt{\rho}$, where ρ is the corresponding electrical resistivity, and the results are shown in figure 4.5. It will be noticed that the result for the terbium ploycrystal lies considerably above the line, showing the necessity of applying a correction for the surface roughness.

2. <u>calibration of the 10 cm. cavity at 3000Mc/sec. with specimen centre conductors of 4.2mm. diameter.</u>

This is the diameter of the terbium single crystal, and to fit this and the non-magnetic calibrating specimens into the cavity, the collets are packed with copper collars of appropriate size. The experimental graphs of $\delta\nu$ against $\sqrt{\rho}$ are shown in figure 4.6. The gradients at 77°K, 195°K and 273°K are, to within experimental error, equal, and so confirm the temperature independence of the parameter B.

3. <u>calibration of the 4 to 5cm. wavelength cavity (figure 3.4) at 6377Mc/sec.</u>

The centre conductor in this case has a diameter of 4.75mm., the diameter of the holmium rod. It was found relatively difficult to obtain bandwidth measurements as consistent as for the 10cm. cavity. This probably because the specimen is not completely rigid in the collet

Figure 4.5

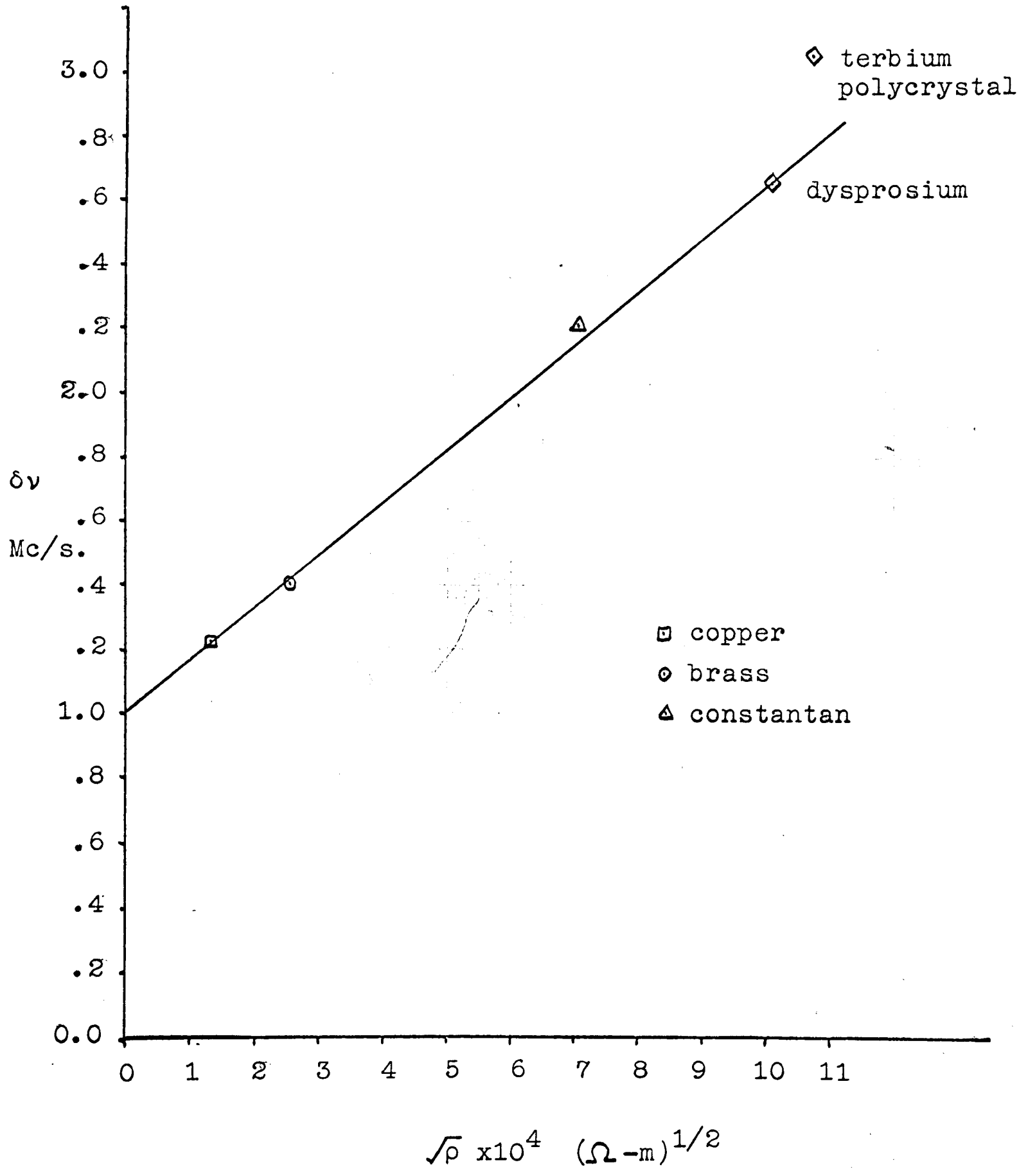
terbium polycrystal
dysprosium
copper
brass
constantan
δν
Mc/s.
3.0
.8
.6
.4
.2
2.0
.8
.6
.4
.2
1.0
.8
.6
.4
.2
0.0
0 1 2 3 4 5 6 7 8 9 10 11
√ρ x10^4 (Ω-m)^1/2

Figure 4.6

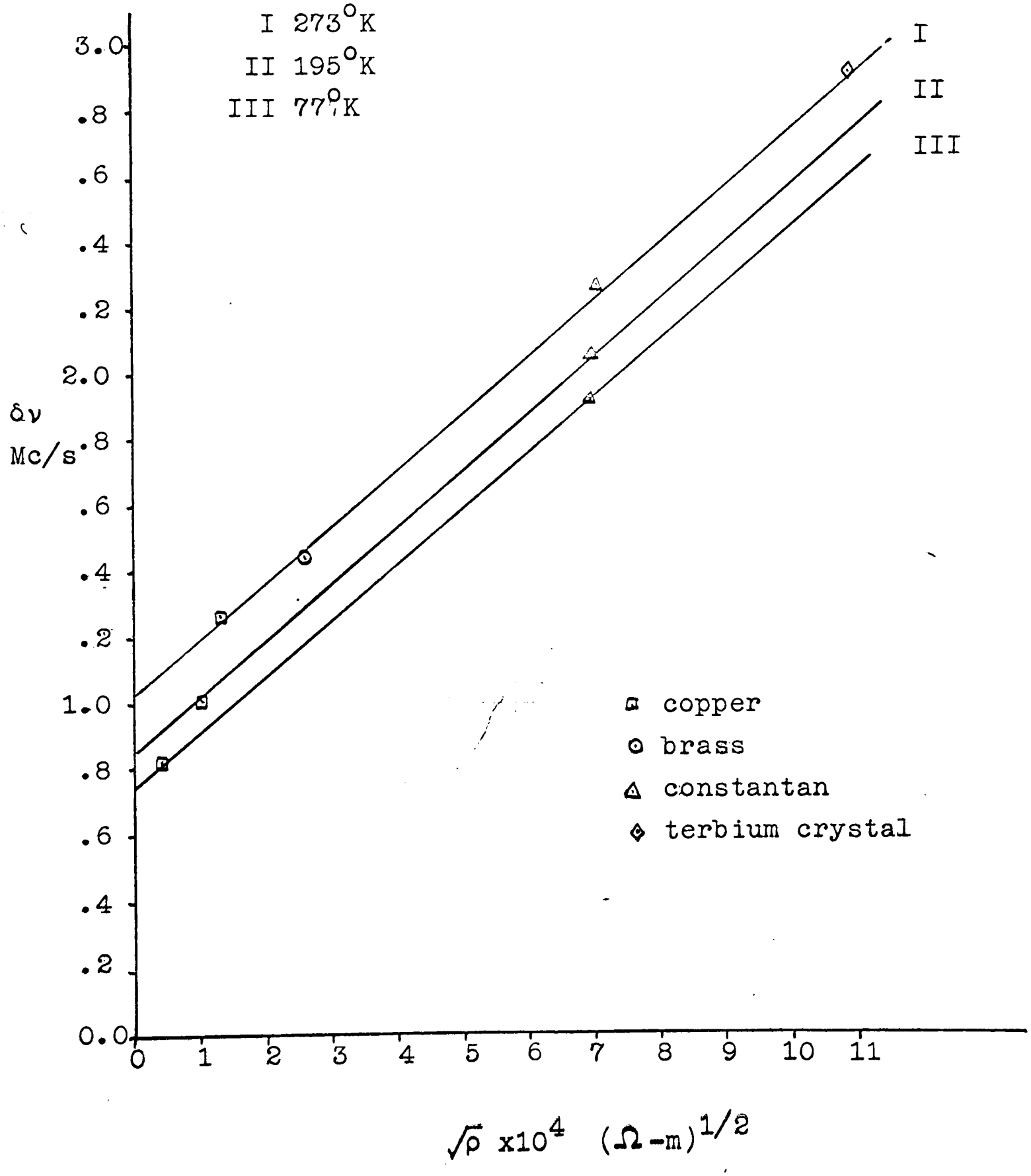
I 273°K
II 195°K
III 77°K
I
II
III
3.0
.8
.6
.4
.2
2.0
δν
Mc/s
.8
.6
.4
.2
1.0
.8
.6
.4
.2
0.0
0
1
2
3
4
5
6
7
8
9
10
11
copper
brass
constantan
terbium crystal
√ρ x10^4 (Ω-m)^1/2

Figure 4.7

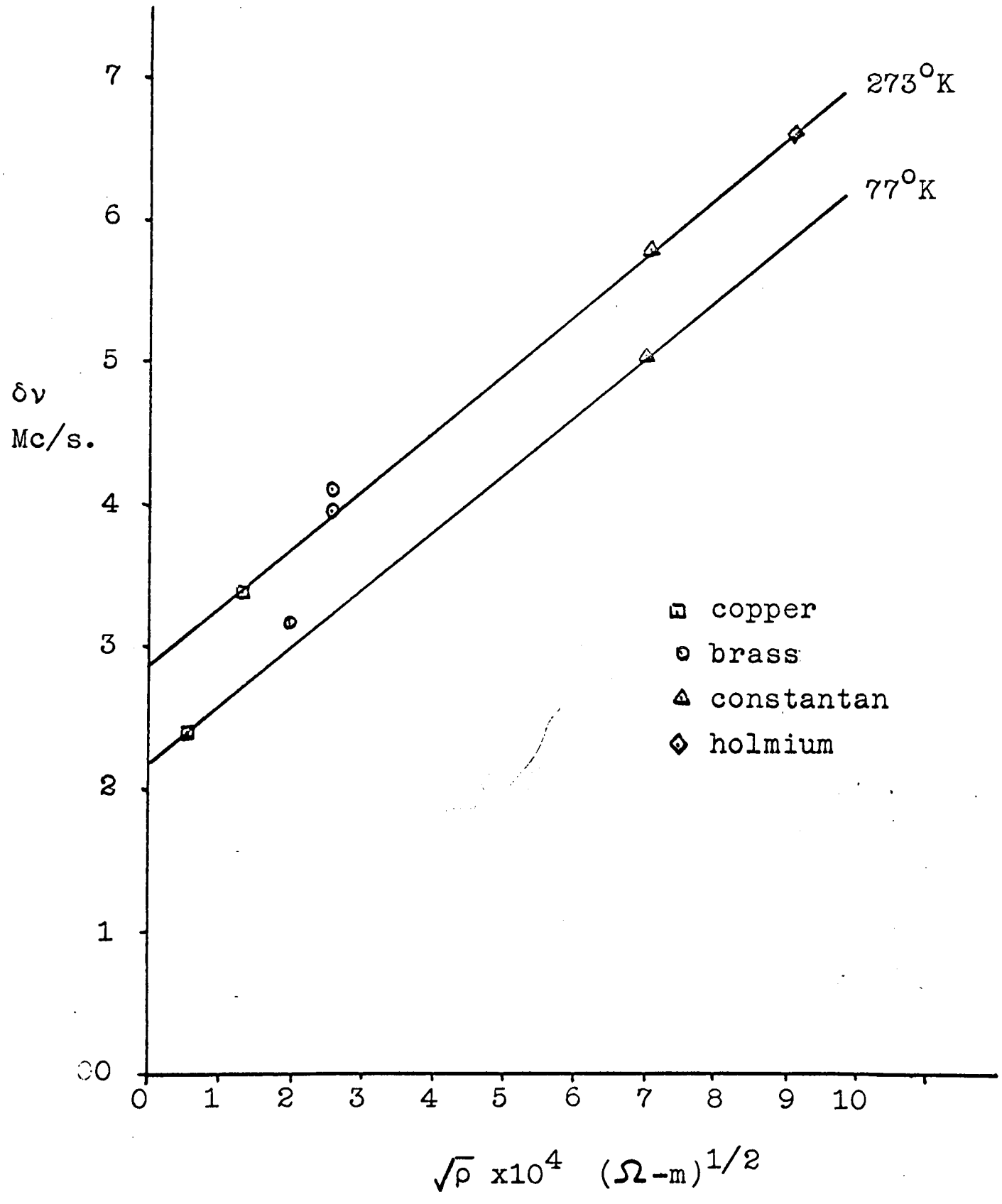
7
6
5
δν
Mc/s.
4
3
2
1
0
0
1
2
3
4
5
6
7
8
9
10
273°K
77°K
copper
brass
constantan
holmium
√ρ x10⁴ (Ω-m)^1/2

at the end of the german silver tube from the tuning micrometer, and small lateral movements are possible. Figure 4.7 shows the experimental values of δv plotted against the corresponding values of $\sqrt{p}$ and, to within experimental error, the values of B at the two temperatures are the same.

As we noted in section 4. (i), approximate values of B may be calculated relatively easily for a coaxial cavity. In Appendix we have calculated the values corresponding to the cavity configurations described above, and these are compared with the experimental results in Table 4.2:-

Table 4.2

frequency	centre conductor	B(experiment)	B(theory)
Mc/sec.	Diameter (mm.)		
3060	4.90	$1.64 \pm .02 \times 10^3$	1.64×10^3
3060	4.20	$1.70 \pm .02 \times 10^3$	1.76×10^3
1377	4.75	$4.3 \pm 0.1 \times 10^3$	4.80×10^3

B is expressed in $(\text{Mc/sec.})/(\text{ohm-m})^{1/2}$.

The calculated values of B make no allowance for the considerable discontinuity in the centre conductor diameter at the collets when the 4.2mm. diameter specimen is used in the 10cm. cavity. In the 4 to 5cm. cavity

complicated end effects arise, and these are not allowed for in the calculation. The discrepancies between the simple theory and the experimental results are presumably due to these omissions.

In all experiments at ≐9,000c/sec., the parameter A(T) in equation 5 is obtained by using either a copper or a constantan centre conductor of appropriate diameter, and measuring the corresponding value of δv as a function of temperature by the point by point method of 4. (ii)c. For the single crystal specimens μ_R is then evaluated from equation 5 using the corresponding experimental values of A(T), B and β. For the terbium polycrystal, our measurements of B are rather unreliable, and published data is used instead.

The measurements of μ_R for the dysprosium crystal were made several months after those for the terbium polycrystal and the corresponding calibration measurements described above. In the later series of experiments, which were conducted at 30500c/sec., the bandwidths at all temperatures were 0.11kc/sec. larger than those obtained in the earlier series. The value of B is assumed to be the same in both cases, and so A(T) differs from the earlier value by a temperature independent correction of this amount.

In the case of the 4 to 5cm wavelength cavity,

using a constantan centre conductor, measurements of $\delta\nu$ by the method of 4. (ii)b at 11°K and 20.3°K give the same result. These measurements were made at 9377Mc/sec. We therefore assume that A(T) is constant throughout the range 11°K to 22°K and, as before, it is determined from equation 5 using the measured values of $\delta\nu$, B, and electrical restivity ρ.

4. (iii)c. Experimental values of μ_R for terbium, holmium and dysprosium.

In this section we present measurements of cavity bandwidth as a function of temperature made with the 10 cm. cavity, with either the dysprosium or terbium specimens as centre conductor, and the 4 to 5 cm. cavity with the holmium as centre conductor. The calibration and electrical resistivity data of the previous sections are used to obtain the corresponding values of μ_R. Some experiments on terbium, on the dependence of μ_R on static magnetic field are also mentioned, but apart from these, all the results in this section are obtained in zero applied static field. The experimental conditions and results for the individual specimens are dealt with separately below. The significance of the error bars in the graphs of μ_R is discussed at the end of the section.

1. terbium polycrystal. (figures 4.8 and 4.9)

The bandwidth measurements shown in figure 4.8

Figure 4.8

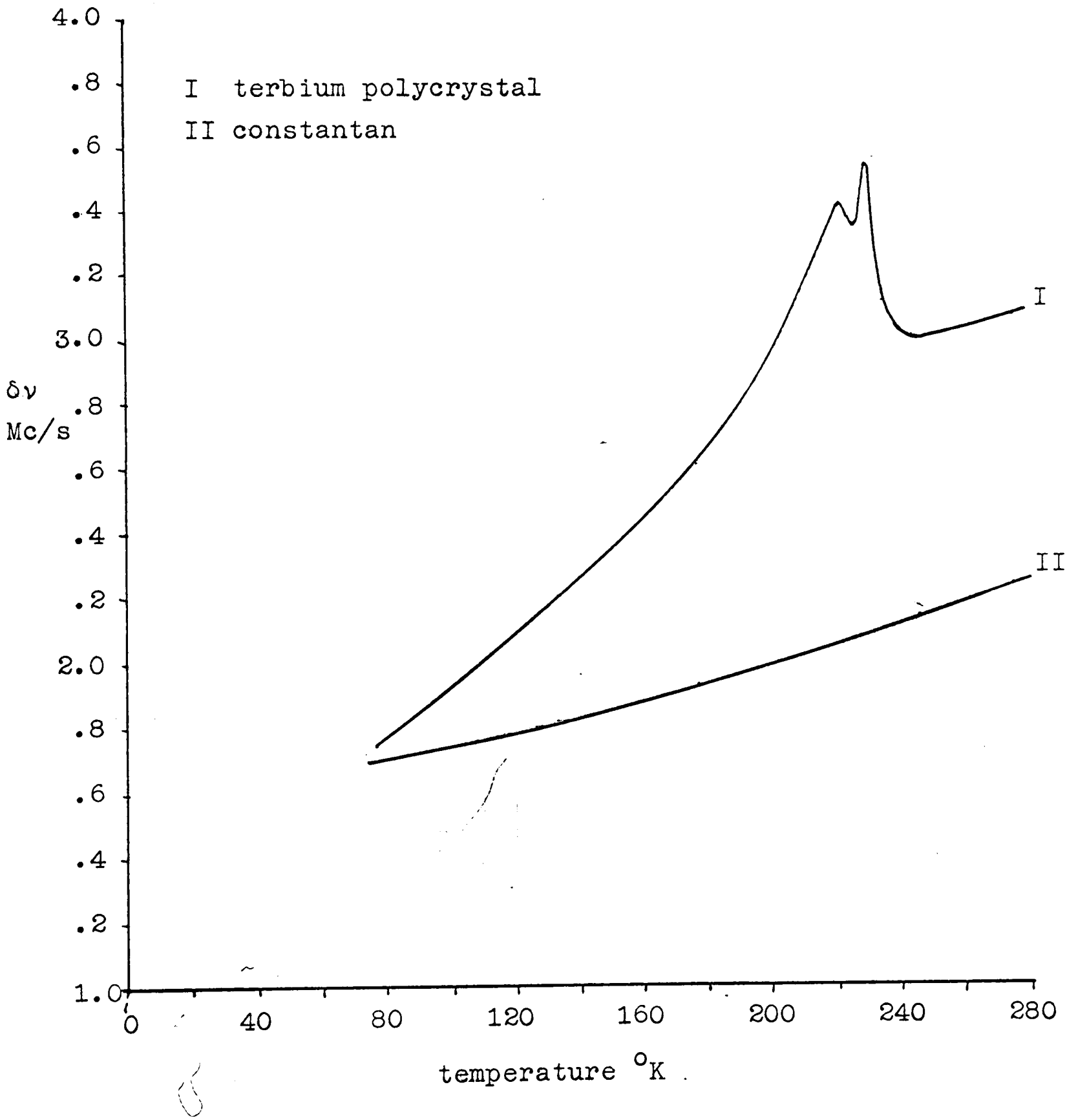
I terbium polycrystal
II constantan
δν
Mc/s
4.0
.8
.6
.4
.2
3.0
.8
.6
.4
.2
2.0
.8
.6
.4
.2
1.0
0
40
80
120
160
200
240
280
temperature °K
I
II

Figure 4.9

permeability μ_R of terbium polycrystal at 3060 Mc/sec.

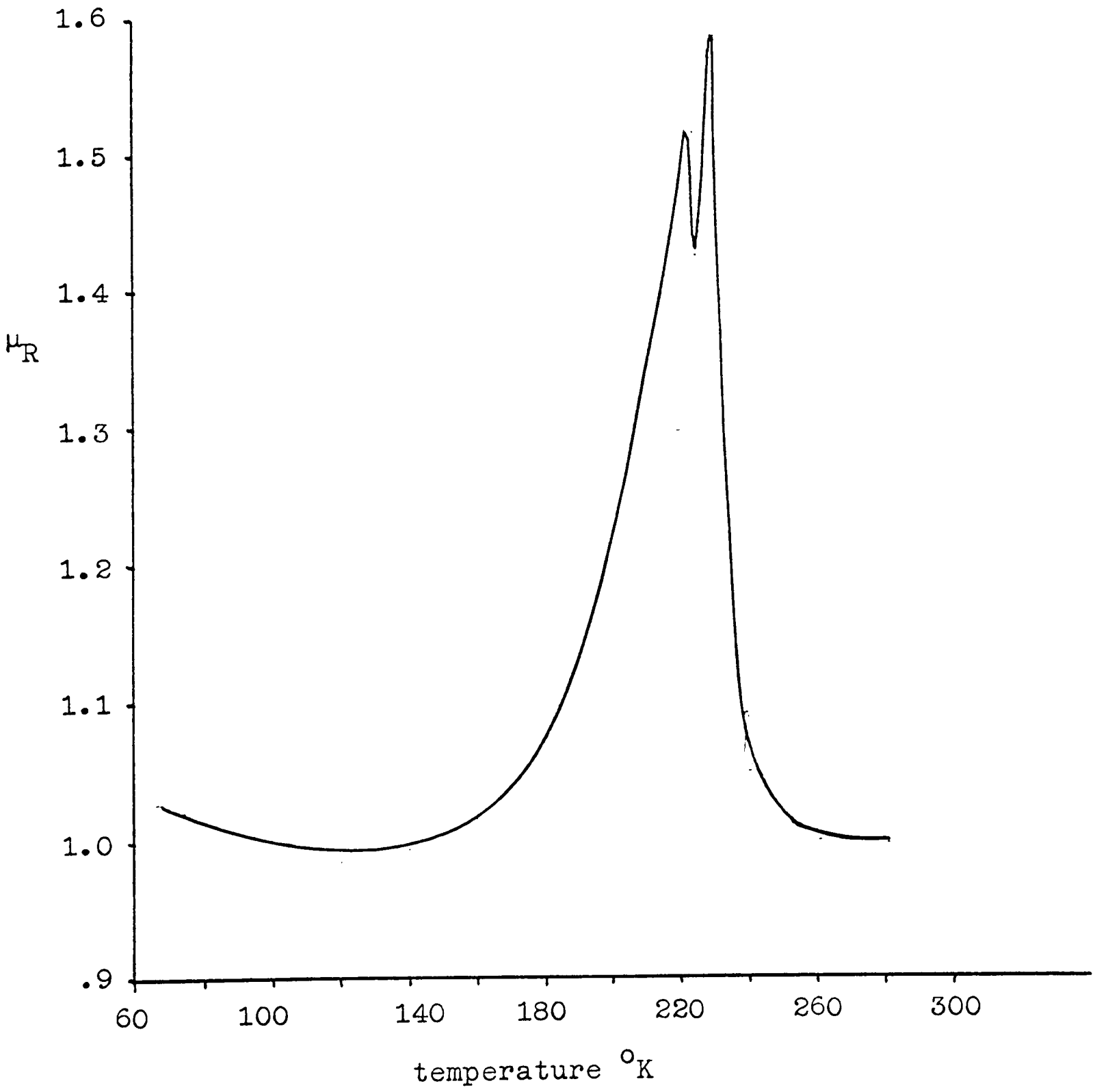

were made at 3060Mc/sec. and are obtained throughout the temperature range 77°K to room temperature by the continuous recording method of 4. (ii)c, as the 10cm. cavity freely warms up through the range. The temperature is measured using a thermocouple soldered to the outside of the cavity, and it is found that for the warming up rate used in this particular experiment, the recorded Neel temperature maximum in δv occurs when this reads about 237°K. The Curie point maximum occurs 8° below this. In calculating μ_R a temperature correction is applied to the bandwidth data so that the Neel point maximum corresponds to 230°K, the value determined from the electrical resistivity data.

As we noted in 4. (iii)b, it is necessary to apply a roughness correction in evaluation of μ_R for this specimen. From equations 5 and 6, section 4. (i) we have:-

$$\delta v = A(T) + B\sqrt{\rho\mu_R(1 + C/\delta)}$$

writing $\delta = \left\{\frac{\pi\nu\mu_0\mu_R}{\rho}\right\}^{1/2}$

$$\left\{\frac{\delta v - A(T)}{B}\right\}^2 = \rho\mu_R\left(1 + C'\sqrt{\frac{\mu_R}{\rho}}\right) \quad \text{equation 7.}$$

Due to the pitted surface of the specimen, the value of used in extraction of μ_R from equation 7 is not, in fact, the measured value given in section 4.(iii)a. Instead, a published value (9) is used, assuming rather arbitrarily a residual resistivity of 4.0×10^{-8} ohm-m. From experience with the single crystals it is probable

that, after annealing, the polycrystal residual resistivity is less than 7×10^{-8} ohm-m. An error of 2 or 3×10^{-8} ohm-m. will make little difference to the final result, especially at the higher temperatures when ρ is large. The value of C' determined at 273°K is 3.9×10^{-4}(ohm-m.)$^{1/2}$. This leads to a maximum roughness correction R(δ) of 1.7, applied at 77°K. From equation 7, μ_R is calculated at various temperatures by a method of successive approximation, the first approximation being that the roughness correction is due to the resistivity only. A continuous curve in then interpolated to give the results shown in figure 4.9.

2. terbium crystal. (figures 4.10 and 4.11)

As in the case of the polycrystal specimen, the variation of δν with temperature from 77°K to room temperature shown in (figure 4.10) is obtained by continuously recording the cavity power reflection coefficient as the 10 cm. cavity gradually warms up. An additional measurement of δν is made at 20.3°K by the method of 4.(ii)b. In the region of the magnetic ordering transitions the warming up rate is about 1°K in two minutes, and the temperature registered by the thermocouple when δν passes through the Neel point maximum is 232°K. Again, as for the polycrystal, the Curie point maximum occurs 3° below this, and a temperature correction is applied to

Figure 4.10.

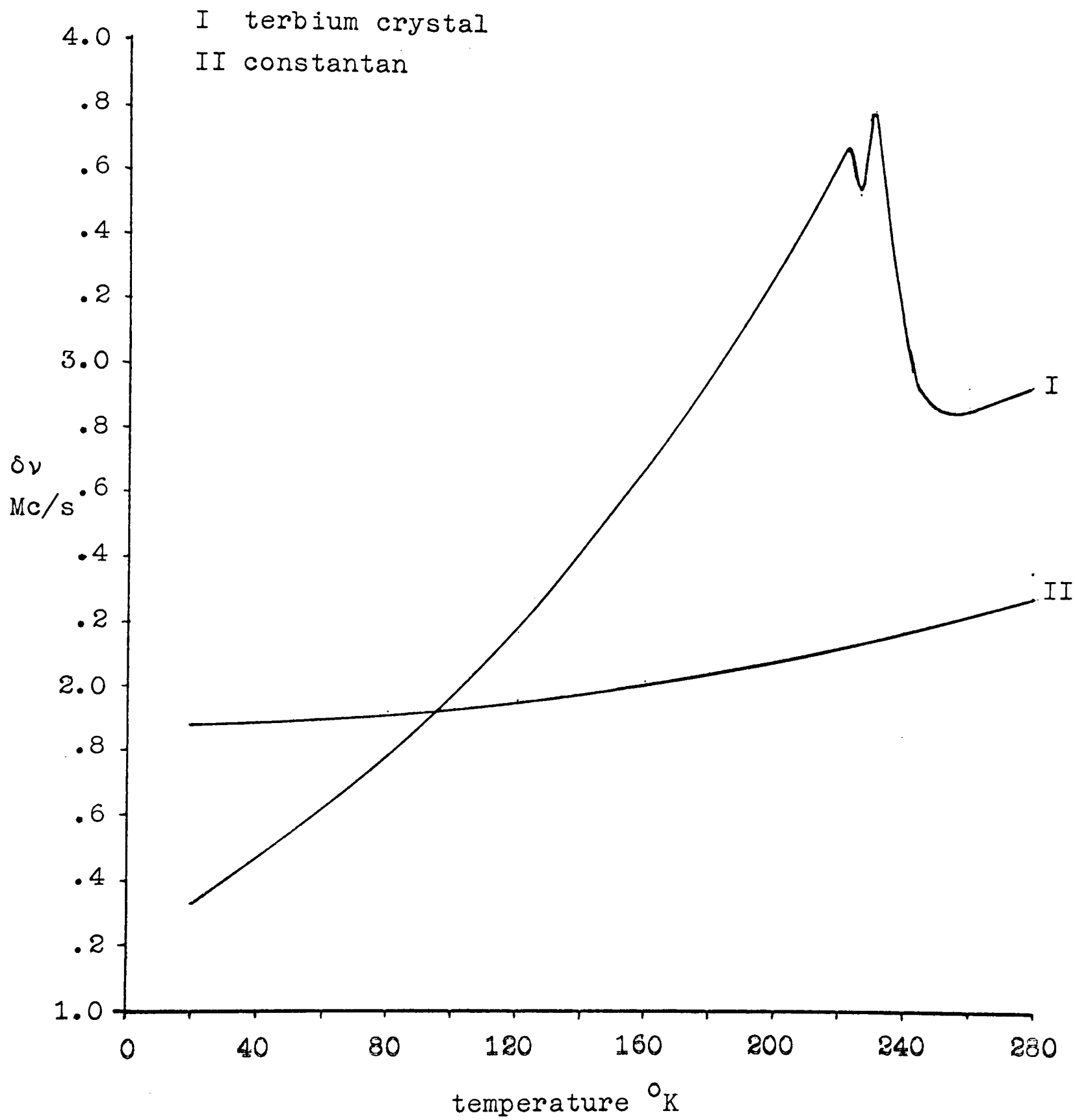
I terbium crystal
II constantan
4.0
.8
.6
.4
.2
3.0
.8
δν
Mc/s
.6
.4
.2
2.0
.8
.6
.4
.2
1.0
0
40
80
120
160
200
240
280
temperature °K
I
II

Figure 4.11

permeability μ_R of terbium crystal at 3060 Mc/sec.

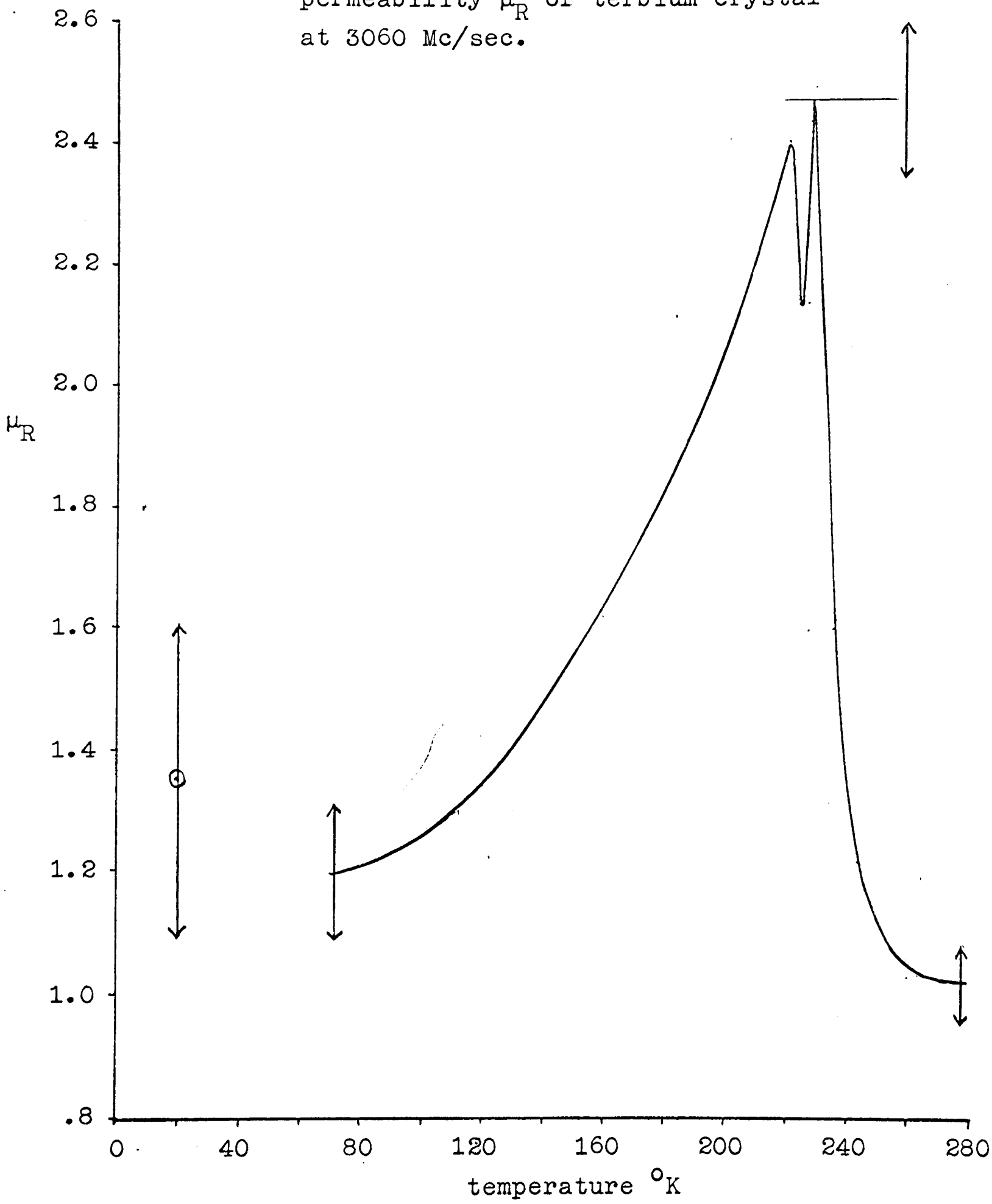

bring the maximum in δv at the Neel temperature into coincidence with the Neel temperature obtained from the electrical resistivity data. The electrical resistivity data used in this case is that obtained on the same specimen (figure 4.4).

Power reflection coefficient measurements taken on another warming up run are averaged with those obtained during a cooling run of comparable rate, yielding a value of $T_N = 230.5^{\circ}K$. This verifies that, to the accuracy of the present work, the Neel temperatures obtained from the electrical and magnetic measurements are the same. There is some evidence that the Curie temperature T_c shows a temperature hysteresis of about a degree, the value of T_c obtained on a transition from the ferromagnetic to antiferromagnetic state being about this amount higher than that obtained on re-cooling. However, this may be a spurious effect, and we discuss it in more detail in Chapter 5. The variation of δv with temperature corresponding to a constantan centre conductor is also shown in figure 4.10. A(T) is evaluated from this, and combined with the corresponding values of B and the terbium resistivity to give μ_R as a function of temperature (figure 4.11).

Up to about 15° above T_N, $\mu_R - 1$ is an order of magnitude less than the static magnetic susceptibility measured by Hegland et al. (8). Above this, our results

become very uncertain. The large temperature hysteresis in μ observed below T_c at low frequencies (10) was not observed in our high frequency measurements.

The dependence of μ_R on applied static magnetic field shows several complicated features, especially in the temperature range where the terbium is antiferromagnetic in zero field. We defer a more detailed presentation and discussion of these features to the following chapter and only make a general observation at this stage. At temperatures in the region of T_N and T_c, as a static field applied perpendicular to the crystal c-axis is increased, it finally produces a substantial decrease in μ_R. At lower temperatures, less and less field dependence of μ_R is observed, and at temperatures below about 140°K, to the accuracy of the experiment, μ_R shows no field dependence up to 5.5kOersted. Similar behaviour is observed in the terbium polycrystal.

3. <u>dysprosium crystal</u>. (figures 4.12 and 4.13)

The variation of δv with temperature shown in figure 4.12 is calculated from power reflection coefficient measurements made at 4° to 6° intervals as the 10cm. cavity gradually cools from room temperature to 77°K. Additional point measurements of δv are made at 14°K and 20.3°K using the method of 4.(11)b. $A(T)$ is calculated from the temperature dependence of δv corresponding to a copper

Figure 4.12

I dysprosium crystal
II copper

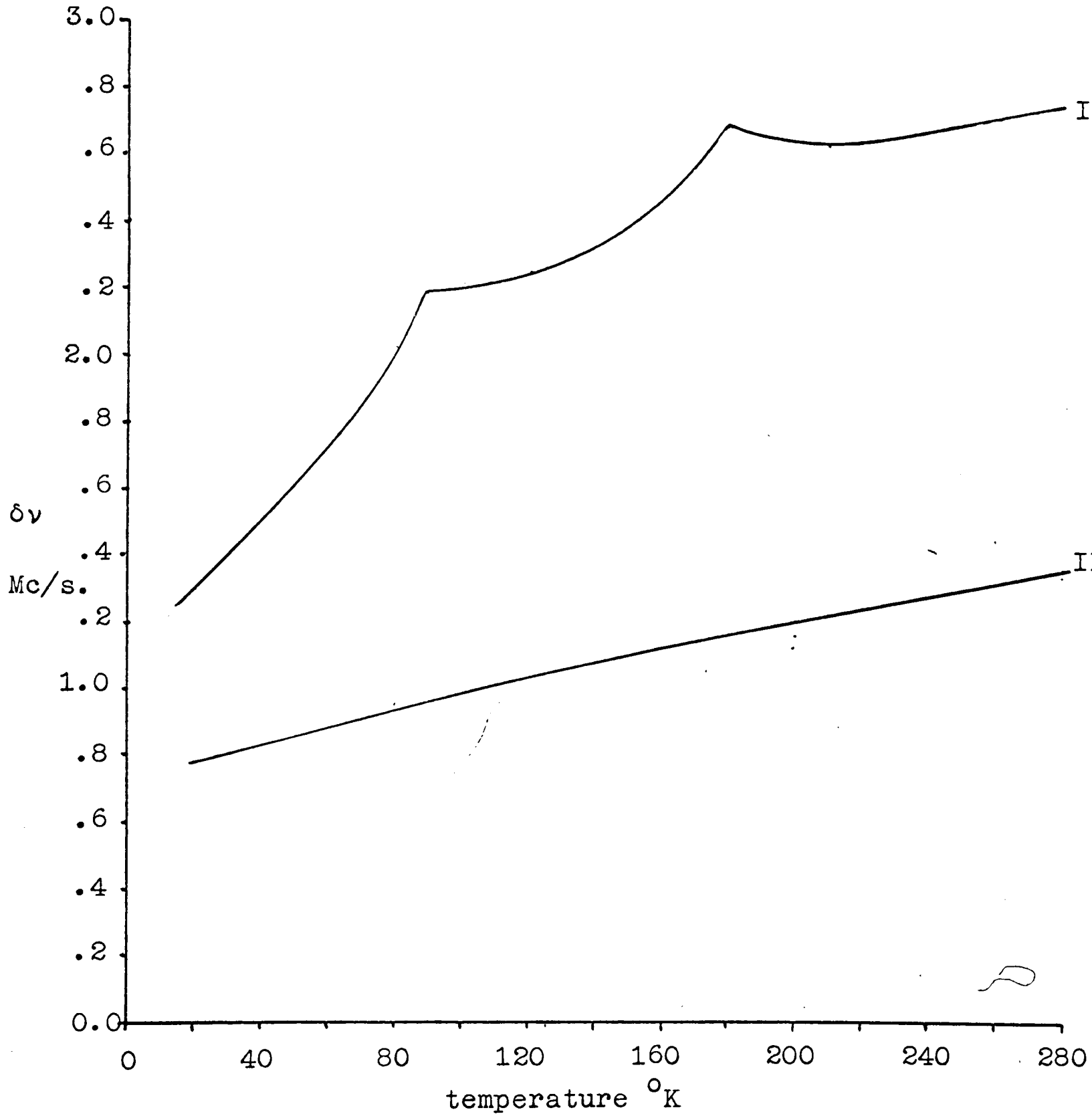

Figure 4.13

permeability μ_R of dysprosium crystal at 3050 Mc/sec.

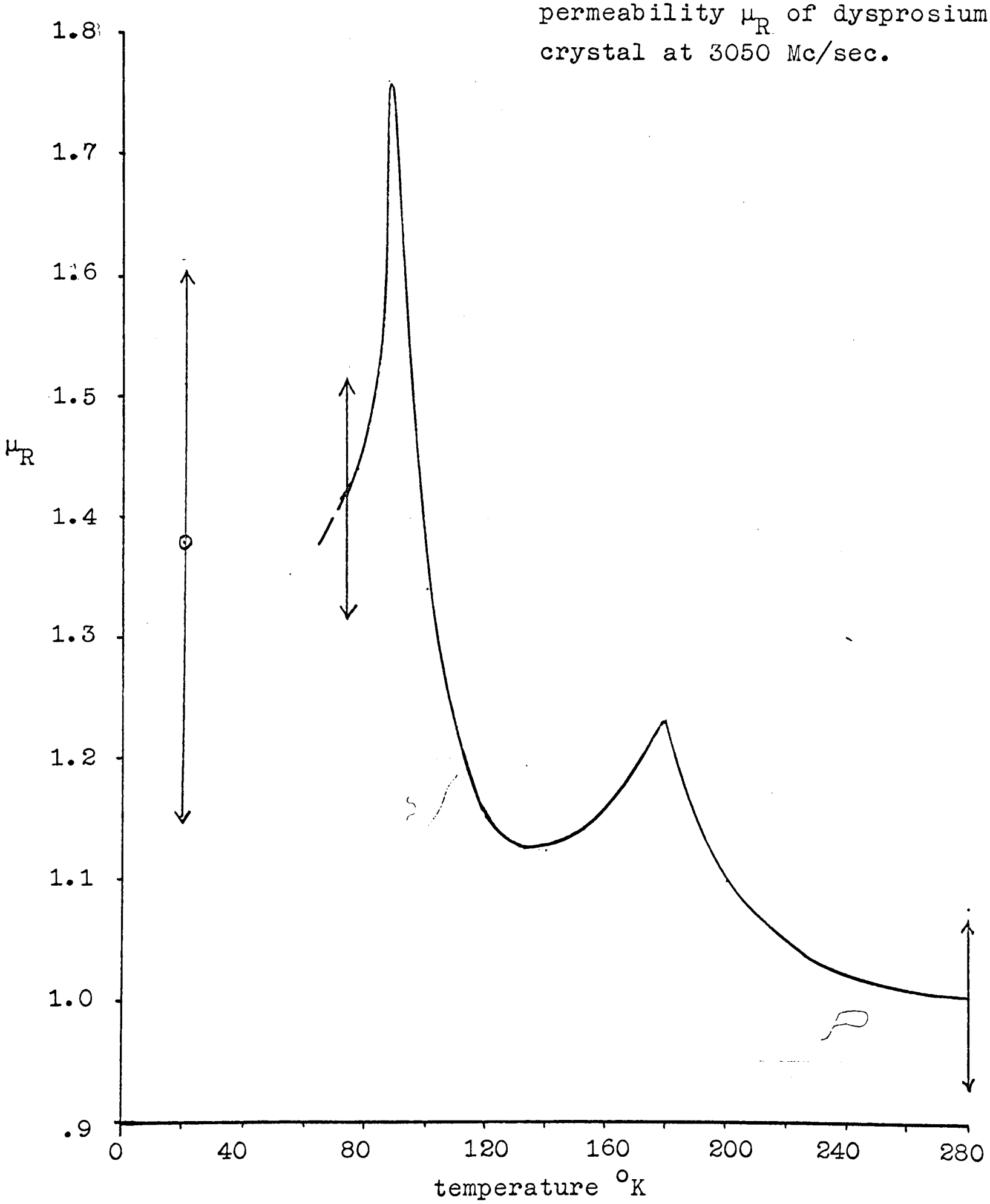

centre conductor, also shown in figure 4.12, and the calculated values of μ_R for the dysprosium appear in figure 4.13.

No investigations have been made of the effect on μ_R of a static magnetic field nor of possible thermal hysteresis effects in either μ_R or the magnetic ordering transitions.

4. <u>holmium crystal</u>. (figure 4.14)

Detailed measurements of μ_R for the holmium crystal are confined to the temperature range 11°K to 22°K, and were made at 6877Mc/sec. With the holmium mounted as centre conductor in the 4 to 5cm. cavity, δv is measured directly at 14°K and 20.3°K. The values obtained are combined with measurements of power reflection coefficient throughout the range to give the corresponding values of δv. The temperature variation of μ_R shown in figure 4.14 is then evaluated using bandwidth measurements made with a constantan centre conductor.

The peak observed at 19°K corresponds closely to the onset of conical ferromagnetism determined by Strandberg et al. (5), their value being 19.4°K. It is probable that in the present experiment, the specimen temperature is slightly above that of the cryogenic liquid surrounding the cavity. A point measurement of μ_R

Figure 4.14

permeability μ_R of holmium crystal at 6377 Mc/sec.

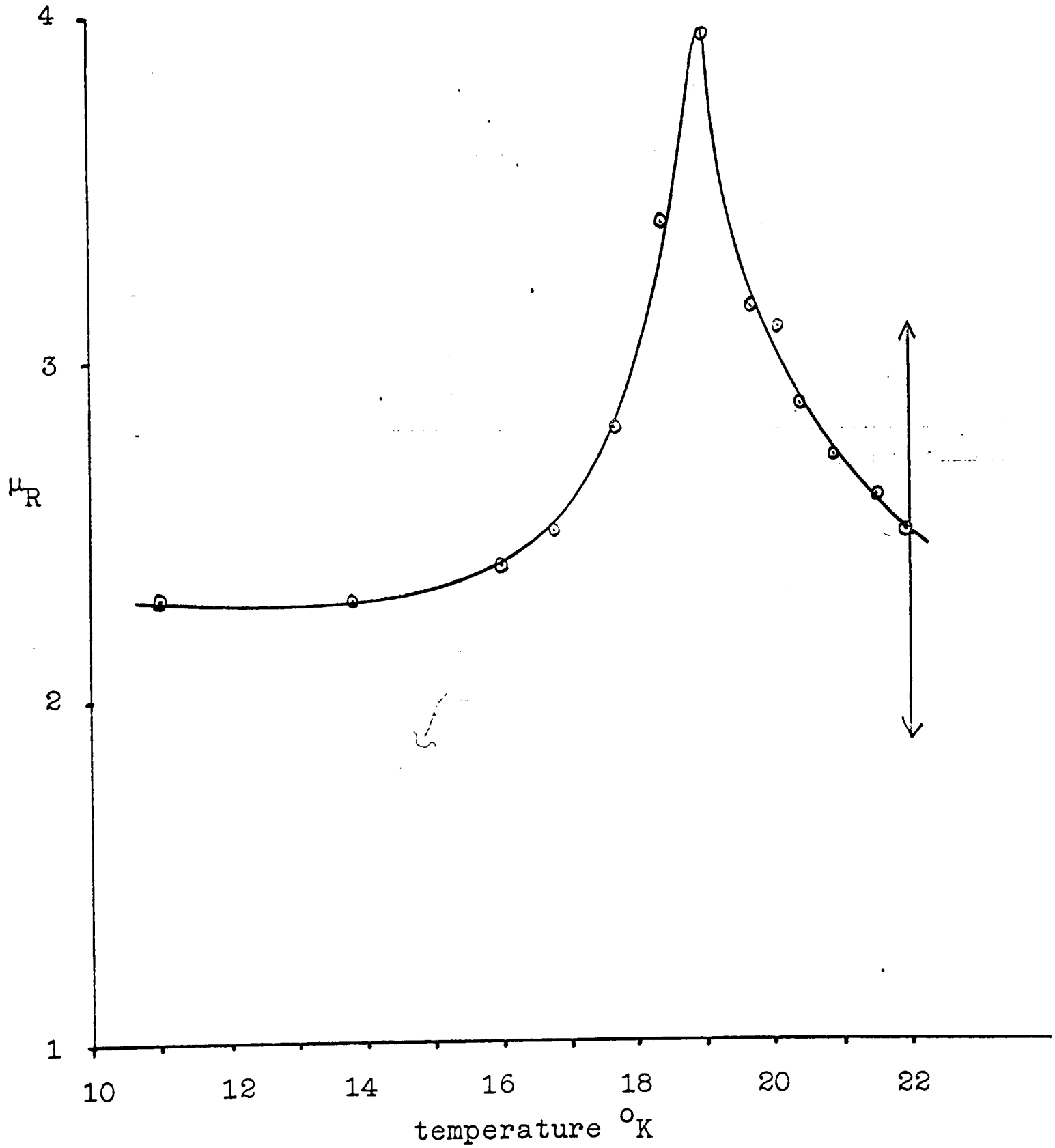

at 77°K gives the value 1.35±0.15, and a qualitative observation of power reflected from the cavity as a function of temperature shows that a peak in μ_R occurs between 130°K and 135°K, corresponding to the antiferromagnetic to paramagnetic transition.

b. Limitations of accuracy of the μ_R measurements.

The main source of uncertainty in the preceding measurements of μ_R lies in the limitations of the method (4.(11)b) used to determine the intrinsic bandwidth $\delta\nu$ at fixed temperatures. μ_R is evaluated from an expression containing the difference in two experimental bandwidths (equation 7), as $\delta\nu$ corresponding to a calibration centre conductor is implicit in A(T).

$\delta\nu$ at all temperatures for the 10cm. cavity is found to be reproducable to within about ±.03 Mc/sec. With the terbium single crystal as centre conductor, for example, this leads to an uncertainty in $\delta\nu$ of ±1°/o at room temperature, increasing to about 2°/o at 20°K. The experimental values of B are subject to uncertainty from the same source and, allowing for a ±.03Mc/sec. uncertainty in all bandwidth measurements, the error bars in figures 4.11 and 4.13 are obtained. The roughness correction applied for the terbium polycrystal normalizes μ_R to unity at room temperature. The correction is becoming considerable by 77°K and, as the linear approximation $R(\delta) = 1 + C/\delta$

at 77°K gives the value 1.35±0.15, and a qualitative observation of power reflected from the cavity as a function of temperature shows that a peak in μ_R occurs between 130°K and 135°K, corresponding to the antiferromagnetic to paramagnetic transition.

5. Limitations of accuracy of the μ_R measurements.

The main source of uncertainty in the preceding measurements of μ_R lies in the limitations of the method (4.(11)b) used to determine the intrinsic bandwidth $\delta\nu$ at fixed temperatures. μ_R is evaluated from an expression containing the difference in two experimental bandwidths (equation 7), as $\delta\nu$ corresponding to a calibration centre conductor is implicit in A(T).

$\delta\nu$ at all temperatures for the 10cm. cavity is found to be reproducable to within about ±.03 Mc/sec. With the terbium single crystal as centre conductor, for example, this leads to an uncertainty in $\delta\nu$ of ±1°/o at room temperature, increasing to about 2°/o at 20°K. The experimental values of B are subject to uncertainty from the same source and, allowing for a ±.03Mc/sec. uncertainty in all bandwidth measurements, the error bars in figures 4.11 and 4.13 are obtained. The roughness correction applied for the terbium polycrystal normalizes μ_R to unity at room temperature. The correction is becoming considerable by 77 K and, as the linear approximation $R(\delta) = 1 + C/\delta$

used in equation 7 will by then be a poor approximation, we can expect the corresponding value of μ_R to be rather more uncertain than for the terbium single crystal.

The bandwidths measured for the 4 to 5cm. cavity are reproducable only to about ±.2Mc/sec. This corresponds to an error of order ±5%/o in the measurements at 20°K and below, leading to the rather large overall uncertainty in the final evaluation of μ_R for the holmium crystal.

In all the single crystal measurements any roughness correction which has not been allowed for will become more apparent at low temperatures when the electrical resistivity has become small. If, for example, R(δ) = 1.05 at 273°K for the terbium crystal, a roughness correction of order 1.?, assuming electrical losses only, would be applicable at 20°K. Such a correction could well be concealed in the experimental uncertainty of the room temperature measurements, and the possibility of its existence leads us to treat with caution the apparent tendancy of μ_R to increase with decreasing temperature between 77°K and 20°K. Similarly, an undetermined roughness correction may have caused appreciable increase in the apparent low temperature values of μ_R for all the crystals.

4. (iv) Discussion of results: application to n.m.r.

(a) General discussion.

If domain wall motion is making a major contribution to the high frequency permeability of a ferromagnet, a static magnetic field sufficient to substantially decrease the number of domain walls will also decrease the permeability. The absence of a field dependence in the 3,000 Mc/sec. value of μ_R at 77°K in terbium for fields up to 5.5 kOersted suggests that the small permeability at this temperature is not associated with domain wall motion. This is further substantiated by the difference between the qualitative variations of μ with temperature in zero static field at low frequencies (10) and the high frequency results. In the low frequency measurements a large "bulge" in μ is observed below T_c when the specimen is cooled, and this shows considerable temperature hysteresis. At 3060 Mc/sec., μ_R decreases much more rapidly with decreasing temperature below T_c, and the only temperature hysteresis detected is a possible small hysteresis in T_c. This qualitative difference may be interpreted in the following way. At low frequencies the domain wall motion will make a large contribution to μ in the ferromagnetic phase. For a given applied alternating field, the domain wall motion will have the largest amplitude when M_s, the saturation magnetization is least. This will occur at

temperatures just below T_c. The measured permeability in this temperature region will therefore be most sensitive to the details of the ferromagnetic domain structure, and thermal hysteresis in this structure will lead to thermal hysteresis in μ. The absence of such hysteresis at 3060Mc/sec. is taken as an indication that domain wall motion is no longer significantly contributing to the permeability.

The rapid decrease in μ_R with temperature below T_c at high frequencies is also found in dysprosium (figure 4.13) and may again be compared with the much more gradual decrease at low frequencies (10), where it is also accompanied by thermal hysteresis.

In the case of holmium there is no direct evidence that domain wall motion is not appreciably contributing to μ_R at 6377 Mc/sec. However, it seems reasonable to suppose that at a frequency fully an octave higher that than at which domain wall motion is insignificant in terbium, the measured permeability will be due to non-domain wall processes.

In each of the specimens, peaks in μ_R are found at the known magnetic ordering transitions. A comprehensive theoretical treatment of these is exceedingly difficult, and various attempts have been made to derive the behaviour of the static magnetic susceptibility in the

region of the transition from the paramagnetic to the magnetically ordered phase (11). The peaks occuring when the metal is switching from one magnetically ordered phase to another occur both in the absence of applied static field, as in the present work, and also at constant temperature when a field sufficient to switch the ordering from one state to another is applied (12). One might qualitatively think of these peaks in μ_R as being due to a general instability in the magnetic system, when two kinds of ordering are more or less equally favoured. Under such conditions it will be energetically relatively easy to move the spins from one orientation to another, leading to an increase in the magnetic susceptibility.

In terbium, at temperatures above T_N, the fact that $(\mu_R - 1)$ at 3,000Kc/sec. is at least an order of magnitude smaller than the static magnetic susceptibility shows that the relaxation of the spin system has a characteristic time τ greater than or of order of 10^{-9}sec. This is consistent with the theory reviewed by Winter (13), where he shows that in the paramagnetic region $1/T_1 \doteq 1/T_2 \doteq (\nu_e)/(\nu_n)^2$, using the notation of 2.(iv)a. For terbium, the estimate of this quantity made in chapter 2 is$\doteq 10^{-7}$ sec.

(b) Application to n.m.r.

In absence of measurements of μ_L, it is impossible

to evaluate $X'_e = \mu' - 1$ and $X''_e = \mu''$ separately. However, the expression on page 2.8 we derived for the fractional change ($\delta Q/Q$) in the quality factor Q of a cavity due to n.m.r., shows that both components of X_e contribute to the observed enhanced signal. A knowledge of the individual components is therefore not necessary provided we only want an estimate of the magnitude of $\delta Q/Q$. The estimates of enhancement in this section are made assuming that $(\mu_R - 1)$ measures an effective electronic susceptibility X_e leading to enhancement of the microwave field of $X_e\beta$. On this assumption, and using the values of given in table 2.1, the effective enhancement for terbium and holmium is obtained, and the result is shown in figures 4.15 and 4.16.

In the case of holmium, it is an attractive possibility to gain enhancement of n.m.r. by working on the permeability peak at about 19°K. The search for n.m.r. in holmium was made with the cavity in liquid hydrogen at atmospheric pressure (T = 20.3°K) and under these conditions μ_R is appreciably increased by the presence of the ordering transition. The ordering on the high temperature side of the transition is plane helical, and from the point of view of n.m.r. linewidth this may be preferable to the conical ordering on the low temperature side (2.(iv)b). However, it is possible that relaxation of n.m.r. will be faster near an ordering transition, as the tendancy to instability in the electronic spin system will have

Figure 4.15

enhancement factor $X_e\beta$ for terbium crystal

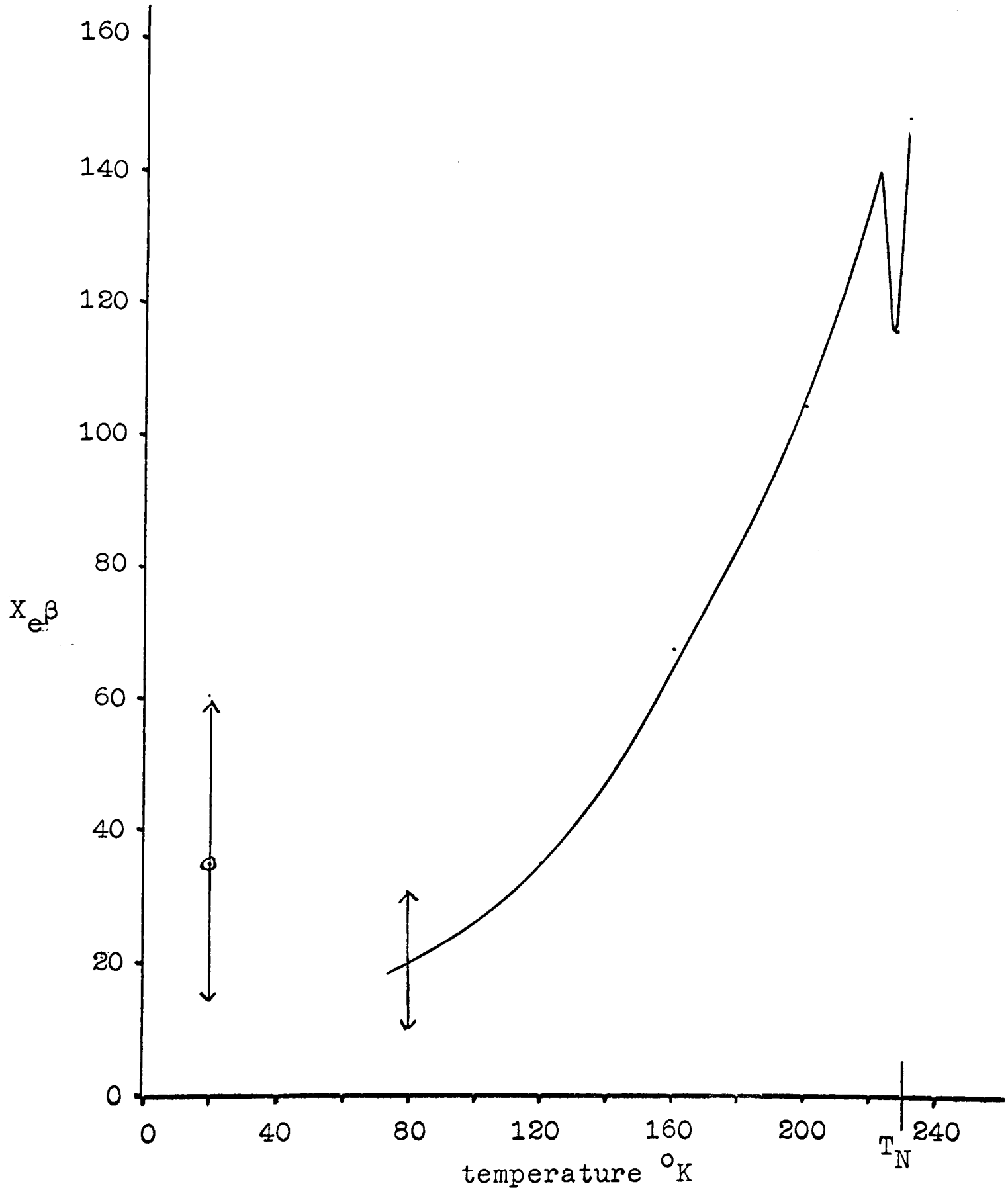

Figure 4.16

enhancement factor $X_e\beta$ for holmium crystal

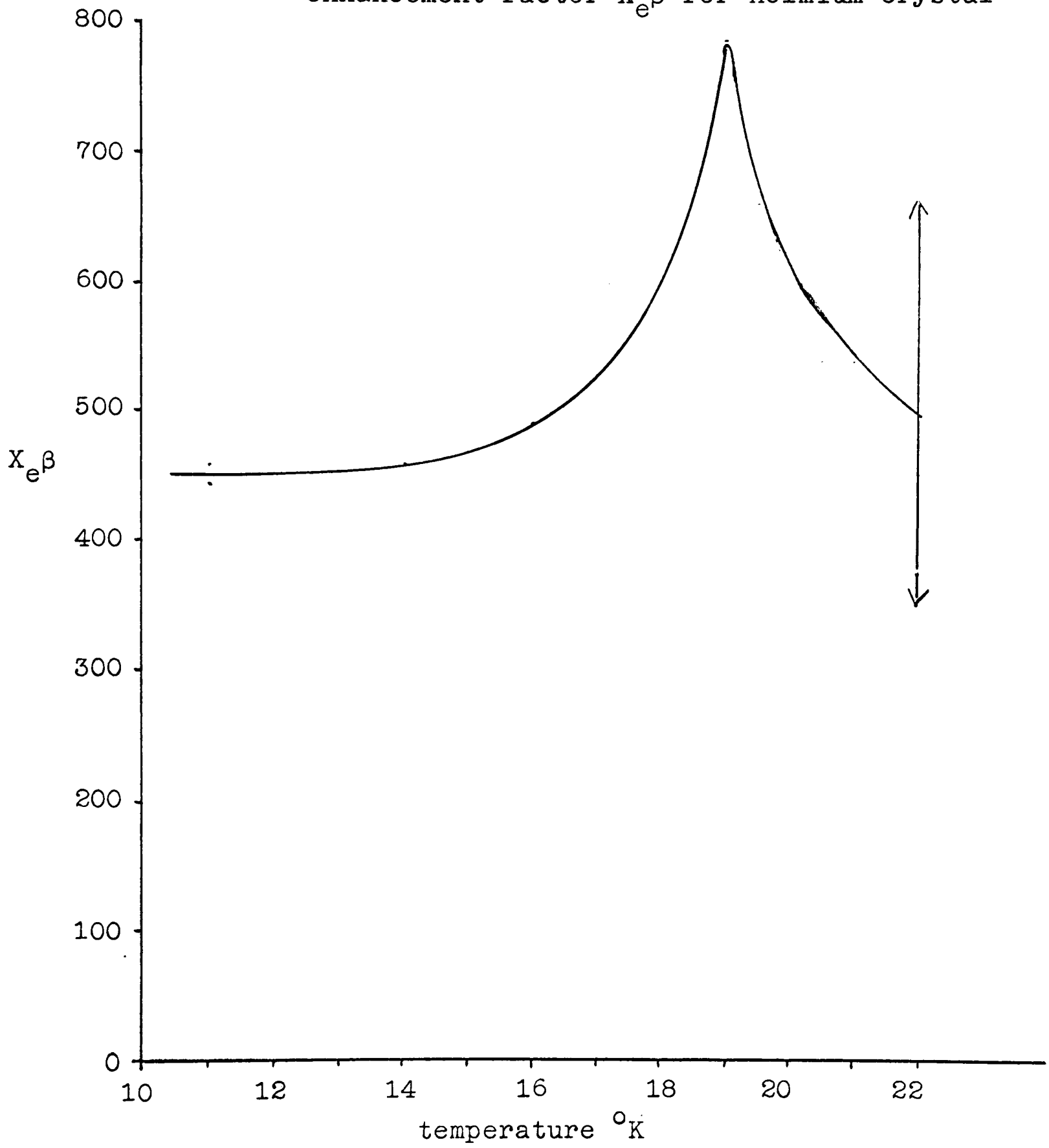

Figure 4.17

mininum enhancement factor $X_e\beta$
for dysprosium crystal

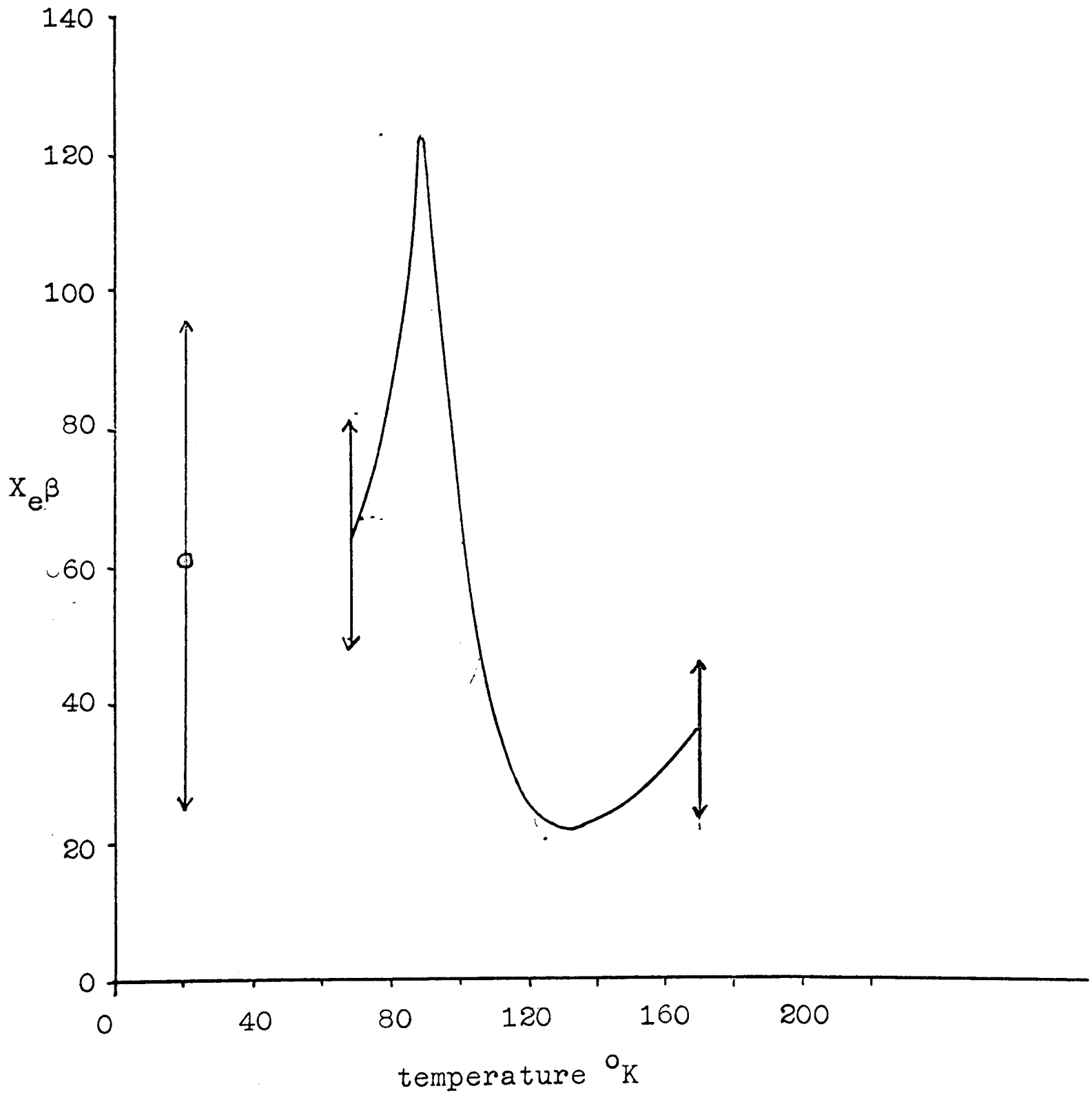

associated with it fluctuations in the directions of the individual moments. As we noted in chapter 2, the relaxation times are already probably shorter than is desirable, and it may be unwise to add to the problems this leads to for the sake of additional enhancement.

In the case of terbium, the enhancement at low temperatures is particularly uncertain, but it is not likely to be greater than 30 at 77°K. Below this the apparent increase of $\mu_R - 1$ may be deceptive due to a possible undetermined roughness correction, but if at least it does not decrease below 77°K, it will be advantageous to search for n.m.r. at as low a temperature as possible to obtain long relaxation times. The search for n.m.r. in terbium was performed on the crystal at 72°K and 77°K, partly because it was feared that the enhancement would, in fact, decrease further at lower temperatures.

In terbium the enhancement increases with temperature up to T_c, at about 220°K. However, we anticipate that fast relaxation will become an ever increasing problem as the temperature is increased. Also, the rate of change in the n.m.r. frequency with temperature, which is about 5 Mc/sec./°K at 77°K from saturation magnetization data, will steadily increase with temperature. As the n.m.r. frequency rapidly decreases towards zero at T_N, very close temperature control will be necessary. Furthermore, the

hyperfine interactions are well known at low temperatures, and an additional drawback to searching for n.m.r. at temperatures near to T_c or T_N would lie in the considerable uncertainty in knowing what frequency to use.

The n.m.r. frequencies at 0^oK in dysprosium are 1140Mc/sec. and 820Mc/sec., both much lower than 3060Mc/sec., that at which our measurements of μ_R were made. As mentioned at the end of chapter 2, domain wall enhancement may possibly operate at the n.m.r. frequency, but whichever enhancement mechanism operates, the values of μ_R at 3060Mc/sec. may be regarded as providing a lower limit on enhancement. This lower limit enhancement factor $(\mu_R - 1)\beta$ is shown in figure 4.17. Unfortunately, as in the case of terbium, the experimental values of μ_R are least certain in the temperature range most interesting for attempts to observe n.m.r., that is, as $T \rightarrow 0^oK$, and the relaxation is becoming as slow as possible.

Chapter 4: References.

1. G.T. Rado in "Advances in Electronics" II 1950 (Academic Press)

2. M.H. Johnson and G.T. Rado: Phys. Rev., 75, 841 1949

3. B.I. Bleaney and B. Bleaney: "Electricity and Magnetism" 247 (1st edn.) Oxford University Press.)

4. "The Microwave Engineer's Handbook and Buyer's Guide" 1963 Edition. T-62.

5. D.L. Strandburg, S. Legvold and F.H.Spedding: Phys. Rev. 127, 2046 1962.

6. P.M. Hall, S. Legvold and F.H. Spedding: Phys. Rev. 117, 972 1960.

7. M.D. Wilding: (University of Sheffield) Presented at Conference on Rare Earth Metals, Durham, May 1965.

8. D.E. Hegland, S. Legvold and F.H. Spedding: Phys. Rev. 131, 158 1963.

9. R.V. Colvin, S. Legvold and F.H. Spedding: Phys. Rev. 120, 741 1960.

10. L.B. Robinson, S-I Tan and K.F. Sterrett: Phys. Rev. 141, 548 1966.

11. C. Domb: Chapter 1 in "Magnetism" IIA, G.T. Rado and H. Suhl editors, (Academic Press 1965).

12. R.B. Flippin: J.App. Phys. 34, 2026 1963.
J. Leisegang: D.Phil. Thesis, Oxford University 1965.

13. J.M. Winter: Jour. Phys. et le Rad. 23, 556 1962.

Chapter 5.

Field Dependence of Microwave Absorption in Bulk Terbium, and some Magnetic Properties of Terbium Powder.

(i) Introduction.

Both the microwave and the low frequency experiments described in this chapter are performed using the appropriate adaptations of the variable temperature apparatus described in 3. (ii)c. The microwave frequency used is ≙ 3,000 Mc/sec. The temperature is measured by a copper-constantan thermocouple soldered to the outside of the experimental chamber which is, in the first case, the microwave cavity, and in the second, the brass cylinder holding the mutual inductance. When applied, the static field is perpendicular to the axis of the cavity.

The qualitative static magnetization of the powder is measured using a Faraday balance described elsewhere (1). In the present work the source of static magnetic field and field gradient is a small solenoid with its axis coincident with the line of the thread suspending the specimen.

(ii) Field dependence of microwave absorption in bulk terbium.

We have made qualitative observation of microwave

power absorption in the terbium crystal using the continuous recording method described in 4.(ii)c. The investigations of this section are confined to the temperature range 210°K to 240°K, and the variation of temperature is achieved by submerging the vacuum jacket of the variable temperature apparatus in liquid nitrogen, and passing the necessary current through the 350ohm heater coil. Two maxima in power absorption are observed in this temperature range, associated with the two terbium ordering transitions. It is found that if a static field is applied perpendicular to the c-axis of the crystal and the temperature continuously varied through the ordering transitions, the Curie temperature remains almost constant as the field is increased to 5kOe, but the Neel temperature decreases steadily. The maximum in power absorption at T_N becomes less pronounced as the field is increased and the maximum at T_c broadens considerably. Above about 4kOe, the maximum at T_N is no longer distinguishable from the high temperature wing of the maximum at T_c. The transition temperatures indicated by the thermocouple on warming up and on cooling down through the ordering transitions in various fields are given in Table 5.1.

Table 5.1

H(kOe)	warming			cooling			average
	T_c	T_N	T_N-T_c	T_N	T_c	T_N-T_c	T_N
0	222.2	230.7	8.5	229.7	219.4	10.3	230.2
1.5	222.2	230.4	8.2	229.0	219.4	9.6	229.7
2.0	222.5	230.0	7.5	228.8	219.9	8.9	229.4
3.1	222.5	229.4	6.9	228.4	219.9	8.5	228.9
4.0	222.5	228.4	5.9	227.4	219.9	7.5	227.9
5.0	223.2	-					

The warming and cooling rate in all cases is approximately constant at about one degree in two minutes. If we assume that the apparent differences in Neel temperatures obtained between cooling and warming is only due to the temperature gradient between the specimen and the thermocouple, the true value of T_N will be obtained by averaging the two results. The average value plotted against static field is shown in figure 5.1.

The magnetization data of Hegland et al. (2) shows that the "bump" in the magnetization-temperature curves at T_N becomes indistinguishable when, due to an increasing applied field, T_N has moved by about 2°K. Our microwave measurements are consistent with this. The difference of about 1.6°K between T_N-T_c obtained on cooling and

Figure 5.1

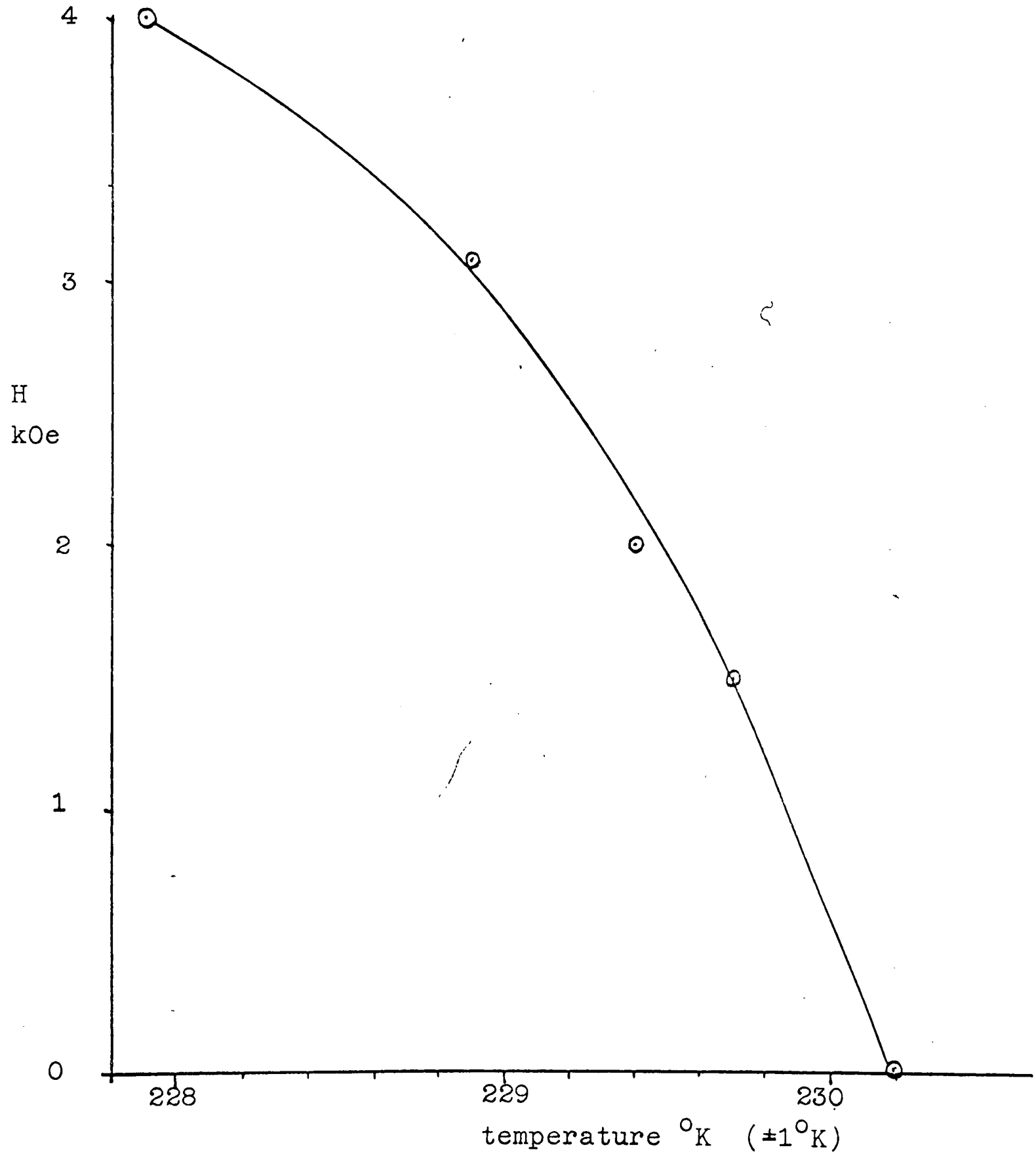

that obtained on warming does not necessarily indicate thermal hysteresis in T_c. We discuss this point in more detail in section (iii).

A preliminary measurement of microwave power absorption as a function of temperature and in zero applied field was made on this terbium specimen before it was either etched or annealed. The surface was then the relatively strained one left by the spark-lathe process used to make the crystal into a uniform diameter rod. Only one maximum in power absorption was observed, occuring at the normal Neel temperature.

(iii) Some Magnetic Properties of Terbium Powder.

(a) Absorption of microwaves at 3,000Mc/sec.

The qualitative temperature variation of microwave absorption in the terbium powder sample (3.(i)) is observed again, the same method as that outlined in the preceding section for the terbium crystal rod. A copper centre conductor is used in the cavity, and the powder is held in paraffin in a p.t.f.e. boat. Only one peak is observed in the variation of microwave absorption with temperature, and this occurs at 230°K, the normal terbium Neel temperature. The microwave absorption results give no evidence of a second magnetic ordering transition down to 77°K.

Application of a static field to the powder at

77°K measurably reduces the absorption of the microwaves. The rate of decrease of absorption with field is steadily increasing up to 5.5kOe, the limit of our observations. The same effect has been observed by Gossard in annealed terbium powder (3),* and it reveals the presence of a considerably greater μ_R than that found at 77°K in the bulk terbium.

(b) Low frequency susceptibility and static magnetization measurements.

Using the mutual inductance method described in 3. (iv), observations have been made of the qualitative variation with temperature of the magnetic susceptibility of the terbium powder at 135c/sec. The results are compared with those obtained for the terbium polycrystal and single crystal rods under the same conditions (figure 5.2). The peak in powder susceptibility occurs at 230°K, and down to 77°K there is no indication of any other magnetic ordering transition.

---

* Gossard used 25 gms. of terbium powder in a coaxial line. His microwave frequency was ≐3,000Mc/sec. and the temperature 77°K. We quote from page 75 of his thesis:- "On warming above the ferromagnetic Curie temperature and on placing the sample in fields of more than 1,000 gauss, the r.f. sample losses decreased by 70°/o, indicating that a considerable portion of the sample losses are magnetic in character".

Figure 5.2

comparison of the qualitative variation with temperature of magnetic susceptibility χ at 135 c/sec. for bulk and powder terbium samples.

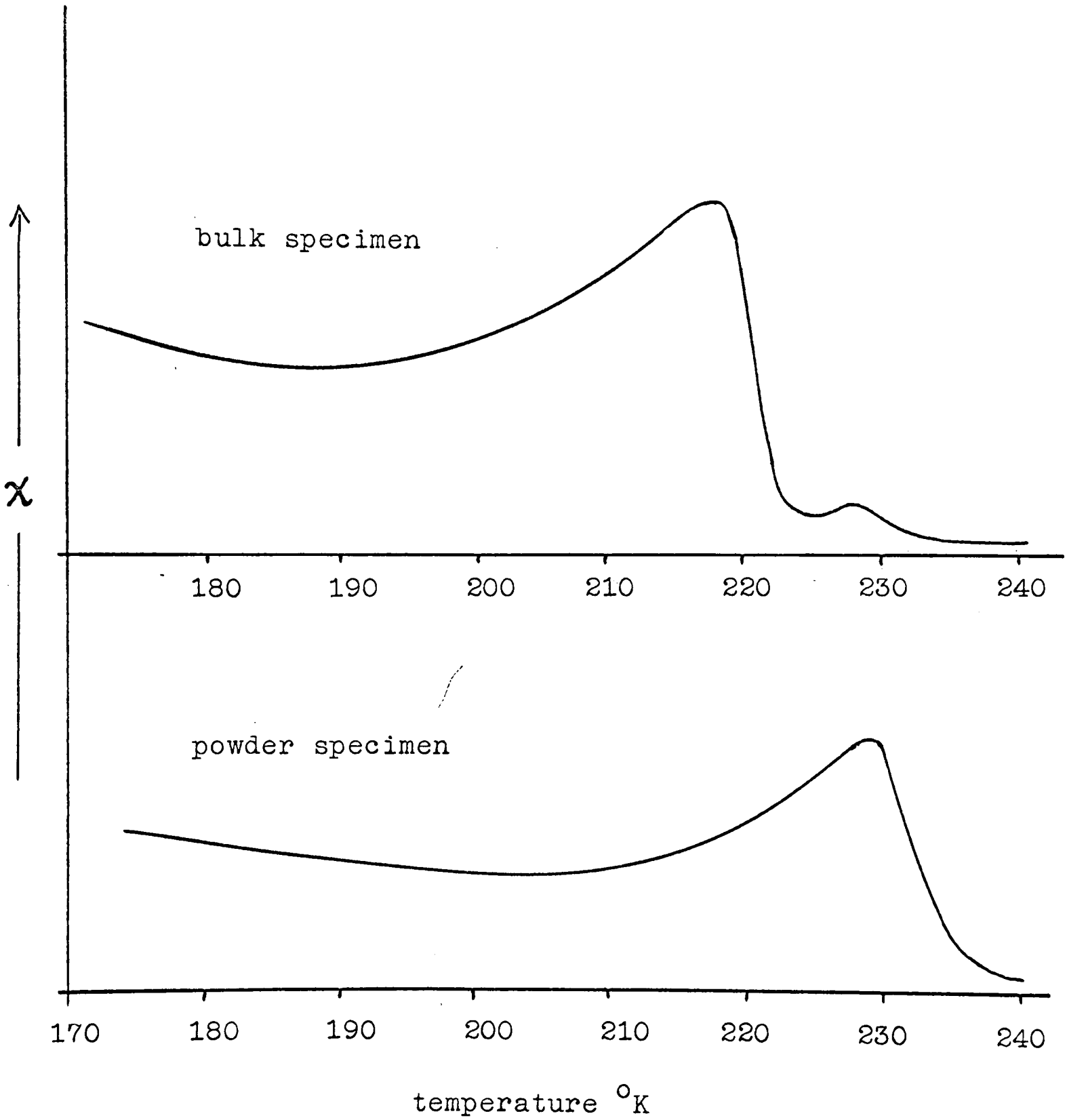

Static magnetization measurements made on the powder on warming up from 77°K are shown in figures 5.3 and 5.4. The readings of magnetization are taken by applying at a fixed temperature a field of 30 Oe followed by one of 70 Oe, and reducing again to zero field while the specimen is warmed up to the next temperature. The results in figure 5.3 are obtained when the only field present during cooling is the earth's field. If the specimen is cooled in presence of a static field of order 40 Oe, the results in figure 5.4 are obtained. It appears that in this case the specimen acquires a "frozen in" magnetic moment during cooling. In either case, hysteresis effects are observed at 77°K if the field is cycled between 0 and 200 Oe. Only one magnetic ordering transition is observed in these magnetization measurements, and this occurs at 227±3°K.

(iv.) Discussion of results.

All the results obtained with the terbium powder indicate that only one magnetically ordered phase occurs. This sets in at the normal Neel temperature and persists to low temperatures. The static magnetization measurements show both hysteresis, and under some conditions a nett magnetic moment at low temperatures. Both features are characteristic of ferromagnetism. The microwave absorption in the strained surface of the terbium crystal also

Figure 5.3

magnetic moment σ (arbitrary units) vs. temperature for terbium powder after cooling to 77°K in zero applied field.

measuring fields: I. 70 Oe
II. 30 Oe

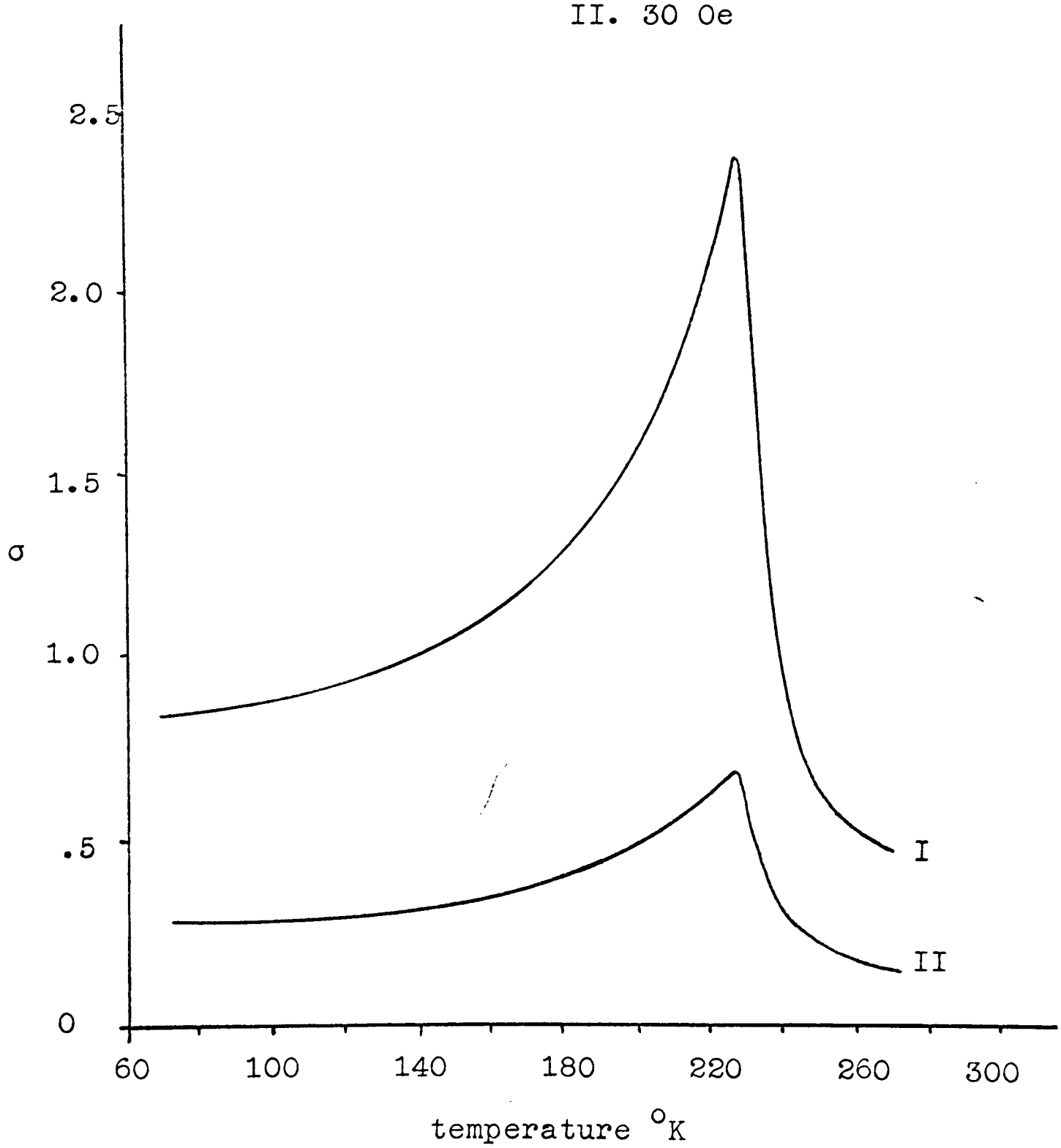

Figure 5.4

magnetic moment σ (arbitrary units) vs. temperature for terbium powder after cooling to 77°K in a static field of 40 Oe.

measuring fields: I. 70 Oe
II. 30 Oe

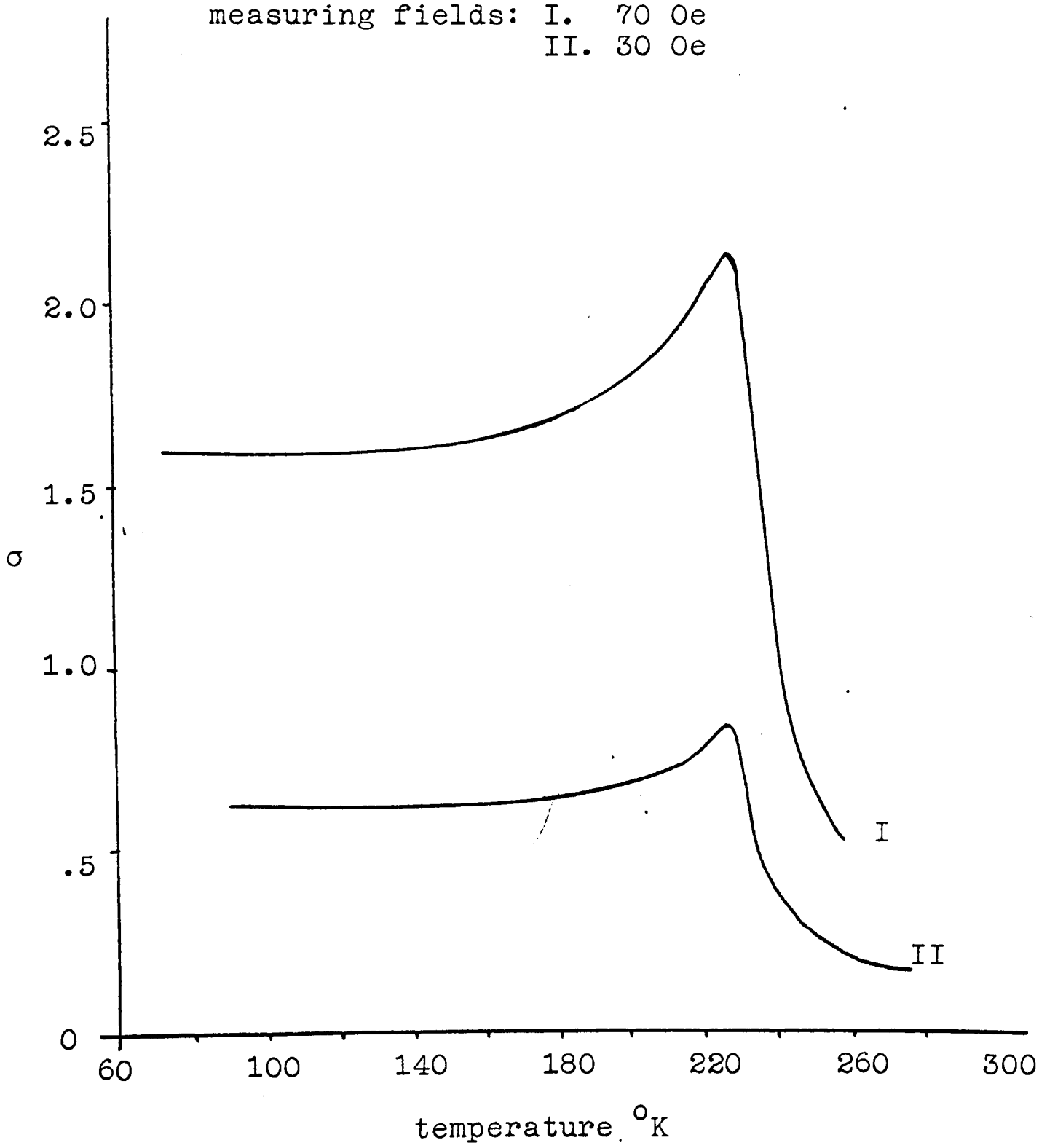

indicates the presence of only one magnetically ordered phase, suggesting that strains supress the helical ordering. Further evidence for this is found in neutron diffraction measurements on bulk terbium, which show that the turn angle in the helical phase is very sensitive to the purity and possibly also the state of anneal of the specimen (4). X-ray diffraction measurements made on some of the powder sample show it to be about 90°/o terbium and 10°/o unidentified terbium compounds, probably mostly oxide. The grinding process used to produce the powder will have introduced considerable strain into the particles, and the X-ray patterns show some broadening due to this.

The large field dependence of microwave absorption at 77°K shows that the ferromagnetism of the powder must differ in some way from that of the bulk terbium. We note that this is found both in annealed (3) and unannealed powder, and it is therefore presumably associated with the particle size or impurity, rather than strain. One possible difference is that the particles may not have any domain walls. Kittel (5) shows that the critical radius for a particle to be a single domain varies as σ_w / M_s^2 , where σ_w is the energy required to form the domain wall, and M_s is the saturation magnetization. He takes MnBi as an example of a ferromagnet with high axial

magnetic anistropy and shows that the critical radius is about 4×10^{-5}cm., corresponding to an M_s of order 600 emu/cc. This radius is comparable to that of our terbium particles. However, the saturation magnetization is very much greater in terbium, being about 2.4×10^{3}emu/cc. Detailed calculation of the energy of the most favoured domain wall configuration in terbium would be necessary before a reliable estimate of the critical radius could be made, but it is certainly possible that the particles do not have domain walls. If this is so, an applied field will directly affect the bulk magnetization without first having to overcome demagnetising fields arising from displacement of domain walls, and we may expect a more rapid field dependence of absorption than in the domain wall case. However, if μ_R in zero field is the same both for the powder and bulk samples, the greatest effect of a field will be to reduce μ_R from its value of $\simeq$ 1.2 in zero field to unity when total saturation is reached (we exclude possible resonance effects). The observed change in μ_R in the powder samples is probably much greater than this. It is not obvious why monodomain behaviour should produce a large microwave permeability at low temperatures, and further investigation of the structure of the powder is necessary.

Irrespective of the exact details of the magnetic ordering of the powder, the large μ_R at 77°K still provide

enhancement of the n.m.r., and this will be much greater than that expected in the bulk material. Unfortunately, the difficulty in obtaining a pure, strain free powder sample probably off-sets this advantage at present. In general, n.m.r. measurements on metal powders show that strain free specimens are necessary to obtain tolerable n.m.r. linewidths (6).

In bulk terbium, the apparent thermal hysteresis in the antiferromagnetic to ferromagnetic transition could be a spurious effect due to latent heat emitted or absorbed by the magnetic system, assuming the transition to be a first order one (7). This will modify the warming or cooling rate of the specimen and, as the thermocouple is soldered to the relatively massive brass cavity, this modification has probably escaped notice. More detailed measurements at much slower cooling rates and with more carefully arranged thermometry are necessary to confirm this.

Chapter 5: References.

1. M.R. Brown: D.Phil. thesis, Oxford University 1961.
2. D.T. Hegland, S. Legvold and F.H. Spedding: Phys. Rev. 131, 158 1963
3. A.C. Gossard: Ph.D. thesis, University of California 1960.
4. J.W. Cable: verbal communication 1963.
5. C. Kittel and J.K. Galt: in "Solid State Physics" vol.3 (Academic Press 1956).

6. A. Abragam: "The Principles of Nuclear Magnetism" ch.7 (Oxford: 1961).

7. R.J. Elliott: Ch.7 in "Magnetism" IIA, G.T. Rado and H. Suhl editors. 1966.

Chapter 6

The Search for n.m.r. in Terbium and Holmium Metals.

(i) Introduction

One of the basic problems encountered in attempts to detect n.m.r. in magnetically ordered heavy rare earth metals lies in constructing a spectrometer suitable for the purpose. The frequency of the n.m.r. is almost completely independent of applied static magnetic field, and so the technique usual in magnetic resonance work, of using constant frequency and variable magnetic field with field modulation, is no longer applicable. A variable frequency spectrometer with either frequency modulation, or using a spin-echo technique, is now necessary. At the frequencies of less than 500kc/sec. at which n.m.r. occurs in most magnetically ordered materials, both approaches have been used extensively. One of the major problems arising from use of frequency modulation, that of eliminating unwanted amplitude modulation, may then be minimized by using a marginal oscillator in which the frequency is determined by a resonant circuit containing the specimen. Marginal oscillators have been used up to frequencies as high as 700kc/sec. (1), but the technique becomes increasingly

difficult to apply at higher frequencies, especially if the specimen has to be kept at a low temperature.

Use of spin-echoes(2) avoids these problems arising from frequency modulation and also partly eliminates effects due to inhomogeneous broadening of the n.m.r. To apply the spin-echo technique, it is necessary to invert the spin system in a time short compared to the spin-spin relaxation time T_2. This requires that $\gamma H_1' >> 1/T_2$, where γ is the gyromagnetic ratio of the nucleus and H_1' the oscillatory field at the nuclear sites. It is notable that in europium and gadolinium, where domain wall enhancement operates giving a large H_1', and the values of T_2 are likely to be relatively long, n.m.r. has been detected by this method (3). However, in the non S-state heavy rare earth metals we have noted that T_2 is likely to be less than 10^{-5} sec. (see ch. 2. (iv)a). H_1' must then be at least 1 kOe. When domain-wall enhancement operates, a value of H_1' as large as this is relatively easy to obtain. Unfortunately, it is doubtful if this enhancement mechanism does operate in most of the non S-state heavy rare earth metals, and the problems of obtaining sufficient microwave power, combined with those arising from the necessary very short pulses ($<T_2$) will then be very difficult to overcome.

In our attempt to detect n.m.r. in terbium and holmium we chose to use a continuous wave spectrometer.

In these metals the resonances at 0°K occur respectively at 3,000 Mc/sec. and 9,500 Mc/sec. both of which lie well within the microwave range. After abandoning an attempt to develop a marginal oscillator, we finally constructed a spectrometer using the double modulation method applied by Gossard (4) at lower frequencies to observation of n.m.r. in Ne^{57}. The principle of this method is outlined in chapter 2, section (iv), and a block diagram of the spectrometer we have used to apply it at microwave frequencies is given in figure 3.1. The microwave equipment shown in this diagram refers to the application in the region of the holmium n.m.r. frequency (9,500 Mc/sec.). That used in the region of the terbium n.m.r. frequency (≈9,000 Mc/sec.) is shown in figure 4.1. The associated electronics is the same in both cases.

The form of the Redfield equations (2.(iv)) shows that, for successful operation of the spectrometer it is necessary that the inverse of the spin-lattice relaxation time should lie between the two modulation frequencies. These are chosen to be 25 c/sec. and 100 kc/sec. The discussion of 2.(iv)c suggests that it is unlikely that the spin-lattice relaxation time at the working temperature (20.3°K for Ho, 77°K or 72°K for Tb) will be greater than 1/25 sec., and if it is less than $1/10^5$ sec. it will not be possible to meet the necessary saturation conditions, and

Figure 6.1

Microwave Spectrometer

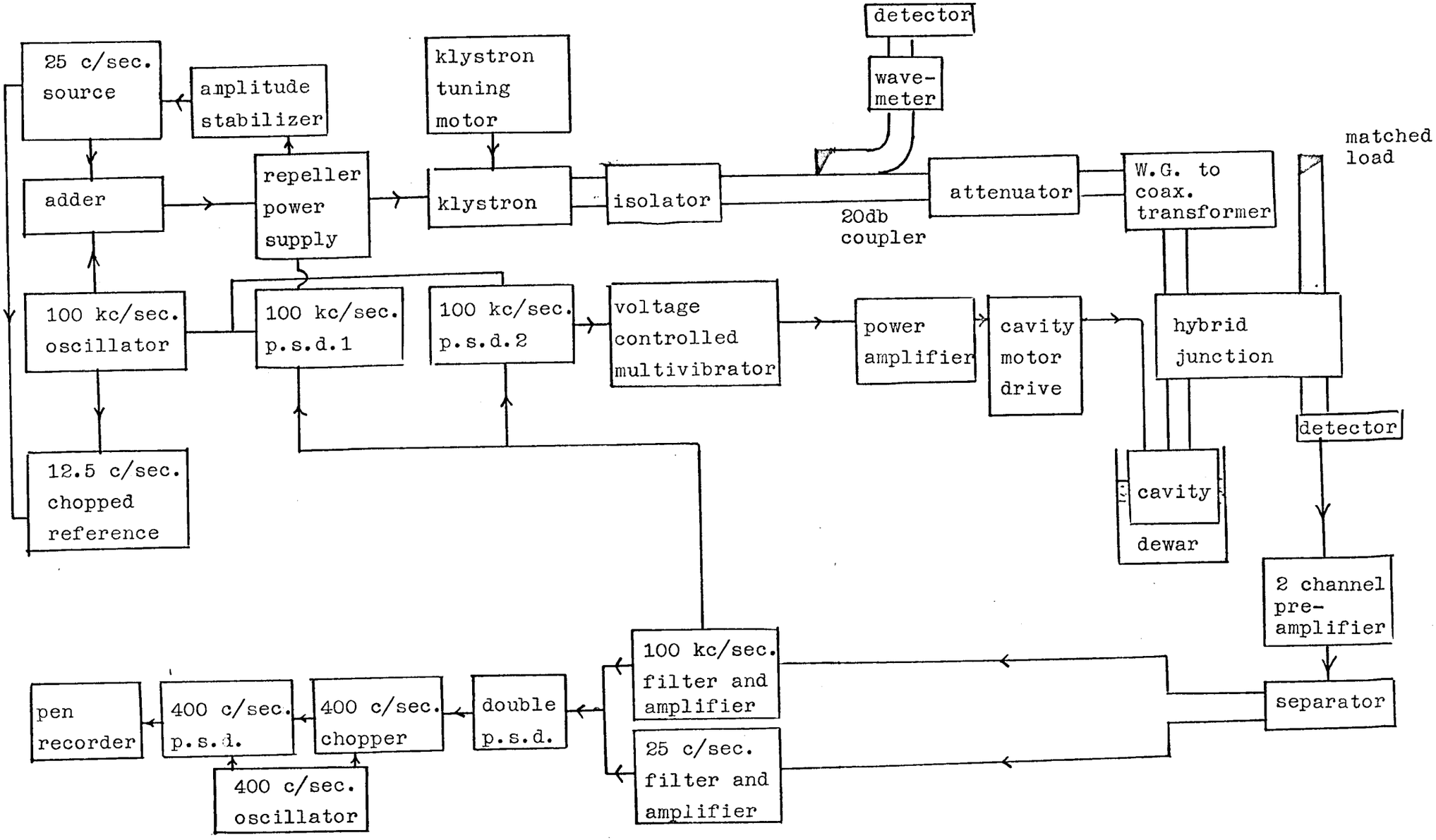

the n.m.r. will be observed more or less equally at both frequencies in any case.

The operation of the spectrometer is, in principle, quite simple. As the specimen cavity resonant frequency and the microwave frequency are continually varied, close coincidence is maintained between them. The microwaves are frequency modulated at the two frequencies, reflected from the cavity and detected. The second harmonic signals and other unwanted mixing term signals are rejected by various filters and the two fundamental signals at 35 c/sec. and 100 kc/sec. are fed into the double phase sensitive detector, which converts them into a d.c. voltage proportional to the difference between their amplitudes. This final signal is amplified using a 400 c/sec. chopper and phase sensitive detector, and is monitored by a pen recorder.

A more detailed description of the microwave equipment and some of the electronics, and also of some of the problems arising in practice, is given in the following sections.

6. (11) <u>Microwave generation, handling and detection.</u>

The microwave source used in the search for n.m.r. in terbium is an E.M.I. klystron type 2K6112[a] mounted in an external cavity. It may be tuned mechanically from 2,700 Mc/sec. to 3,500 Mc/sec., and in the middle of this

range generates a nominal 150 milliwatts of microwave power. The main klystron mode is about 18 Mc/sec. wide, and the whole mode is traversed by varying the repeller potential through about 50 volts. The klystron works directly into a continuously variable waveguide attenuator followed by a waveguide to coaxial line transformer. The remainder of the microwave apparatus consists of coaxial line fittings, and is shown in figure 4.1. The specimen cavity is the tunable cavity shown in figure 3.3.

In the search for n.m.r. in holmium an E.M.I. klystron type R9701 is used. This also is mounted in a mechanically tunable external cavity, and generates a nominal 150 milliwatts of microwave power in the middle of its range. It may be tuned mechanically from 5,800 Mc/sec. to 8,000 Mc/sec. and has a mode width of about 15 Mc/sec. The whole mode is traversed by varying the repeller potential through about 35 volts. The remaining microwave equipment consists of the waveguide and coaxial line components shown in figure 6.1. The specimen cavity is that shown in figure 3.4.

In both frequency ranges the microwaves are detected using A.E.I. crystal diodes type CS9B or CS10B.

6. (iii) Modulation, stabilizing and signal processing.

(a) Modulation.

Frequency modulation of the microwaves is provided by applying the appropriate voltage waveform to the klystron repeller. The waveform is obtained by adding the outputs of a 100 kc/sec. quartz-crystal stabilized oscillator and a 25 c/sec. (a.f.) source. The a.f. is generated by subdividing the mains frequency using an Eccles-Jordan bi-stable circuit. Use of the 25 c/sec. subharmonic of the mains frequency has advantages later in the spectrometer when it is desired to reject the second harmonic of the a.f. The filters tuned to reject 50 c/sec. then also serve to remove all spurious mains frequency pick-up from heater supplies, earth loops and so on.

The amplitudes of the 25 c/sec. and 100 kc/sec. modulations are approximately equalized by taking a sample of the "adder" output, amplifying and detecting this to give a d.c. signal proportional to the difference between the two amplitudes. This is then used to operate an amplitude control on the a.f. source output, in such a way as to minimize the difference.

The depth of modulation which may usefully be applied is limited by the bandwidth of the specimen cavity, which acts as a discriminator producing a large depth of amplitude modulation (a.m.) on the microwaves. Under

working conditions, when the cavity resonant frequency is coincident with the microwave frequency, the principal a.m. occurs at 100 kc/sec.±25c/sec., 50c/sec. and 3.0kc/sec. If this amplitude modulation is too large, saturation of the preamplifier occurs. The maximum depth of frequency modulation which is conveniently applied is about 300 kc/sec. peak to peak overall.

(b) Stabilizing systems.

During operation, the microwave frequency is varied continuously by driving the klystron mechanical tuning with a synchronous motor running off the mains supply. It is necessary that the specimen cavity resonant frequency should remain as close as possible to the microwave frequency, and this is achieved by a combination of two methods. Both depend on the 100 kc/sec. amplitude modulation produced by discrimination at the cavity when the resonant frequency differs from the microwave frequency. This error signal is detected, amplified and separated from the other frequencies present, and fed into the two phase sensitive detectors p.s.d.1 and p.s.d.2. The d.c. voltage output of p.s.d.1 is fed onto the klystron repeller to move the microwave frequency toward the cavity resonant frequency. The output of p.s.d.2 controls the frequency of a multivibrator about some free running value. The multivibrator free-running

frequency (i.e. that at which it operates in absence of an error signal) is chosen so that the corresponding cavity tuning rate is approximately equal to the klystron tuning rate.

In practice, this double method of stabilizing the microwave and cavity resonant frequencies on a common continuously changing frequency proves very successful. The practical limitation in its efficiency is due to periodic instability known as "hunting". When the error signal amplification exceeds a certain value the stabilizing tends to overshoot, and a periodic variation of the microwave frequency results. This may be damped out by using a long time constant in the phase sensitive detectors. With this particular apparatus, a time constant of 20 sec. allows sufficient error signal amplification to produce the necessary frequency stabilizing.

With this double stabilizing system, both adaptations of the spectrometer may be continuously run over the full fine tuning range of the respective cavities. For the 10cm. cavity, the motor speeds are chosen so that the full frequency sweep of 30 Mc/sec. takes about 3 hours. For the 4 to 5 cm. wavelength cavity, the full frequency sweep is arranged to take about 1.5 hours, covering 35 Mc/sec.

In both cases it is found that there is considerable variation of cavity power reflection coefficient with

frequency. This is due to dependence of the cavity quality factor Q on frequency (Appendix C), and it makes it impossible to maintain over a wide frequency range the nearly critical cavity coupling conditions (i.e. power reflection coefft. ≃ 0) necessary for use of superheterodyne detection. This is a serious limitation, as the dominant source of noise in the spectrometers is the microwave detector. We return to this point in section (iv) of this chapter.

(c) Signal processing.

After detection of the microwaves, all information relevant to n.m.r. is carried at either 25 c/sec. or 100 kc/sec. It is therefore necessary to reject as thoroughly as possible all other frequencies. The 50 c/sec. and 200 kc/sec. signals produced by discrimination of the microwaves at the specimen cavity are rejected using respectively a twin-tee filter tuned to 50 c/sec. and a low pass filter which passes 100 kc/sec. but not 200 kc/sec. A more difficult problem is presented by the sidebands at 100 kc/sec.$\pm$25c/sec. These are rejected by a filter consisting of two series resonant circuits based on quartz crystals and tuned to 100 kc/sec.$\pm$3 or 4 c/sec. This filter reduces the sidebands by 40 decibels, which is entirely adequate for the present purpose. It is necessary for the oscillator and filter to be sufficiently stable to keep the nominal 100 kc/sec. at the centre of the filter pass-band. This is

achieved by using a quartz crystal to control the 100 kc/sec. oscillator, and by maintaining this crystal and the two in the filter at constant temperature using thermostatically controlled ovens.

After filtering and amplification, the 100 kc/sec. and 25 c/sec. signals are fed into the double phase sensitive detector (figure 6.2). This operates using a switched beam tube ((c), and figure 6.3). The reference signal is produced by switching at 12.5 c/sec. between the 100 kc/sec. and 25 c/sec. sources, giving the waveform shown in figure 6.3. This switches the electron beam between the anodes 1 and 2 at 100 kc/sec. for 1/12.5 sec., and at 25 c/sec. for 1/12.5 sec., and so on. The phases of the 100 kc/sec. and 25 c/sec. on the reference are adjusted so that a signal at 25 c/sec. gives maximum electron beam intensity when the beam is incident on anode 1, and a signal at 100 kc/sec. gives maximum intensity when the beam is incident on anode 2, or vice versa. This leads to a d.c. voltage at "d.c. out" proportional to the difference between the two signal amplitudes. A chopper converts this signal into an a.c. signal at 400 c/sec., and this is amplified and re-formed into a d.c. signal using a 400 c/sec. phase sensitive detector, and used to drive the pen recorder.

If a small discrepancy between the cavity resonant frequency and the microwave frequency develops, this produces

Figure 6.2

double phase sensitive detector

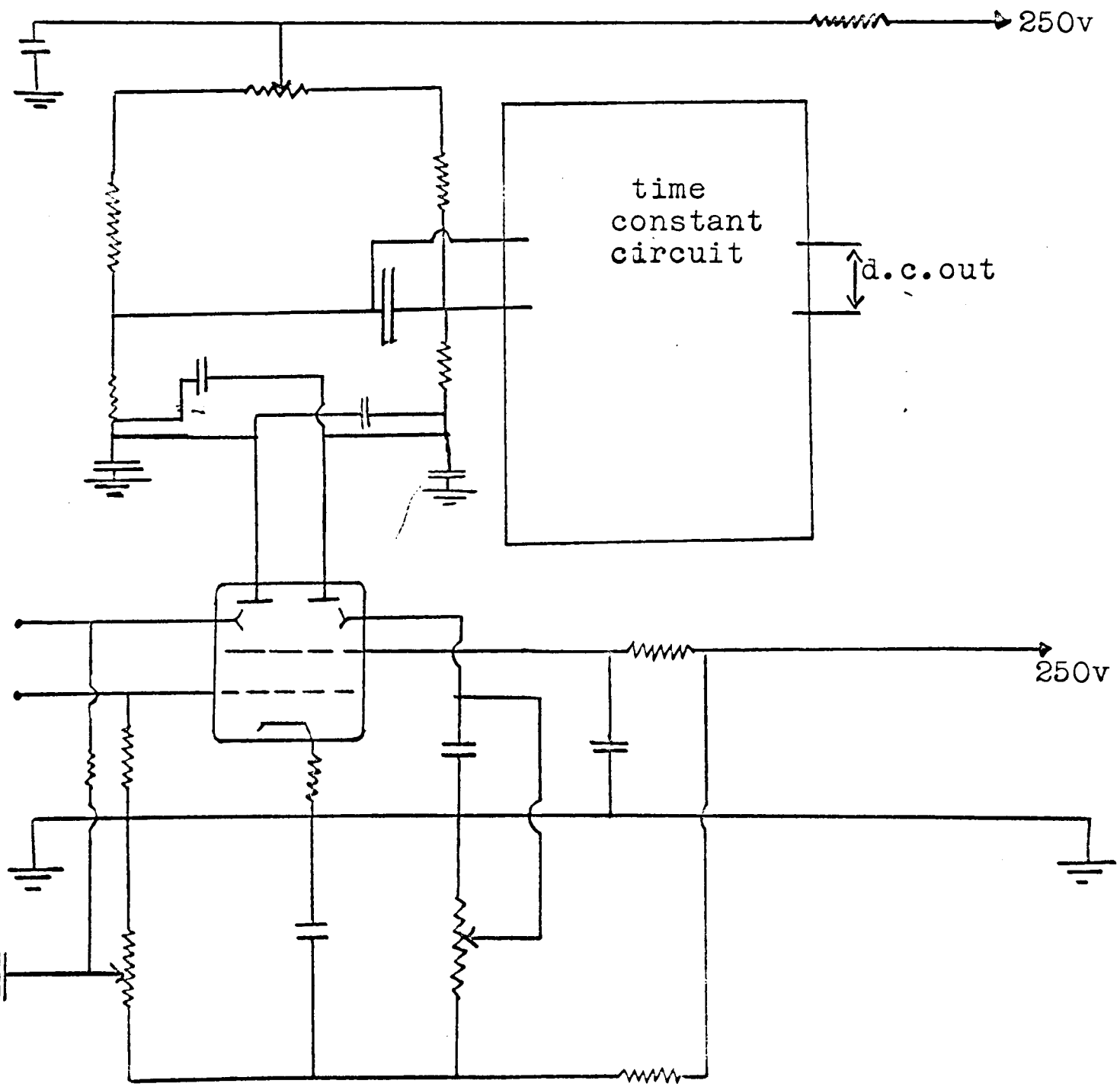

Figure 6.3

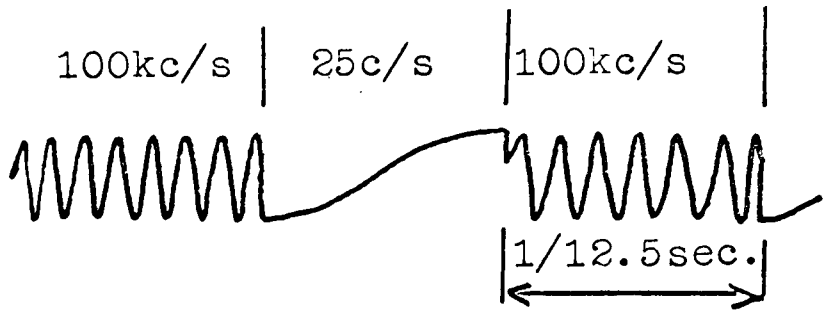

reference signal

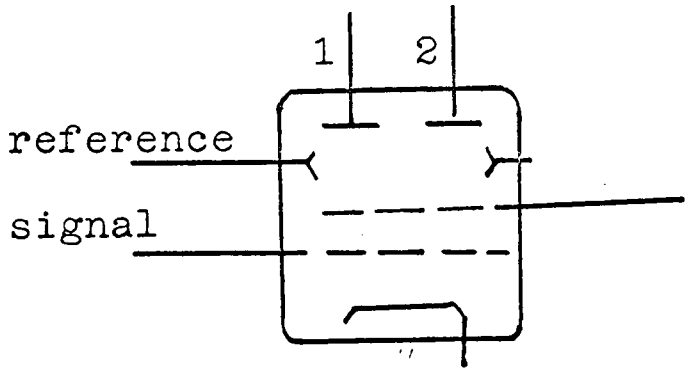

split beam tube

signals with the same phase and amplitude at both 25 c/sec. and 100 kc/sec. Provided the amplification of both signals is the same, they balance out in the double phase sensitive detector. In the 25 c/sec. channel, provision is made for the necessary amplification control.

During operation, a spurious 100 kc/sec. signal is sometimes observed. This is in quadrature with the signal produced by imperfect frequency tracking between the microwaves and the specimen cavity, and its origins are somewhat obscure. Some of it seems to be due to amplitude modulation of the microwaves at the klystron, and it may be partially removed by careful choice of operating position on the klystron output mode. Such a signal would be caused by n.m.r. under conditions of partial saturation (2.(iv)), but the signal we observe persists when a non-magnetic centre conductor is used in the cavity, and it is also found at room temperature, and so it is evidently an instrumental effect. Provided the phases of the 100 kc/sec. phase sensitive detectors are carefully adjusted, this quadrature signal may be efficiently rejected. Its presence is nevertheless unfortunate, as it would be interesting to attempt to detect the signal in quadrature with the frequency modulation produced by the partially saturated n.m.r.

6. (iv) Sensitivity of the Spectrometers.

If the fractional change $\delta Q/Q$ in the cavity quality factor due to the resonant absorption of microwave power in a specimen is sufficiently large, a measurable change is produced in the steady voltage output of the microwave detector. The corresponding change in cavity power reflection coefficient is then easily measured by determining with the microwave attenuator how much attenuation produces the same effect. Using the relation derived in Appendix C, this may then be applied to absolute determination of $\delta Q/Q$.

This approach forms the basis of our experimental determination of the limiting sensitivity of the spectrometers. The electron spin resonance in a sample of an organic compound (d.p.p.h.) is used to produce the necessary change δQ in Q. The resonant conditions are produced by applying a static field of appropriate strength perpendicular to the axis of the cavity, the change in cavity power reflection coefficient is measured and the corresponding fractional change in Q calculated. The frequency modulations are then switched on and the signal detection and processing units adjusted as if under normal running conditions. The field is then modulated at 25 c/sec. to a depth producing a known fraction of the measured $\delta Q/Q$ over the modulation cycle. The electron spin resonance produces a signal in the 25 c/sec. detection channel only, and a corresponding signal is

registered by the pen recorder. The size of this signal is compared with the noise level encountered when the spectrometer is in full operation, and the value of $\delta Q/Q$ corresponding to a signal $\doteq$ x2 greater than the noise is calculated.

In this way it is found that the smallest detectable $\delta Q/Q$ in both the 3,000 Mc/sec. and 9,500 Mc/sec. adaptations of the spectrometer is $\doteq 5 \times 10^{-5}$. The pen recorder displacement remains within a value corresponding to this order of signal size over a frequency sweep typically of 10 Mc/sec. Beyond this, long term drift in the detection system produces larger displacements.

The following calculation shows that the experimental limiting sensitivity is compatable with the limitations imposed by noise generated in the crystal detector. We assume that the microwave power reflected from the cavity is sufficient to put the crystal detector into the region where the rectified current is proportional to the incident power. This is likely to be the case on our spectrometer since, as we have observed, it is impossible to maintain nearly critical coupling over a wide range of frequencies. Following Feher (6) the crystal output of noise power under these conditions is given by-

$$P_N = \left\{ \frac{\gamma P_M}{f} + 1 \right\} kT\delta f,$$

where P_M is the incident microwave power, δf the bandwidth of the detection system, f the frequency about which this is situated, and T is the detector temperature. The dominant contribution to this expression will be due to the first term, describing the flicker noise, and the contribution at 25 c/sec. will completely outweigh the contribution at 100 kc/sec. The detection system bandwidth around 25 c/sec. is of order 10 c/sec. and so

$$P_N = \frac{P_M}{25} 10\ kT$$

If we assume that the crystal is about as noisy as the 1N23 used by Feher, γ is $\doteq 10^{11}$ $(watt\text{-}sec)^{-1}$. The crystal is operated at room temperature, and therefore $kT \doteq 4x10^{-21}$ joules. The noise power generated by the crystal is then

$$P_N \doteq \frac{10^{11} x 4x10^{-21} x 10 P_i}{25}$$

$$\doteq 1.6x10^{-10} P_i .$$

If P_o is the microwave power incident on the cavity and the cavity power reflection coefficient is 20db, the power incident of the crystal detector for the bridge system shown in figures 4.1 and 6.1 is $(1/4)(1/100)P_o$ and hence $P_N = 4x10^{-13} P_o$.

If the signal produces a fractional change $F = (\delta Q/Q)$ in the cavity quality factor, this leads to a power change $P = \frac{1}{4}.\frac{1}{4} P_o F^2$ at the detector when the cavity is critically coupled, and a smaller change otherwise. A typical crystal conversion factor of about 1/3 then leads to a signal after the crystal of $(1/48)P_o F^2$. If this is about x10 above the noise, corresponding to a signal to noise ratio on the recorder chart of about 3, the corresponding value of F is given by:-

$$10 \doteq \frac{\frac{1}{48} P_o F^2}{4 \times 10^{-13} P_o}$$

$$\text{hence} \quad F^2 \doteq 10^{-11}$$

$$\text{and} \quad F \doteq 3 \times 10^{-5}$$

which is consistent with the measured value.

Experimentally, the detected noise level is constant for any given microwave power incident on the detector crystal, regardless of whether or not the microwaves are frequency modulated, or whether they are reflected off the cavity or have come directly from the klystron. Reduction in the power level leads to reduction in the noise. This test at least shows that the noise arises before the signal processing electronics, and that it is not due to microphonics in the cavity. It does not, however, distinguish between oscillator (i.e. klystron) noise and

crystal detector noise. It is possible that the rather poor sensitivity of the spectrometers could be improved by using a higher a.f. modulation frequency. If, for example, 250 c/sec. were used, the crystal noise would decrease by a factor 10, improving the signal to noise ratio, which is a ratio of voltages, by $\sqrt{10}$. However, this would cease to be advantageous when the modulation frequency became comparable to the inverse of the spin-lattice relaxation time. Furthermore, drift in the detection system is beginning to be a problem even at the present level of sensitivity, and it is doubtful if any substantial improvement could easily be effected.

6. (v) The search for n.m.r.

Using the spectrometers described above, we have searched unsuccessfully for n.m.r. in both terbium and holmium metals. The frequency ranges and operating temperatures of this search are given in Table 6.1. We also give the predicted n.m.r. frequencies corrected to approximately the working temperatures using the method and magnetization data referred to in chapter 1.

Table 6.1

metal	working temperatures ^{o}K	predicted frequency Mc/sec.	extent of search Mc/sec.
Tb	77	2980±50	2954 to 3078
Tb	72	3020±30	2957 to 3010
Ho	20.3	6450±50	6320 to 6570
Ho	21.3		6350 to 6390

From the expression for the fractional change $\delta Q/Q$ in the cavity quality factor due to n.m.r. (page 2.8), the estimated enhancement of n.m.r. (chapter 4) and the measured sensitivity of the spectrometer, an estimate may be made of the maximum permissible n.m.r. linewidth, above which spectrometer sensitivity will probably be inadequate. In making those estimates, we assume that the necessary partial saturation conditions are satisfied, and that the signal therefore appears only at 25 c/sec. It is also assumed that the measured permeablility gives a susceptibility $X_e = \mu_R - 1$ effective for enhancement. The expression on page 2.8 is then simplified to:-

$$(\delta Q/Q)_{mod} \doteq \frac{aF}{8\pi|\mu|} \frac{(X_{no})(X_e\beta)^2 \nu_o (\delta\nu)_{mod}}{(\delta\nu_o)^2}$$

In the present application, $(\delta\nu)_{mod} \doteq 0.3$ Mc/sec., and $(\delta Q/Q)_{mod} \doteq 5\times10^{-5}$. The maximum permissible linewidth $(\delta\nu_o)$ is then given by:-

$$(\delta\nu_o)^2 \doteq 2.4\times10^2 \frac{aF}{|\mu|} (X_{no})(X_e\beta)^2 \nu_o .$$

For terbium at 77^oK, $\nu_o \doteq 3{,}000$ Mc/sec., $X_e\beta \doteq 20$ and $|\mu| \doteq 1.2$ (from chapter 4), $a \doteq 0.6$ (Appendix A), and from Table 2.1, $X_{no} \doteq 2\times10^{-9}$ and $F \doteq 2/5$. From these figures $(\delta\nu_o)_{max.} \doteq 0.4$ Mc/sec.

For holmium at 20.3^oK, $\nu_o \doteq 8{,}500$ Mc/sec.,

$X_e\beta \doteq 300$ and $|\mu| \doteq 2.5$ (from chapter 4), $a \doteq 0.4$ (Appendix A), and from Table 2.1, $X_{no} \doteq 2.6\times10^{-8}$ and $F = 4/21$. From these figures $(\delta\nu_o)_{max} \leq 10$ kc/sec. From the considerations of chapter 2, section (iv), it is probable that the lifetime broadening contribution to the n.m.r. linewidth in both cases will exceed the values calculated above. As we noted in chapter 2, it is also possible that the necessary partially saturation conditions are not fulfilled, especially in terbium, and our failure to observe n.m.r. may be explained on either or both grounds.

6. (vi) Conclusion.

Fundamental to the magnetic properties of the ions of the non S-state heavy rare earths is the large unquenched orbital angular momentum of the 4f electron shell. This is responsible for the large hyperfine interactions which result in several features contributing to the difficulty of observing n.m.r. in the magnetically ordered phases of the metals. Most notable among these features are the probable very short spin-spin relaxation times, arising through the Suhl-Nakamura coupling, and the high n.m.r. frequencies. The latter add to the problem of n.m.r. observation both by a diminution of enhancement compared to the low frequency case, and also by the sheer difficulty of making a suitable spectrometer. The possibilities of the spectrometer described in this chapter are by no means

entirely exhausted. For example, use of a thinner specimen will lead, for any particular available microwave power, to an increased microwave field at the surface of the specimen and a correspondingly increased field at the nuclei, and likelihood of obtaining the necessary partial saturation conditions. It is possible that loss of enhancement away from ordering transitions or at very low temperatures will be more than compensated by gains in the relaxation times. The properties of the terbium powder described in chapter 5 suggest that use of the powder, at least for this particular metal, may overcome some of the problems arising from a relatively small enhancement of the oscillatory field.

It would be advantageous to build a spectrometer that did not depend on partial saturation of the resonance. However, the ideal of a microwave system with a highly uniform frequency response is a very difficult one to achieve, and some reliable means of discriminating between spurious instrumental resonances and n.m.r. is essential. It is likely to prove exceedingly difficult to make any kind of continuous wave spectrometer with high sensitivity and a sufficiently uniform response over a large frequency range to observe broad n.m.r. lines (e.g. 20 kc/sec. or more). We have seen that such broadening may well occur throughout the series due to Suhl-Nakamura coupling. At the same time, this coupling will make the alternative spin-echo approach difficult to apply.

The relatively small hyperfine interactions in dysprosium and terbium bring together the possibilities of some domain wall enhancement and the longest spin-spin relaxation times in the series. Because of this, these metals, which appear at first sight relatively unfavourable for attempts to observe n.m.r. may, in the end, prove most accessible. The features of terbium and holmium, large nuclear moments and 100% abundant nuclei, which make them appear most favourable on the sort of assessment table given in chapter 2 (Table 2.1) will at the same time contribute both to the high n.m.r. frequencies and direct Suhl-Nakamura coupling. The corresponding reduction in enhancement and short spin-spin relaxation times will greatly add to the difficulties of observing n.m.r.

In this thesis we have sought to detail and assess some of the problems encountered in attempts to observe n.m.r. in the non S-state heavy rare earth metals. Taken together, these difficulties probably account for the lack of progress in this field of research since Lossard's first unsuccessful experiment on terbium in 1960 (7). There is little doubt that a successful n.m.r. experiment would give a wealth of information on these materials, and despite the technological problems involved, we may expect continuing research in the field for some years to come.

References: Chapter 6.

1. K.B. Jefferts and E.D. Jones: Rev. Sci. Inst. 36, 983 1965.

2. E.L. Hahn: Phys. Rev. 80, 580 1950.
see also ref. 3.

3. R.E. Gegenwarth and J.I. Budnick: Bull. Am. Phys. Soc. (11) 10, 591 1965.
G.A. Uriano and R.L. Streever: Phys. Lett. 17, 205 1965.

4. A.C. Gossard, A.M. Portis and W.J. Sandle: Phys. and Chem. of Solids 17, 341 1960.

5. B.V. Rollin: Jour. Sci.Inst. 41, 239 1964.

6. G. Feher: Bell System Tech. Jour. 36, 452 1957.

7. A.C. Gossard: Ph.D.thesis, University of California 1960, (unpublished).

Appendix A.

From Chapter 4, equations 2.3 and 4 we have:-

$$1/Q_i = \frac{1}{2\pi r \nu \mu_o V} \left(A_a R_a + A_r R_r \right)$$

The fractional change $\delta Q_i/Q_i$ in Q_i due to an incremental change δR_a in R_a is given by:-

$$\delta Q_i/Q_i^2 = - \frac{A_a \delta R_a}{2\pi r \nu \mu_o V}$$

$$\text{therefore } \delta Q_i/Q_i = - \frac{A_a R_a}{A_a R_a + A_r R_r} \cdot \frac{\delta R_a}{R_a}$$

$$= - a \frac{\delta R_a}{R_a} .$$

From Chapter 4, equation 1a, $R_a = \sqrt{\pi p \nu \mu_o} \left(|\mu| + \mu'' \right)^{1/2}$

But $\mu' = 1 + X'$ and $\mu'' = X''$ hence:-

$$R_a = \sqrt{\pi p \nu \mu_o} \left\{ \left[(1+X')^2 + X'' \right]^{1/2} + X'' \right\}^{1/2}$$

and the fractional change $\delta R_a/R_a$ in R_a due to small changes $\delta X'$ and $\delta X''$ in X' and X'' is:-

$$\frac{\delta R_a}{R_a} = \frac{1}{R_a} \left\{ \frac{\partial R_a}{\partial X'} \delta X' + \frac{\partial R_a}{\partial X''} \delta X'' \right\}$$

$$= \frac{1}{2\mu_R |\mu|} \left\{ (1+X') \delta X' + (X'' + |\mu|) \delta X'' \right\}$$

$$= \frac{1}{2|\mu|} \left\{ \frac{\mu'}{\mu_R} \delta X' + \delta X'' \right\}$$

$$\text{hence } \delta Q_1/Q_1 = \frac{-a}{2|\mu|}\left\{\frac{\mu'}{\mu_R}\ \delta X' + \delta X''\right\}$$

Unless explicity stated otherwise, when Q and δQ are referred to in the text the instrinsic factor is signified, and we shall omit the subscript 1. We also omit the minus sign before a, as our primary interest is in estimating the magnitude of $\delta Q/Q$. Hence, from the definition of μ_R (equation 1a, Chapter 4):-

$$\delta Q/Q = \frac{a}{2|\mu|}\left\{\frac{\mu'}{|\mu|+\mu''}\ \delta X' + \delta X''\right\}$$

$$\text{The parameter } a = \frac{A_a R_a}{A_a R_a + A_r R_r}$$

$$= \frac{\text{power dissipated in the specimen}}{\text{total power dissipation in cavity}}$$

As we have seen (Chapter 4, equation 5) the bandwidth $\delta\nu$ is the sum of two parts; A(T), which is proportional to the power dissipation in the rest of the cavity, and $B\sqrt{\rho\mu_R}$ to that in the specimen.

For the 10 cm. wavelength cavity at $77^{\circ}K$, A(T) = 0.72 Mc/sec. (figure 4.8) and $\delta\nu = A(T) + B\sqrt{\rho\mu_R}$ = 1.77 Mc/sec. (figure 4.10) hence $a = \frac{1.05}{1.77} \doteq 0.6$

For the 4 to 5 cm. wavelength cavity at $20.3^{\circ}K$, the measured values of A(T) and $\delta\nu$ are respectively $\doteq$ 2.5 Mc/sec. and 4.45 Mc/sec.

hence $a \doteq \frac{1.95}{4.45} \doteq 0.4$

Appendix B.

From equations 1a,4 and 5 in Chapter 4,

$$\delta\nu = A(T) + \sqrt{\frac{\pi\nu\mu_o}{2\pi\mu_o}} \left(\frac{A_a}{V}\right) \sqrt{\rho\mu_R}$$

where $A_a = \int_a H^2 dS$ and $V = \int_V H^2 dV$

$$\text{hence } B = \frac{1}{2}\sqrt{\frac{\nu}{\pi\mu_o}} \quad \frac{A_a}{V}$$

In a coaxial cavity, the magnitude of a field at a point (r,z) is given by $H = \frac{K}{r} \cos \frac{2\pi z}{\lambda}$, where the z-axis is the axis of the cavity, r the radial distance from z and K is a constant. We measure z from the top end of the two cavities (figures 3.3 and 3.4). If a and b are the radii of the inner and outer conductors, we then have for the 10 cm. cavity:-

$$A_a = 2\pi a \frac{K^2}{a^2} \int_{\lambda/4}^{3\lambda/4} \cos^2 \frac{2\pi z}{\lambda} \, dz$$

$$\text{and } V = \int_0^{\lambda} \left\{ \int_a^b \frac{K^2}{r^2} \cos^2 \frac{2\pi z}{\lambda} \, 2\pi r \, dr \right\} dz$$

$$= 2\pi K^2 \ln(b/a) \int_0^{\lambda} \cos^2 \frac{2\pi z}{\lambda} \, dz$$

$$\text{and hence } B = \frac{1}{4a \ln(b/a)} \sqrt{\frac{\nu}{\pi\mu_o}} \qquad \text{equation B.1.}$$

In the 4 to 5 cm cavity, the centre conductor extends the full length of the cavity (neglecting end effects) and hence

$$B = \frac{1}{2a \ln(b/a)} \sqrt{\frac{\nu}{\pi \mu_o}} \qquad \text{equation B.2.}$$

In both cavities, 2b = 27.4 mm. Using this and the values of 2a and ν given in Chapter 4, B is calculated from B.1 and B.2. The results are given in Table 4.2.

Appendix C.

As an equivalent circuit for a microwave cavity terminating a coaxial line we adopt the circuit below (see ref. C1):-

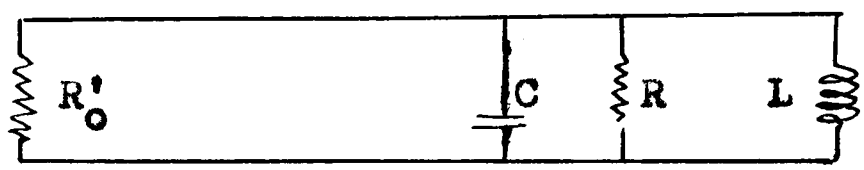

R'_o is the transformed characteristic impedance of the line, as viewed from the cavity.

The total power dissipation in this circuit, and hence the loaded bandwidth $\delta\nu_L$ is proportional to $1/R'_o + 1/R$. The first of these terms describes losses external to the cavity, and the second those intrinsic to the cavity. Hence:-

$$\delta\nu_e = \frac{D}{R'_o} \quad \text{and} \quad \delta\nu = \frac{D}{R} \text{ , where D is a constant.}$$

On resonance the cavity impedance is R, and the power reflection coefficient is therefore (see ref. C2):-

$$\rho_P = \left\{ \frac{R'_o - R}{R'_o + R} \right\}^2$$

$$\text{hence} \qquad \rho_P = \left\{ \frac{\delta\nu - \delta\nu_e}{\delta\nu + \delta\nu_e} \right\}^2$$

References:-

C 1. D.D. King: "Measurements at Centimeter Wavelength", page 131, van Nostrand 1952.

C 2. Bleaney and Bleaney: "Electricity and Magnetism" p.285, Oxford University Press, 1957 (1st edition).